MSc Thesis

Modelling and optimization of insertion maneuvers at Mars

Cristina Riti

Student ID 5229405
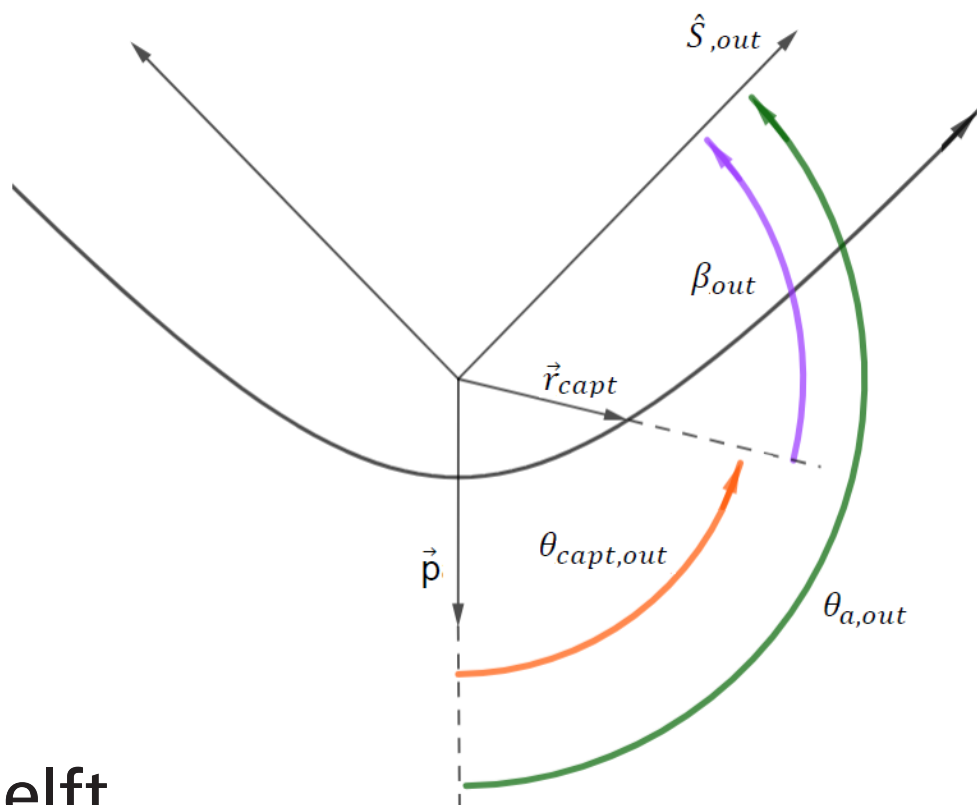
TUDelft

MSc Thesis

Modelling and optimization of insertion maneuvers at Mars

by

Cristina Riti

to obtain the degree of Master of Science
at Delft University of Technology,
to be defended publicly on August 30th 2023

Student number:	5229405
Project duration:	July 2022 – July 2023
Thesis committee:	Ir. R. Noomen, thesis supervisor
	Dr.ir. E. Mooij, chair
	Dr. R.T. Rajan, examiner

An electronic version of this thesis is available at `http://repository.tudelft.nl/`.

TUDelft

Preface

Cristina Riti
Delft, July 2023

I have started this thesis moved by my faith in Murphy's law: "Anything that can go wrong will go wrong", which applied to Space Engineering translates into trying to figure out all the possible failure modes and recovery procedures for a Space mission, or how to "expect the unexpected". While developing the thesis, many events influenced my direction both academically and personally. All of them have challenged me and made me think differently about myself, my future and even the objective of my thesis project. Despite all of that, I am glad I still managed to conclude my journey at TU Delft.

It's been an odd and complicated thesis year, which I began last July as part of Lunar Zebro, a student team I will be grateful to as a whole, for teaching me how to be part of an engineering team while connecting with so many talented and brilliant individuals.

I sadly had to leave the team to dedicate myself to the thesis, as well as my first part-time job in a space company, ISISPACE. For six months, until June 2023, I've been part of its Ground Segment department. I want to thank everyone there for welcoming me, but especially my closest colleagues of the Ops room for making me believe in my capabilities again. I was struggling with my thesis, as much as thinking about leaving Delft and moving back to Italy. And even if it may seem counter-intuitive, spending half a day on a job was the best way to save time, because it allowed me to continue the thesis instead of abandoning it.

A special thanks goes to Ron Noomen, my supervisor, who had the patience to follow me at my pace, even when it was not the fastest or the most consistent. For almost two years (considering the literature study as well) he supervised my progress and was always there to cheer for any step forward.

The list of people I met here in the Netherlands would be too long, but I want to thank my roommates Erik, Nathaniel and Iliana, for supporting me and making sure I did not spend way too much time alone in my room.

The end of this preface is reserved for team Italy, all the people I had to live far from for three years and missed terribly. First, my parents and my brother and sister. My family is the reason I am a science nerd who had the strength and possibility to move out of their country. Then, my boyfriend, who listened to all the times I complained about how busy I was and how much I wanted to see him. And finally all the girls I am so lucky and honored to call friends. Aurora, who I know will answer me any time and tell me everything about her life to not make me feel like I missed out on anything. Martina, who was my thesis buddy for a whole year, and with whom I shared the trials and tribulations of such final project. She always gave me strength and unconditional words of support, even in the most dire times. Imen, who always put a smile on my face during our super-loud calls which could be heard through walls, and was always interested in listening to me blabbering about TV series and how the world goes.

TU Delft was my dream university and reconciling that dream with challenging conditions (living in a different country and a global pandemic) has been an experiment in cognitive dissonance. However, I will always cherish these years. The best lesson I learnt here is to always go for any opportunity that seems interesting. It takes courage, especially to accept that you cannot always figure out beforehand what an experience will be like, or what it will give you. Instead of "expecting the unexpected", I learnt how to enjoy the unexpected.

Abstract

Insertion maneuvers are used to move a spacecraft from an open orbit (parabolic or hyperbolic) into a closed orbit around a target body. These maneuvers are key components in any space mission considering orbiting a body for a large amount of time, for exploration or landing; the hyperbolic orbit will be the one that will be used to transfer between Earth and the target, while the closed orbit will be the one on which the spacecraft will station. In preliminary mission studies, insertion maneuvers are often assumed as being performed at pericenter, and with the two velocity vectors (before and after the maneuver) having the same direction. However, this method does not account for the relative orientation of the two orbits, which are often constrained by separate optimization studies, which may not grant the necessary conditions for a tangential insertion. This study aims to provide a simple method to perform preliminary studies on insertion maneuvers, while ensuring the continuity between the two trajectories, even when those are subject to shape or orientation requirements. The objective is to optimize the insertion maneuver for a crewed mission to Mars, and via this case study gain insight in the best maneuver available (instead of assuming a pericenter, tangential insertion), as well as the best shape and orientation of the trajectories before and after the maneuver.

Contents

Abbreviations and Symbols

List of Abbreviations

ABC	Artificial Bee Colony
ARM	Asteroid Redirection Mission
DE	Differential Evolution
DRA	Design Reference Architecture
DSM	Deep Space Maneuver
EM	Emergency Maneuver
EMC	Evolvable Mars Campaign
EOL	End Of Life
ESA	European Space Agency
GER	Global Exploration Roadmap
HAT	Human spaceflight Architecture Team
ISS	International Space Station
JPL	Jet Propulsion Laboratory
LDHEO	Lunar Distance Highly Elliptical Orbit
LDRO	Lunar Distant Retrograde Orbit
LEO	Low Earth Orbit
LPO	Lunar Parking Orbit
MC	Monte Carlo
MERF	Mars Equatorial Reference Frame
MPO	Mars Parking Orbit
NASA	National Aeronautics and Space Administration
ONS	Off-Nominal Situation
PEOL	Premature End Of Life
PO	Parking Orbit
RAAN	Right ascension of the ascending node
S/C	Spacecraft
SEP	Solar Electric Propulsion
SOI	Sphere Of Influence
SSB	Solar System Barycenter
TEI	Trans Earth Injection
TMI	Trans Mars Injection
TOF	Time Of Flight
TU Delft	Technical University Delft
TUDAT	TU Delft Astrodynamics Toolbox
TudatPy	TU Delft Astrodynamics Toolbox with Python interface

List of Symbols

^	Unit vector notation
→	Vector notation
e	Referencing the elliptical orbit characteristics
h	Referencing the hyperbolic orbit characteristics
♈	Direction of Aries constellation
α	Right Ascension [rad]
β	Angle between radial position and reference asymptote [rad]
γ	Flight path angle [rad]
δ	Declination [rad]
Δt	Time interval [s]
ΔV	Cost of a maneuver [m/s]
θ	True anomaly [rad]
θ_A	True anomaly of the hyperbolic asymptote [rad]
$[\theta]_i$	Rotation matrix of angle θ around axis i
μ	Gravitational parameter [m^3/s^2]
τ	Longitude [rad]
χ	Angle between the local north and the projection of the velocity vector on the horizontal plane [rad]
ψ	Flight path angle analogue [rad]

Ω	Right ascension of the ascending node [rad]		h	Specific angular momentum vector [m^2/s]
ω	Argument of pericenter [rad]		i	Inclination [rad]
$\hat{S}$	Asymptote direction		J2	Spherical harmonics coefficient corresponding to radree 2 and order 0
$\hat{W}$	Angular momentum direction		NP	Population size
$\mathcal{E}$	Specific orbital energy [m^2/s^2]		p	Semi-latus rectum [m]
$\vec{n}$	Ascending Node vector		r	Radial position [m]
$\vec{p}$	Pericenter direction unit vector		r_p	Pericenter radius [m]
$\vec{r}_{capt}$	Radial position at capture		$r_{MARS,SOI}$	Radius of the SOI of Mars [m]
a	Semi-major axis [m]		r_{PO}	Parking orbit radius [m]
C_3	Energy integral [m^2/s^2]		sol	mean solar day on Mars [s]
CR	Crossover coefficient		T	Orbital period [s]
d	Mean solar day on Earth [s]		t	Time [s]
e	Eccentricity [-]		v	Velocity [m/s]
F	Mutation coefficient		v_∞	Velocity on an hyperbolic trajectory at infinite distance from central body [m/s]
G	Generation number			
h	Altitude of a point over a target body [m]		V_g	Groundspeed [m/s]

1

Introduction

The future of space missions has recently seen a resurgence of human missions outside of Earth orbit with plans of exploration of the Moon (with the ARTEMIS program). The Moon missions will serve as a stepping stone for an even more ambitious objective, that of landing a crew on Mars [16], [19].

As part of the mission design process, there is a need to perform preliminary studies of each phase of the mission, from the transfer between Earth and Mars to the daily operations once in the vicinity of Mars. These studies have critical requirements, different from the ones of current robotic missions around Mars, due to the presence of a human crew, such as those highlighted in a study by Goodliff [8]. Only preliminary studies have been published at time of writing, detailing the objectives, tentative launch windows and architectures of such missions, for example the studies by Percy [19], [20].

While these studies already contain a lot of detailed information, documentation is often incomplete, in particular on the exact mathematics and computations behind the trajectory and maneuver models employed in their analyses. Studies such as those performed by Joyner ([12], [11]) and Merrill ([15]) on the subject often mention models without providing their implementations, as will be explained in this study. The idea of this thesis study stems from this obstacle, with the intention of charting a clear way of solving the problem, specifically focusing on the insertion maneuver, a key component in any propellant budget. The insertion maneuver is the link between the transfer trajectory between Earth and Mars and the stay time in the orbit of Mars (while the mission is being accomplished). Ensuring the continuity between these two phases is a non trivial problem, which will be examined in the study, attempting to find a suitable method to model and optimize the problem.

This study will use as a reference the case of a crewed mission to Mars, based on a series of NASA studies on future missions to Mars called the Evolvable Mars Campaign ([19]). This reference will provide useful information on environmental variables, parameters and constraints applicable to crewed missions to Mars.

The research question is:
"What are the optimal conditions for an insertion in an operational orbit around Mars in terms of cost of the maneuver and characteristics of the trajectories involved, ensuring the compatibility of the maneuver with the transfer trajectory and resulting parking orbit, and considering a single maneuver?".

Chapter 2 provides background on the choice of the insertion maneuver problem, as well as introducing the EMC frame. Chapter 3 details the assumptions that characterize the case studies selected, derived from different studies on missions to Mars. Chapter 4 presents the theoretical background into the insertion maneuver problem and its analytical solution. Chapter 5 is dedicated to the presentation of the optimization problem, from its definition to the choice and tuning of an optimizer algorithm. Chapter 6 will present the results of the optimization and lessons learned, while Chapter 7 will conclude the study and give recommendations for future studies.

<div style="text-align: right">

2

Heritage

</div>

This chapter will describe how the thesis topic selection has evolved through the first months of the project. The literature study [22], which was done in preparation for the current study, was focused on the area of off-nominal scenarios in space missions, more specifically due to an incomplete maneuver or an error while performing it. The suggestion for the thesis was to study how an appropriate trajectory design could be helpful in both preventing and recovering those situations.

The literature study also covered which types of missions would be more interesting for this application, and the choice fell, among others, on Martian missions. The following sections will build from these results, and expand on the decision and assumptions leading the search for the case study, and how it developed into the final research question and its subquestions, which will be presented at the end of this chapter.

2.1. Results of Literature Study

Off-nominal scenarios are defined as any situations that deviate from the nominal mission. Some off-nominal scenarios do not allow the mission to continue with the planned sequence of trajectories and maneuvers, but require Emergency Maneuvers (EMs) to either continue or prematurely be ended.

The literature study focused on the definition of multiple off-nominal scenarios and the study of the possible solutions that had been described in previous research. The result of the literature review was a selection of interesting aspects and questions that will be summarized below [22].

- **Presence of a human crew**
  The presence of a human crew changes the available options once the nominal mission cannot be completed. A robotic mission can be ended prematurely by, for example, crashing an orbiter on a target body. On the other hand, a human mission must allow for the safe return of the crew to Earth, by planning for appropriate EMs. Human missions are therefore more complex problems when it comes to EMs, and have been selected for further study, also due to the renewed interest in human exploration, with the ARTEMIS program [16].

- **Mission target**
  The next target in the field of human exploration is returning to the Moon. New lunar missions will be the necessary step between the human presence in the ISS and future Martian missions [27]. However, a large number of studies on such missions and their abort scenarios is already present in literature. It was then decided to cover Martian missions instead. The idea was to apply some of the already developed concepts to a different setting, with different conditions and requirements, and identify solutions that could become the new staples in the field of EMs, with specific characteristics dictated by the different target body.

- **Mission stage** In a study on the Apollo missions, Diamant divides the EMs according to when and where in the mission they occur [7]. The main distinction is whether they occur during the insertion in a Lunar Parking Orbit (LPO) or during the escape from it and insertion in the return

4

trajectory to Earth. It also contains suggestions on the transfer trajectories between Earth and the Moon, and how to achieve a "free return" trajectory, or an 8-shaped trajectory that will grant the return of the spacecraft in Earth orbit, without the need of an additional maneuver.

Studies on EMs for missions to Mars have until now only covered maneuvers operated during the transfer between Earth and Mars, both in the studies of Joyner [12], [11] and Patole [18]. These studies cover the characteristics of the transfer trajectory in the travel between Earth and Mars and the addition of Deep Space Maneuvers (DSM) to obtain more favourable conditions (in terms of propellant budget or total time of flight). The emergency tackled is the need for an abort maneuver to return to Earth as soon as possible, instead of continuing the mission. Free return trajectories to Mars have been studied by Joyner [11] and Wooster [28], but tend to have a very high time-of-flight (TOF, a critical quantity for a human crew). On the other hand, abort strategies that tackle the characteristics of the insertion or escape maneuver considering both the transfer trajectory and the parking orbit around the target (such as the ones by Diamant for the Apollo era) are not present in current literature on Martian missions, and represent an interesting subject for the thesis study.

2.2. Evolvable Mars Campaign

The previous section resulted in the choice of a human mission to Mars as case study. In order to employ some more realistic parameters and boundaries for the project, it was decided to use a current mission design as a reference, and the Evolvable Mars Campaign appears the most suitable for this purpose. The next section will present how this mission has been selected and its characteristics.

2.2.1. Choice of mission frame

Several studies have been seminal in the current body of knowledge around planning crewed missions to Mars, from the ones dedicated to robotic missions on the planet to theoretical research and feasibility studies for crewed missions. In recent years a few specific projects have raised to the level of plausible plans for attempting a human mission on Martian soil. The following is a short list of the main ones, compiled by Goodliff [8]:

- NASA's Design Reference Architecture (DRA) 5.0.
- NASA's Evolvable Mars Campaign (EMC)
- JPL's Minimal Mars Architecture
- Inspiration Mars Mission
- Mars One Campaign

In the analysis of these different projects, it was clear that the Mars One Campaign and the Inspiration Mars Mission were not feasible, first from an economical and funding standpoint, secondly from the technological developments they required in a very short time frame.

   The DRA 5.0 was an older project, started in 2009 to study the feasibility of a crewed Martian mission. While different from its successor, the EMC, it was decided to not consider the DRA as the studies that focused on it considered many technological developments which, after almost a decade, will not be achieved in time. It also requires an extremely high number of crews that would be involved in the missions, making it less efficient than the others.

   The EMC and Minimal Mars Architecture shared many similarities, from the same time frame and launch windows, to the idea of starting with the exploration of Phobos as a first step, while allowing more time to research and find solutions for a Mars habitat. The propulsion system is also similar (SEP for cargo and chemical for crew), but the main difference would be in the location of the Trans Mars Injection (TMI) maneuver. The JPL Minimal Mars Architecture considers a LEO insertion, which requires a very costly impulsive maneuver, while the EMC performs the maneuver in a LDHEO orbit (Lunar Distance Highly Elliptical Orbit), which results in propellant savings and the reutilization of services that will be developed for in-between lunar missions (Proving Ground) and the Asteroid Redirection Mission (ARM). Therefore, the sustainability of operations and the use of in-between steps to develop and test relevant technologies make the EMC a more mature plan, and the one chosen for this thesis study.

2.2.2. EMC introduction

The EMC was first proposed in 2014, by the NASA Human spaceflight Architectures Team (HAT), to investigate the possibilities for human exploration of Mars in the 2030s, according to the National Space Policy of the USA [19].

The EMC includes three separate missions, all carrying a crew of four: the first one landing on Phobos, the second and third both landing on Mars (all planned between 2033 and 2045).

In order to allow for such a long and complicated mission, it is necessary to deploy critical components in advance, such as cargo (lander, surface habitat for humans, taxi vehicle). Otherwise the mission would be too heavy and it would be too expensive if not impossible to launch. Those elements can be sent either directly to Phobos, or to a Mars Parking Orbit, via Solar Electric Propulsion (SEP) stages to save propellant, since the absence of a crew can allow for a longer Time Of Flight (TOF).

It is also possible to pre-deploy some propulsion stages for the crew vehicle. The "main" propulsion system (the one of the transfer vehicle) is split between the inbound and outbound legs of the journey, with each maneuver having its own dedicated propulsion stage. The Trans Earth Injection (TEI) and Earth Orbit Insertion (EOI) stages are pre-deployed in the Mars Parking Orbit (MPO) and await there the arrival of the transfer vehicle. This mission architecture is referred to as "split-mission" [19].
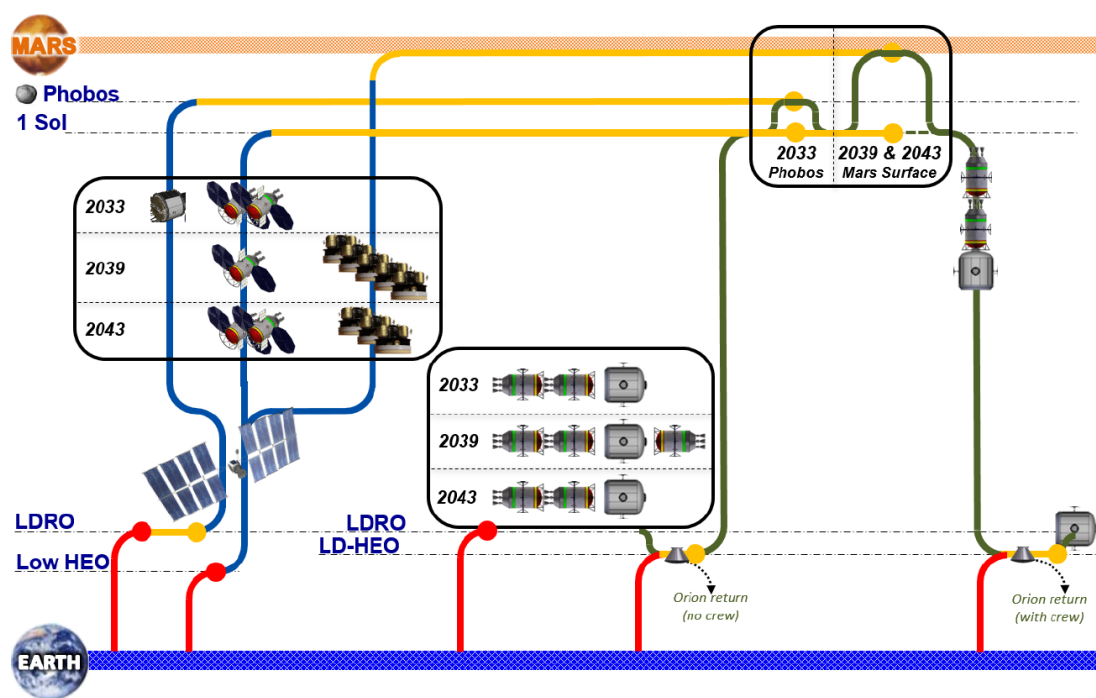
Figure 2.1: Overiew of the flight sequence and stack deployment for the three missions in the EMC campaign, with chemical/SEP split [20].

The following description of the mission phases comes from a study by Percy [20] on the propulsion system for the EMC missions. A summary of the EMC strategy is also shown in Figure 2.1. The crew stack is the only one that will perform the transfer using chemical propulsion. The crew stack is made of the deep space habitat and two propulsion stages (one for the MOI maneuver, and one for the TMI maneuver). This stack is assembled in Lunar Distance Retrograde Orbit (LDRO) and then departs for LDHEO, where it rendez-vous with an Orion capsule carrying the crew, which then moves into the transfer habitat. The maneuvers listed below assume that the stack and crew have already performed such rendez-vous successfully.

The transfer to Mars will begin in cis-lunar space, at perigee of a LDHEO, pericenter altitude of 400 km and apocenter at lunar distance. A TMI maneuver injects the spacecraft into a transfer trajectory; it can either be a direct transfer to Mars, or a DSM can be planned approximately in the middle of the total transfer duration, to achieve more advantageous conditions on arrival into the Mars SOI (this depends

on the launch and arrival conditions).

Once the spacecraft arrives inside the Martian SOI, the Mars Orbit Insertion (MOI) stage is used to position it into a 1-sol MPO. The stack does a rendez-vous with the two propulsion stages needed to return to Earth, forming the transfer stack. In the first mission, an additional "taxi" vehicle is employed, to transfer the crew between Mars and Phobos, while in the other two missions a lander is added to reach the surface of Mars. However, this study will focus on the main stack.

The transfer stack (deep space habitat and return propulsion stages) is then re-positioned in a different MPO, in order to achieve better conditions for the return travel. The TEI stage is used to inject the spacecraft in a direct return trajectory. Upon arrival, the transfer spacecraft is positioned in LDHEO using the EOI stage, and does a rendez-vous with a Orion capsule, which will carry the crew to the Earth's surface. The transit habitat moves to LDRO to be refitted and used in future EMC missions.

2.2.3. Choice of MPO as environment instead of transfer

As mentioned in Section 2.1, the design of EMs for Martian crewed missions has focused mainly on the design of transfer trajectories between Earth and Mars (with or without a DSM).

However, it is worth noticing that, differently from the Apollo mission, the EMC strategy has the crew stack first insert in an elliptical orbit around Mars, but then also perform additional maneuvers to reposition and obtain more optimal conditions for the departure towards Earth. This so-called repositioning strategy is not covered by Percy [19] in the general overview of the EMC missions, but in additional studies led by Merril and Qu [15], [21] on the EMC frame.

Repositioning strategies may also be necessary for future missions to the Moon, due to the long stay time on the surface and the need to rendez-vous with any return stages, or additional cargo that was pre-deployed. However, at time of writing, there are no studies covering EMs in case these maneuvers in the Martian orbit were to fail, which is identified as an interesting gap in the current knowledge. In order to attempt to address it, it is first necessary to understand the necessity and characteristics of repositioning maneuvers in the SOI of a planet.

2.3. PO repositioning history

Repositioning a spacecraft, once it is on a parking orbit, means achieving, via multiple maneuvers, a closed orbit that is more advantageous for escaping the central body. The objective of the repositioning is to minimize the total ΔV spent by the mission in the SOI of the central body (the sum of the insertion, repositioning and escape ΔVs). There are many combinations of repositioning maneuvers available at the mission design stage, which are organized into so-called "strategies", which are a sequence of them starting from the insertion maneuver and ending with an escape maneuver around a central body.

These strategies can be developed both numerically (for example via numerical integration of the equations of motion of the spacecraft) or analytically. This section will explore the analytical studies that have introduced the necessity and usefulness of repositioning techniques for a mission to Mars.

2.3.1. Free repositioning

The repositioning problem has been introduced by Desai in two publications [5] [6] which state that previous studies for human exploration of Mars assumed that a coplanar insertion at pericenter was always possible, without considering the actual relative geometry between the Earth-to-Mars trajectory and the elliptical parking orbit.

Desai is the first to show how this assumption can result in an underestimation of the propellant budget, and to offer a solution for the issue, called "free repositioning". The input are the conditions of the hyperbolic arrival, and the strategy identifies the elliptical parking orbit that would grant a coplanar, pericenter insertion both at arrival and at departure. The innovation by Desai is twofold.

First, the parking orbit selected accommodates both insertion and departure maneuvers, while in the past pericenter coplanar maneuvers were assumed, without considering whether the parking orbits would have had the same orientation in space or not in order to intersect with the transfer legs.

In addition to this, while previous studies assumed Mars to be perfectly spherical, Desai adds the influence of the J2 effect, which causes the precession of the parking orbit. The resulting parking orbit selected maintains the same geometrical properties in terms of shape (same eccentricity and semi-major axis) but changes orientation over time, due to the planet's oblateness (and therefore second-order terms of its gravitational field), as shown in Figure 2.2.
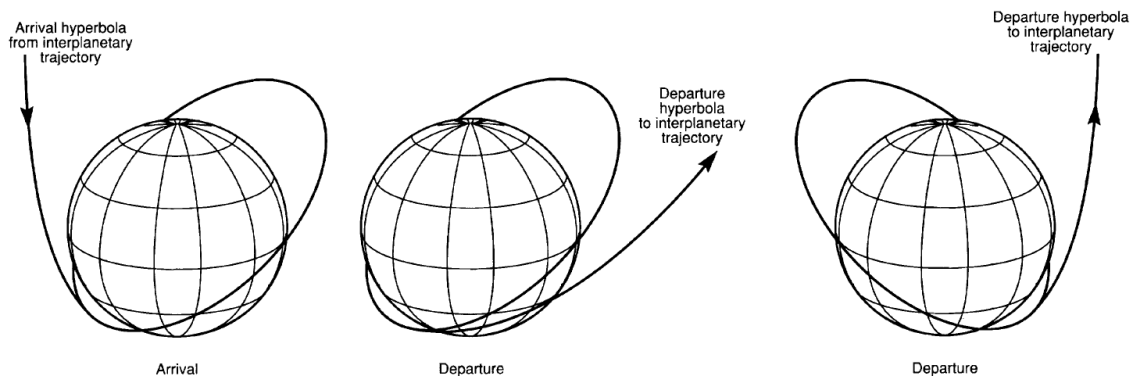
Figure 2.2: Geometry of a transfer between an hyperbolic orbit and an elliptical parking orbit, at insertion (left), departure in the case of a spherical Mars (center) and departure in the case of an oblate Mars (right) [5].

Desai's strategy results in a parking orbit that matches correctly the orientation of the arrival hyperbola for the insertion maneuver, and then precesses over the total stay time (based on the required time in the orbit of Mars for the selected mission) to match the orientation of the return hyperbola for the escape maneuver. No additional maneuvers are necessary, and the strategy is therefore called "free repositioning".

Another study by Desai [4] considers orbit precession but instead of having the orbit perfectly precess to have a pericenter tangential escape, the study computes the propellant budget for a non-tangential, non-coplanar escape maneuver (after 60 days of orbit precession and a fixed transfer hyperbola asymptote). The same study varies the true anomaly of the maneuver in the elliptical orbit, finding that pericenter is not always the best position for out-of-plane escape maneuvers, demonstrating how even assuming that pericenter is always the best position for insertion and escape maneuvers is a limiting hypothesis. The same study suggests that the use of retrograde parking orbits applied to this problem can reduce the total propellant budget for the mission (considering the total cost of the insertion and escape maneuver).

2.3.2. 3-step repositioning

Landau introduces an additional maneuver, to offer a higher degree of flexibility to the problem, with the so-called 3-step strategy [13]. The study applies all the conclusions of Desai (need of considering the orbit orientation and J2 effect) and adds a maneuver to "supplement" the change in orientation, so that the desired final orientation of the parking orbit can be achieved in virtually any amount of time (instead of having to wait for the precession effect). Landau explains that the method suggested by Desai results in "rare" solutions, which usually do not correspond with the conditions for minimum transfer time and ΔV.

The initial assumption of Landau's problem is that the angles characterizing the asymptote for the incoming and departure hyperbolas are different (which is usually the case for these orbits). The initial parking orbit is selected to achieve a pericenter tangential insertion. However, the stay time of the mission does not allow the parking orbit to precess enough to match exactly the departure hyperbola for another pericenter tangential maneuver (therefore Desai's method cannot be applied). Landau then suggests two solutions:

- A 2-step strategy, which allows for an off-tangential escape maneuver at periapsis. The maneuver would be quite expensive because it would usually require a change in inclination of the orbit, with the higher velocity magnitudes of positions close to pericenter.
- A 3-step strategy invented to minimize the cost of changing the orbit orientation. Both insertion and escape are pericenter tangential maneuvers. The additional maneuver is a so-called apotwist: it is performed at apocenter and it twists the orbit around the apoapsis line, to obtain a change of orientation. An example of apotwist maneuver is shown in Figure 2.3.

Landau's study shows how an off-tangential burn at pericenter for insertion and departure (a 2-step strategy) is generally more expensive than his proposed 3-step strategy, also named apotwist technique.
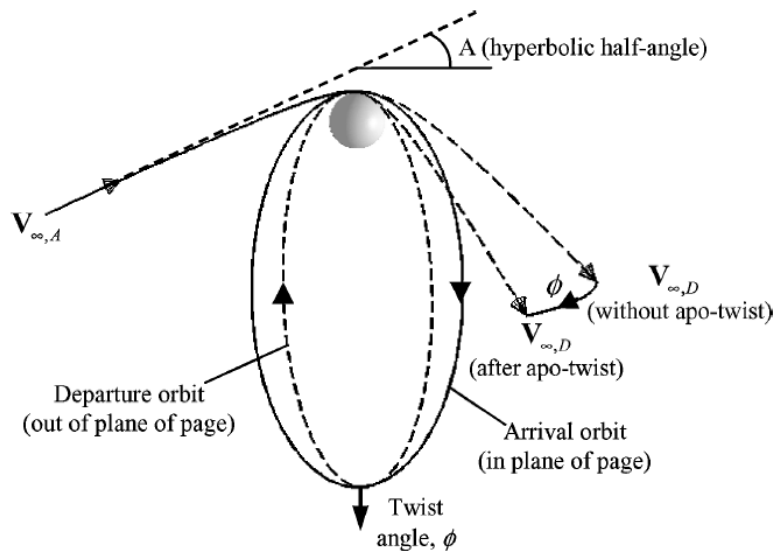
Figure 2.3: Rotation of parking orbit about the line of apsides by twist angle ϕ, from Landau [13]

2.3.3. 7-step maneuver, or bi-elliptic apotwist

Both Desai and Landau start from the characteristics of the transfer hyperbolas and arrive at the definition of the parking orbit ellipse (or ellipses) that would best fit in-between these two maneuvers. However, parking orbits do play an important role in space missions, and some of their characteristics may be fixed in order for the scientific objectives to be achieved.

The bi-elliptic apotwist is a 7-step repositioning strategy that tries to combine the benefit of a low-cost insertion and escape maneuver (by adopting high-eccentricity elliptical orbits after such maneuvers) with the need to reach a specific target parking orbit (usually with a lower eccentricity) during most of the stay time around Mars.

The bi-elliptic apotwist technique was first introduced by Merrill [15] for a study of the EMC maneuvers in the SOI of Mars. The following list will detail the orbits and the seven maneuvers part of the strategy. All orbits have the same pericenter distance, called r_{PO}. In order to understand what is considered parking orbit, and what is a bi-elliptic transfer orbit instead, the reference is in Figure 2.4, since this nomenclature is taken from the original study.

- **Orbit A:** Incoming hyperbola of Earth-to-Mars transfer
- **Maneuver 1:** Off-periapsis, coplanar, non-tangential insertion maneuver
- **Orbit B:** First bi-elliptic transfer orbit
- **Maneuver 2:** Apotwist maneuver (same definition as Landau)
- **Orbit C:** Second bi-elliptic transfer orbit
- **Maneuver 3:** Lower the height of the apoapsis, performed at periapsis
- **Orbit D:** (Arrival) Parking Orbit
- – First Orbit precession (due to long stay time on the target PO, orbit D)
- **Orbit E:** Same shape as parking orbit D, but precessed
- **Maneuver 4:** Second Apotwist maneuver
- **Orbit F:** Parking orbit
- – Second Orbit precession (due to long stay on orbit F)
- **Orbit G:** Departure parking orbit
- **Maneuver 5:** Raise the height of the apoapsis, performed at periapsis
- **Orbit H:** Third bi-elliptic transfer orbit
- **Maneuver 6:** Third Apotwist maneuver
- **Orbit I:** Inbound transfer orbit
- **Maneuver 7:** Off-periapsis, coplanar, non-tangential escape burn
- **Orbit J:** Outgoing hyperbola of Mars-to-Earth transfer
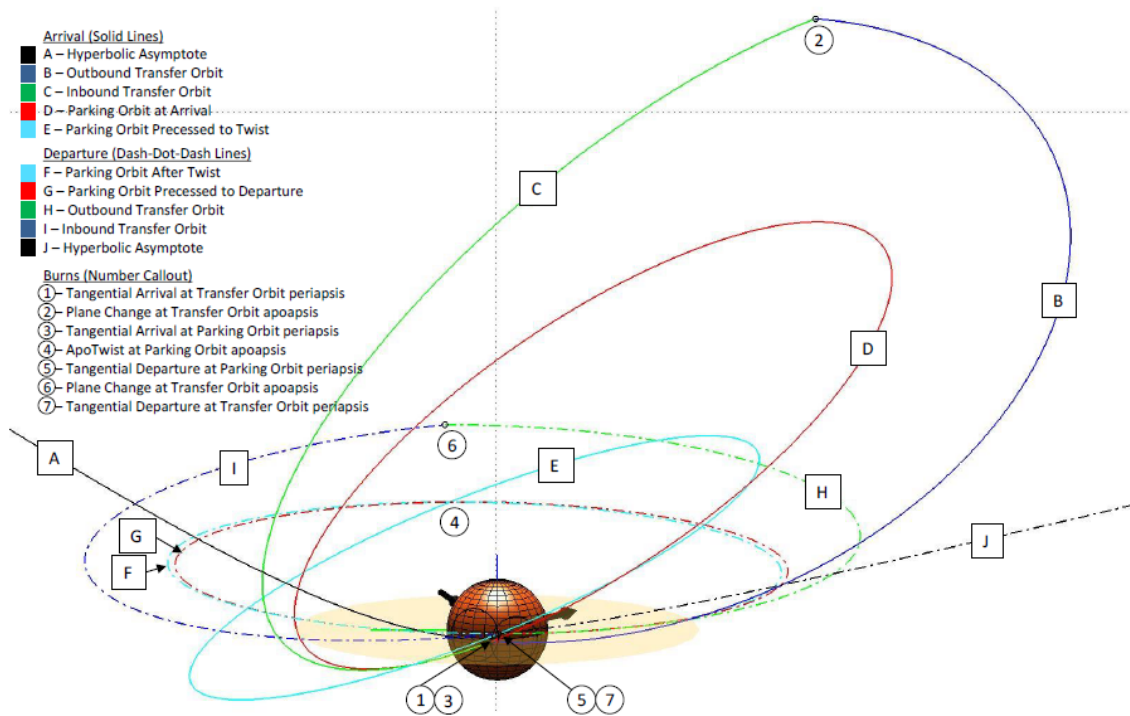
Figure 2.4: Bi-elliptic apotwist technique orbits and maneuvers, concept of operations [15]. For the detailed explanation of the orbits and maneuvers, check the description in this section.

Merril's strategy presents the additional risk of performing a high number of maneuvers; on the other hand, it provides additional degrees of freedom that allow to apply it to missions with very different objectives and duration, like those of the EMC frame, as well as allowing for more room to perform different EMs in case of failures.

2.4. Insertion Maneuver challenges

Having covered the characteristics of different repositioning strategies in the previous section, it was decided that an interesting thesis objective could be to adapt the 7-step repositioning technique assuming that one of the maneuvers was not executed correctly, and which propellant margin would be reasonable to perform an emergency correction maneuver. In order to do so, the first step would have been reproducing the conditions of the nominal mission, using the strategy adopted by Merril, in order to then modify it.

However, some important issues emerged. The largest was that Merrill, while explaining the use of a numerical method (and the selection of input and output variables) for the problem, does not mention any of the equations adopted for their 7-step strategy. While the apotwist maneuver and changing the height of apoapsis are both very straightforward maneuvers under the assumptions of impulsive maneuvers and a two-body problem (more information on those assumptions in Chapter 3), the insertion and escape maneuver were not as easy to model. Merril adopted a coplanar, off-periapse, non-tangential maneuver, but in case of an emergency there was a need to model a non-coplanar, off-periapse maneuver, with an additional degree of difficulty in ensuring that the orbits would intersect at the desired location for the maneuver. Desai's paper mentions non-coplanar maneuvers, but does not include a mathematical model for them as well [4].

A different study on the EMC, performed by Nervo [17], replicates the nominal repositioning strategy of the EMC but adds a non-coplanar insertion maneuver model, first introduced by Cornick [2]. Nervo justifies the adoption of the most generic maneuvers possible (off-periapsis, non-coplanar) to include the largest number of options in their study. Clearly, it pairs a high flexibility with an additional computational challenge.

Cornick's paper includes a full description of the analytical model used to solve the insertion maneuver problem (which will be introduced more thoroughly in Chapter 4). While many papers mention the use of non-coplanar insertions as an option, Cornick is one of the few references that present all the information to replicate their model.

While Nervo goes on to compute the full seven-step strategy via an optimization problem, the study and optimization of the insertion maneuver by itself, paired with the flexibility of performing an off-pericenter, non-coplanar maneuver opened up a new and promising area of research, since insertion and escape maneuvers are the only ones which appear in all the above-mentioned repositioning strategies.

2.5. Rationale for research question

The heritage study has resulted in a better definition of the case study, a human exploration mission to Mars, and the topic of the project, which is insertion maneuvers. With the help of previous studies, it is clear how an oversimplification of the insertion maneuver will result in a high error on the estimation of the maneuver cost (as demonstrated by Desai [4]), which is a relevant metric in preliminary mission studies aimed at sizing the mission such as the one by Percy for the EMC frame [19].

The research question is: *"What are the optimal conditions for an insertion in an operational orbit around Mars in terms of cost of the maneuver and characteristics of the trajectories involved, ensuring the compatibility of the maneuver with the transfer trajectory and resulting parking orbit, and considering a single maneuver?"*.

The research question can be split in the following sub-questions:

- What is the smallest ΔV achievable?

- What is the optimal pairing of transfer hyperbola conditions and target PO?

- What is the difference in ΔV between insertion in the target PO, and insertion in a preliminary PO, which is later modified (as defined by the EMC)?

- How robust are the resulting optimal insertion conditions? What is the sensitivity of the solution to a variation in the input conditions (the relative geometry between the transfer and parking orbits)?.

3

Overview of Methodology

This chapter will present the thesis problem in greater detail. First, all the information from the EMC documentation will be presented as it can be found in literature. After this overview, parameters, assumptions and constraints will be derived in order to replicate the insertion conditions for a mission to Mars as accurately as possible. Four mission scenarios will be presented, as well as their characteristics. Then, the insertion problem will be defined more accurately as well as the strategy selected to solve it.

3.1. Assumptions

This section contains the assumptions made in order to create the environment and acceleration model necessary for the mathematical description of the problem, which will follow in Chapter 4.

3.1.1. Two-body problem and resulting trajectories

The first assumption is describing the movement of the spacecraft as a two-body problem. Under the two-body problem, the movement of the spacecraft is due only to the gravitational influence of a single central body. Vice-versa, the influence of the spacecraft on the central body would be present, but is irrelevant due to the small mass of the spacecraft with respect to the chosen body (usually the Sun, a planet or a moon).

According to the two-body problem, the gravitational influence is approximated to its first-order term, also called the point-mass gravitational acceleration. The assumption is deemed sufficient by Merrill [15] in their study of EMC reorientation strategies, and all the previous studies cited both for Mars transfers and emergency maneuvers in Chapter 2. All other accelerations are assumed small with respect to the gravitational acceleration, and therefore negligible.

The validity of such approximation can be explained by examining the second-largest acceleration, after the point-mass gravitational acceleration. Terms such as any atmospheric effects when closer to Mars, solar radiation pressure or the gravitational influence of different bodies are never mentioned for preliminary studies that focus on maneuvers inside the SOI of Mars (such as the insertion maneuver). The only mentioning of a non-negligible acceleration is in the studies of Desai [5] and Landau [13], presented in Chapter 2 as the source of the repositioning strategies around Mars. In their papers, they both point out the impact of the J2 effect on the choice of the parking orbit for a mission. The J2 effect is a part of the gravitational spherical-harmonics approximation due to the three-dimensional distribution of the mass of Mars. However, Desai and Landau apply the J2 effect only as a perturbation of the two-body problem and exclusively to compute the change in Ω and ω of a long-stay parking orbit. The effect of precession is therefore negligible if the insertion maneuver is considered by itself instead of in a complete repositioning strategy, as there is no need to compute the long-term precession of the parking orbit.

Having considered the options above, the two-body approximation with no additional perturbations is therefore deemed sufficient to model the accelerations of the problem.

A two-body problem in astrodynamics results in so-called "Keplerian" trajectories, or trajectories that can be described via a conic section equation. More information on the subject can be found in

the literature study [22].

For the purpose of the problem, it is sufficient to say that the two-body problem considered is the one between Mars (as central body) and the spacecraft (the body we are describing the state of). At the beginning of the problem the spacecraft is on a transfer orbit, which (once entered into SOI of Mars) is a hyperbolic orbit with sufficient energy to escape the gravitational pull of the central planet. In order to achieve the mission objective, the spacecraft has to perform an insertion (see Subsection 3.1.2) in a parking orbit, which is a closed orbit around the central body. The Keplerian parking orbit is an elliptical orbit. The reference frames and coordinate systems used to describe the state of the spacecraft on such trajectories are introduced in Subsection 3.1.3.

3.1.2. Insertion maneuvers

"Insertion maneuver" is a term that indicates maneuvers that insert the spacecraft in a different orbit. In this study, we will use this terminology to refer to the specific insertion of the spacecraft in a closed orbit around Mars. The maneuver marks the shift between two separate phases of the mission: the transfer phase (between Earth and Mars) and the orbital phase (in which the spacecraft revolves around Mars).

A common assumption in preliminary studies, as first-order approximation, is that of an impulsive maneuver. Impulsive maneuvers happen instantaneously ($\Delta t = 0$) and only cause a change in velocity of the spacecraft ($\Delta \vec{v}$), without a change in position. The hypothesis is that, since the time necessary to maneuver is very small compared to the time spent on the previous and following trajectories, the whole maneuver is applied at the same time, in the same location in space.

Previous studies, such as those of Merrill on the repositioning strategy in Mars SOI [15] do not apply any restrictions concerning the direction of the change in velocity applied ($\Delta \vec{v}$), probably due to the preliminary nature of such studies, usually used as proof of concept and to obtain a preliminary propellant budget. With the intent of comparing results and strategies with those previous studies, the same assumption will be used for the problem at hand.

3.1.3. Reference frames and coordinates

The following reference frames will be used in the model description [25] :

- Heliocentric J2000
- Mars Equatorial
- Perifocal

The reference frame adopted for the heliocentric transfer is the J2000 heliocentric frame. It is an inertial reference frame with its origin at the Solar System Barycenter (SSB), a location very close to the center of the Sun and uses a set of fiducial objects as references. It is usually referred to as the "mean equinox of 2000 reference frame", as the reference for the X axis corresponds to the mean vernal equinox, and the reference plane is the mean equatorial plane (contains both the X and Y axes), both averaged at the beginning of the year 2000. The Z axis is in the direction of the celestial North Pole. This reference frame is used only to introduce the initial conditions of the problem related to the hyperbolic transfer orbit, once the spacecraft enters the SOI of Mars.

The reference frames adopted to describe the state of the spacecraft inside the SOI of Mars are two: an inertial, equatorial reference frame centered in the center of Mars, and the perifocal reference frame. The equatorial reference frame has the x-direction towards the vernal equinox and z-direction towards Mars rotational axis, pointed towards the North Pole. The reference frame is inertial, meaning that the reference directions do not shift according to the movement of the "current" Mars rotational axis, but stay fixed along its mean J200 direction (see the convention above for the J2000 frame). The same holds for the other directions.

The perifocal reference frame has its origin in the center of Mars, and the direction of the x-axis and y-axis are on the orbital plane of the spacecraft. The x-axis is the direction of pericenter, the y-axis is the direction of the semi-latus rectum and the z-axis is in the direction of the angular momentum vector of the orbit of the spacecraft.

To have a more clear description of all the quantities of the problem, all results will be expressed in the Mars Equatorial Reference Frame (MERF). The other two reference frames will only be mentioned to explain how to translate quantities into the MERF, in the description of the analytical model in Chapter 4.
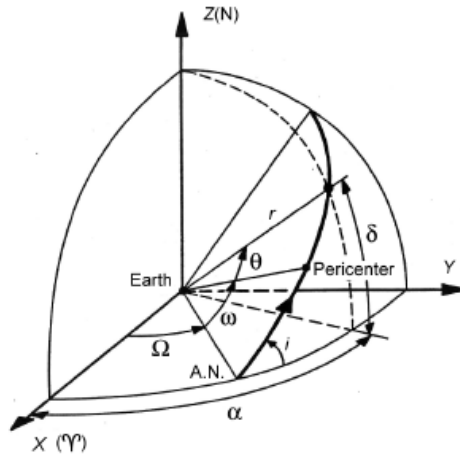
Figure 3.1: Position of a satellite around a central body, in an inertial body-centered reference frame. Definition of orbital elements
(i, Ω, ω, τ) and spherical coordinates (r, α, δ) [25].

Having defined these reference frames, the following coordinates are used to describe the state of the
spacecraft [25]:

- Rectangular coordinates [$x,y,z,\dot{x},\dot{y},\dot{z}$] : used to define the position and velocity vector ($\vec{r}$ and $\vec{v}$)
  and their 3D components, especially at the maneuver location.
- Spherical coordinates [$r, \alpha, \delta, V, \gamma, \psi$]: the right ascension α and declination δ are used to define
  the direction of the asymptotes of the hyperbola in a Mars-centric reference frame. Applied to this
  problem, those coordinates are necessary to approximate the incoming and outgoing direction
  of the position vector direction when modelling a spacecraft on hyperbolic trajectories at infinite
  distance from the target body (Mars, in this instance).
- Orbital elements [$a, e, i, \Omega, \omega, \theta$]: the so-called Keplerian elements are used to describe the trans-
  fer (hyperbolic) trajectory and the target parking orbit (elliptical) around Mars, to highlight their
  geometrical properties and any differences between the two in terms of size and orientation.

For a more in-depth description and definition of these coordinates, the author refers the reader to the
Literature Study prepared in advance of this thesis [22].

The formulas to move from one reference frame to the other, and to convert from one coordinate
system to another have not been cited in this report for the sake of brevity, but can be found in most
astrodynamics manuals (see: [25], [9], [26]). Transformations will be mentioned in Chapter 4 only
when crucial in the problem definition.

3.2. Mission scenarios

The mission scenarios, along with the assumptions, define a set of conditions necessary to move
from a most generic insertion maneuver (with no boundary conditions or environmental settings) to a
problem case with more realistic settings. This section will describe the specific scenarios chosen as
examples, in terms of defining the transfer hyperbolic orbits and elliptical orbits involved (the initial and
final conditions of the problem).

The transfer trajectories, between Earth and Mars, are usually divided in two big categories: with
or without a Deep Space Maneuver (see the NASA reference Handbook on Mission Opportunities [1]).
However, since the Deep Space Maneuver is supposed to be applied during the transfer, and far from
the SOI of Mars, from the point of view of the insertion maneuver both transfer types look the same.
There was no need to derive different case studies based on the two types of transfers.

As mentioned in Subsection 3.1.2, the insertion maneuver chosen is of one kind, the most open-ended
possible, to open up the search space to all the available options. The same insertion maneuver will
therefore be applied to all the cases.

In order to differentiate the case studies and answer the research questions, the choice fell to selecting
different elliptical orbit conditions after insertion.

The main reference papers on the EMC, by Percy [19] and Merril et al. [15], [21] were used to collect information on parking orbit characteristics around Mars. The EMC approach is to first insert the spacecraft in a highly elliptical orbit, advantageous for a low-cost insertion, to then perform additional repositioning maneuvers to achieve the parking orbit of interest for the scientific objectives of the mission (whether they are observation or landing), usually of lower eccentricity and different orientation.

As mentioned in Chapter 2, the idea of this study is to focus on the insertion maneuver, without further considerations on repositioning, applying an analytical method to compute the insertion conditions (rather than the numerical one used in previous studies).

Without performing a new study on parking orbit selection, it is therefore possible to highlight two kinds of elliptical orbits that can be the result of the insertion maneuver:

- Orbit A: arrival orbit, a highly elliptical parking orbit that is advantageous to achieve a low-cost orbit insertion. However, it would require additional follow-up maneuvers to position the spacecraft in a meaningful scientific orbit.
- Orbit P: scientific parking orbit, an orbit that already has the required characteristics (altitude of pericenter, inclination, orientation with respect to the Martian surface) to achieve the mission objectives. Usually, this is an orbit with lower eccentricity.

The mission scenarios will show how different problems result from the choice of a direct insertion or a repositioning strategy. In the first case, the propellant budget is optimized for the single insertion maneuver, but in the second case the scientific orbit is directly achieved, at the expense of a higher propellant budget, but with less risk (performing less maneuvers).

Another area of interest is the exploration of retrograde parking orbits. Qu [21] does not exclude the use of retrograde PO, except for flyby missions of the Martian moons, which are orbiting Mars in prograde orbits. To explore whether prograde or retrograde orbits are more advantageous, given a set of conditions on the hyperbolic arrival trajectory, case A will be divided in A1 and A2, which will consider the same arrival orbit (geometrically) but with opposite inclinations ($i_1 = 180 - i_2$).

When it comes to the parking orbits P, two kinds of missions are considered:

- P1: A landing mission, also mentioned as part of the EMC, which would require to target a specific landing area on Mars surface, and therefore a very strictly defined parking orbit.
- P2: A preliminary observation mission, which would have the option of exploring most of the surface of the planet as scientific requirement, and would generally require a polar, circular parking orbit.

The polar mission is not mentioned in the EMC frame, but has been included as to add another interesting case study, which could work for a non-crewed mission as well.

3.3. Parameters

The relevant fixed parameters, which are set as constant across multiple scenarios, are listed below:

- **Central body**

  As mentioned throughout the study, the central body is Mars. The key parameters derived from this choice are the gravitational parameter μ, the definition of the length of a mean solar day on Mars (1 sol) and the mean radius of Mars and the radius of Mars SOI, as in Table 3.1. The Martian day (sol) is used to quantify the size of a target elliptical orbit, based on its period, and will be mentioned in Section 5.6. The table contains the definition of 1 sol in mean solar days (d), which are defined in seconds.

Quantity	Value
μ	4.2828×10^4 km^3/s^2
1 sol	1.027490 d
1 d	86400 s
r_{MARS}	3389.5 km
$r_{MARS,SOI}$	0.57×10^6 km

Table 3.1: Definition of parameters related to the Martian environment [17], [25], [14].

- **Launch window**

  The EMC frame considers three missions, departing from Earth in 2037, 2041 and 2045. The values of the transfer hyperbolas selected by Qu [21] for their EMC study refer to those three missions. The values of velocity at infinite distance from Mars v_∞, right ascension α and declination δ of the hyperbolic asymptote are reported in Table 3.2. The ideal ΔV is for a tangential insertion at pericenter, in a 1-sol coplanar orbit around Mars with a pericenter altitude (h_p) of 250 km.

Launch Year	Mars Arrival	v_∞ [km/s]	α [deg]	δ [deg]	Ideal ΔV [km/s]
2037	8/2/2038	2.789	19.4	38.7	0.966
2041	7/27/2042	2.920	113.8	-1.7	1.033
2045	10/6/2046	3.334	162.9	-34.0	1.257

Table 3.2: Earth-Mars transfer conditions for EMC missions using chemical propulsion, as reported by Qu [21].

Instead of repeating the case studies (A1, A2, P1 and P2) for three different launch years, it has been decided to select a single window. The launch window selected is the one for 2041, as the corresponding mission in the EMC frame includes a landing portion (case P1 would then make the most sense considering that window), while the 2037 mission does only consider a Mars fly-by. The input values for the hyperbolic arrival used in the optimization problem will be derived from this assumption, the process will be explained in Chapter 5.

- **Elliptical orbits**

  The pericenter altitude of all elliptical orbits is assumed at h_p = 250 km.
  For A1 and A2, the period is set to 10 sol. For P1, the orbital period is set to 1 sol. Both cases are referencing the values used in the EMC. For P2, there is no previous reference; it has been chosen to fix the eccentricity of the orbit (e = 0.001), which along with the fixed pericenter altitude does define the shape of the orbit univocally.

3.4. Methods and simulation tools

The mission scenarios will be implemented using all the assumptions, parameters and constraints mentioned before. In addition to those elements, a final definition of the off-pericenter, non-tangential insertion and a model to obtain the problem solution are necessary.

First of all, the insertion maneuver problem is not simply about computing the ΔV of an insertion maneuver, given two fully-defined orbits, or it would be trivial (under the assumptions selected). The real issue comes from the fact that preliminary mission studies tend to define only partially both the hyperbolic arrival and the parking orbits around Mars, in order to leave the problem open for further refinement, once more data on the mission is available.

As mentioned before, a follow-up step is to make sure that the final stage of the hyperbolic arrival and the parking orbit do intersect, to make sure that the insertion maneuver is indeed feasible. Sometimes this assumption is simply "a given", or is approximated by assuming a forced pericenter insertion, and usually by fully defining the parking orbit, and then deriving the characteristics of an incoming hyperbolic trajectory. An example simplified algorithm for this maneuver is shown in Table 3.3.

However, there is not a clear method to match these resulting hyperbolas with the asymptotes of the hyperbolic transfer trajectory selected with a study on the transfer stage (for example, the values used by Qu and shown in Table 3.2).

Step	Action	Quantities defined
1	Define the elliptical parking orbit Keplerian elements, based on scientific requirements	a_e, e_e, i_e, Ω_e, ω_e
2	Assume pericenter insertion in the elliptical orbit	$\Theta_e = 0$
3	Assume pericenter insertion in the hyperbolic orbit	$r_{p,h} = r_{p,e} = a_e(1 - e_e)$, $\Theta_h = 0$
4	Assume coplanar insertion	$i_h = i_e$, $\Omega_h = \Omega_e$
5	Compute the semi-major axis of the hyperbola via the transfer orbit energy (see Equation 4.15)	a_h
6	At this point you have two fully-defined orbits, and at insertion point their velocities are aligned.	$\vec{v}_h, p \parallel \vec{v}_e, p$
7	Compute cost of pericenter insertion	ΔV

Table 3.3: Simple insertion algorithm, for a coplanar, pericenter insertion problem

Merrill [15] uses a numerical method that relies on a complete repositioning strategy and optimization to approximate consecutive orbits (for example the transfer hyperbola and the parking orbit) as intersecting. However, the strategy includes seven maneuvers (from insertion to escape towards Earth) in the Mars SOI, therefore going well beyond the scope of this study.

Merrill's numerical method cannot be applied to a problem that only considers the insertion maneuver by itself, even if we were to consider the first maneuver of the 7-step strategy (the insertion), separating it from the follow-up repositioning maneuvers. Doing this would only result in an underdetermined system (the unknowns would be more than the equations available to solve the problem). However, it would still be possible to derive a numerical method starting from Merrill's and adding further constraints to the problem.

Cornick [2] is the only available study to provide an analytical method with equations included to solve the problem at hand. The method description includes both how to compute the ΔV budget and at the same time ensure the intersection of the initial and final orbits, even when they do not have coinciding orbital planes.

The method by Cornick has been selected over the "simple" insertion and the numerical method for multiple reasons. First, its implementation was clearer and more easy to reproduce. Secondly, it still had the flexibility of being applicable to more than just a so-called perfect case, in which the orientation of the hyperbola were to match that of the target elliptical orbit. In addition to this, an analytical method allows to develop a tool that yields a clear and quick result for a given set of input values, which is an attractive quality both for the verification of the tool and for its application in preliminary studies.

The definition of Cornick's problem is: *"Given the conditions at infinity of an hyperbolic transfer, and given a completely defined elliptical orbit and a target insertion point on the elliptical orbit, define the required characteristics of the hyperbolic orbit in the MERF and the resulting ΔV budget of the insertion maneuver"*. The complete analytical description of the problem implementation is given in Chapter 4.

$$4$$
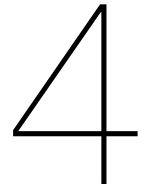
Model formulation

This chapter will introduce the model used for the insertion maneuver implementation. The selection of the model has been covered in Chapter 4. The original model formulation is taken from a study by Cornick [2] and has an analytical solution. The analytical method will be presented in its equations, as well as any additional simplified cases (for example a coplanar case) used for its verification.

The solution of Cornick's insertion problem is a full characterization of the arrival hyperbola and elliptical orbit, intersecting at the insertion maneuver location, as well as the resulting cost of the maneuver ΔV. The results obtained with this method will require optimization, in order to answer the research questions mentioned in Chapter 2. The optimization strategy will be introduced in Chapter 5.

4.1. Input and Output

This study intends to start from the elements that are used in the transfer studies, and those used in the studies of maneuvers inside the SOI of Mars, and find ways to optimize the insertion maneuver, that represents the common element between these two studies. The output of a transfer trajectory optimization study is:

- Transfer orbit specific orbital energy $\mathcal{E}$ or energy integral C_3
- Transfer orbit asymptote, defined as the right ascension (α) and declination (δ) of the hyperbolic asymptote. These values approximate the α and δ of the spacecraft position at infinite distance from Mars, on the transfer hyperbola.

The state of a spacecraft in the SOI of Mars is defined by six values (as explained in the literature study [22]), which means that the transfer hyperbolas, as defined by these studies, still have three "free parameters" which can be used to make sure their conditions are suitable for a transfer to the target parking orbit.

A parking orbit study usually starts from the mission objectives and technical constraints (like spacecraft size, propellant budget, costs and time constraints) dictated by an architecture frame (such as the EMC) in order to design suitable parking orbits to achieve such objectives. The output of the EMC parking orbit reorientation study is (as presented by Qu [21]):

- Definition of PO pericenter radius
- Definition of PO orbital period
- Definition of PO inclination
- Definition of stay time in the SOI of Mars (depending on the mission duration)
- Definition of additional re-orientation maneuvers

The latter two elements are not relevant for this study, obviously. The switch between architecture and parking orbit studies is usually an iterative procedure, to arrive to a feasible mix of technical design and mission design results.

Considering the results from transfer studies and PO studies, Table 4.1 presents the input and output quantities of Cornick's problem, as formulated in Chapter 3.

Symbol	Input	Symbol	Output
$C_{3,h}$	Energy Integral of hyperbola	ΔV	Insertion cost
α_h	Right ascension of hyperbola	a_h	Semi-major axis of hyperbola
δ_h	Declination of hyperbola	e_h	Eccentricity of hyperbola
a_e	Semi-major axis of ellipse	i_h	Inclination of hyperbola
e_e	Eccentricity of ellipse	Ω_h	RAAN of hyperbola
i_e	Inclination of ellipse	ω_h	Argument of pericenter of hyperbola
Ω_e	RAAN of ellipse	θ_h	True Anomaly of hyperbola
ω_e	Argument of pericenter of ellipse		
θ_e	True Anomaly of ellipse		

Table 4.1: Overview of the input and output quantities of Cornick's analytical method to solve the insertion maneuver problem to transfer from a hyperbolic to an elliptical orbit [2].

4.2. Cornick's analytical method

Cornick's analytical method is the most open-ended solution of the insertion problem, as there are no assumptions on the relative positioning of the transfer hyperbola and elliptical orbit. The following section will introduce the equations of the method, as well as some conclusions on its application to the insertion maneuver problem specifically.

4.3. Method description

In order to compute the cost of the insertion maneuver, one has to compute the orbital characteristics of the transfer hyperbola, the characteristics of the elliptical parking orbit of arrival and the position of the maneuver on both, since the maneuver is considered to be potentially off-pericenter.

We will call Orbit A the incoming hyperbola, and Orbit B the first parking orbit post-insertion (Figure 2.4). First, Orbit B will be characterized. Orbit B will have its Keplerian elements (semi-major axis, eccentricity, inclination, argument of periapsis, longitude of the ascending node, and true anomaly of the maneuver point) as already defined, according to Cornick's problem input list (Table 4.1). The idea is to define the radial position and velocity of the spacecraft at the maneuver point in the MERF. First, it is necessary to compute the node vector n (magnitude in Equation 4.1, direction towards the ascending node of the orbit as in Equation 4.2).

$$n_B = \frac{1 + e_B}{1 - e_B} \tag{4.1}$$

$$\hat{n}_B = [\Omega_B]_3 [i_B]_1 \hat{I} \tag{4.2}$$

$$\hat{I} = \begin{bmatrix} 1 \\ 0 \\ 0 \end{bmatrix} \tag{4.3}$$

The following notation has been used for the rotation matrices: a rotation matrix $[\theta]_j$ is a rotation of argument θ about axis j of a specified reference frame. Equations 4.4 to 4.6 show the three basic rotation matrices for a rotation of angle θ, and the three possible pedices.

$$[\theta]_1 = \begin{bmatrix} 1 & 0 & 0 \\ 0 & \cos\theta & -\sin\theta \\ 0 & \sin\theta & \cos\theta \end{bmatrix} \tag{4.4}$$

$$[\theta]_2 = \begin{bmatrix} \cos\theta & 0 & \sin\theta \\ 0 & 1 & 0 \\ -\sin\theta & 0 & \cos\theta \end{bmatrix} \tag{4.5}$$

$$[\theta]_3 = \begin{bmatrix} \cos\theta & -\sin\theta & 0 \\ \sin\theta & \cos\theta & 0 \\ 0 & 0 & 1 \end{bmatrix} \tag{4.6}$$

The rotation matrices $[\Omega_B]_3, [i_B]_3$ are rotation matrices to transform vectors from the orbital plane reference frame of Orbit B in the Mars-centric equatorial reference frame (frame XYZ in Figure 4.1). For more information about this transformation, see Wakker [25].
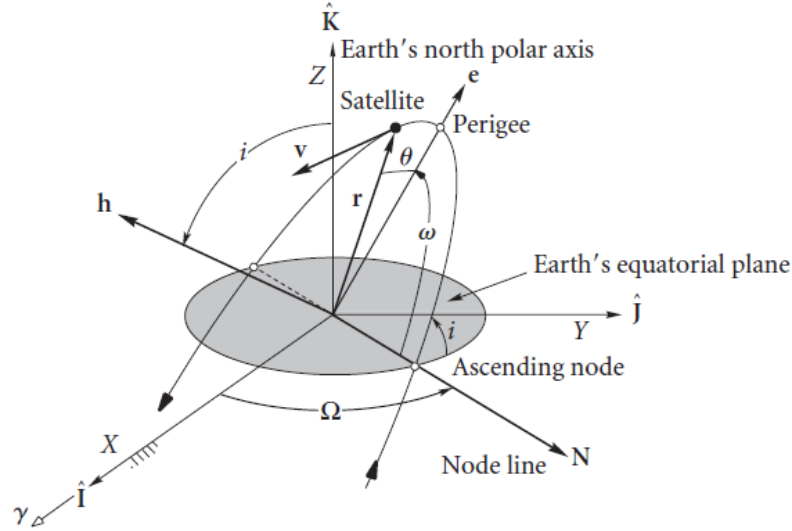
Figure 4.1: Earth geocentric frame (XYZ), same assumptions as the MERF used in the study (except for the central body), ascending node and node line N highlighted [3].

Knowing the true anomaly at capture, $\theta_{B,capt}$, it is possible to compute the angle ρ_B :

$$\rho_B = \theta_{B,capt} + \omega_B \tag{4.7}$$

The angle ρ_B is the angle measured from the ascending node to the position of the spacecraft, in the orbital plane. The position vector at capture, r_{capt} direction and magnitude are defined as follows:

$$r_{capt} = \frac{a_B\left(1 - e_B^2\right)}{1 + e_B \cos\theta_{capt}} \tag{4.8}$$

$$\hat{r}_{capt} = [\Omega_B]_3 [i_B]_1 [\rho_B]_3 \hat{I} \tag{4.9}$$

$$\vec{r}_{capt} = r_{capt}\hat{r}_{capt} \tag{4.10}$$

One can formulate the velocity vector in the Mars Equatorial Reference Frame (MERF), for a generic true anomaly of Orbit B, as in Equations 4.11 and 4.12, and then apply these equations to derive the velocity at capture, on the arrival orbit ($\vec{V}_{B,capt}$):

$$V_B = \sqrt{\frac{2\mu}{r_B} - \frac{\mu}{a_B}} \tag{4.11}$$

$$\hat{V}_B = [\Omega_B]_3 [i_B]_1 [\rho_B]_3 [\psi_B]_3 \hat{I} \tag{4.12}$$

Cornick, in the description of the method, uses an outdated definition of flight path angle, which will be referred here as the angle ψ, or the angle between the direction of the position vector and the velocity vector, positive in the direction of motion of the orbit, see Figure 4.2.
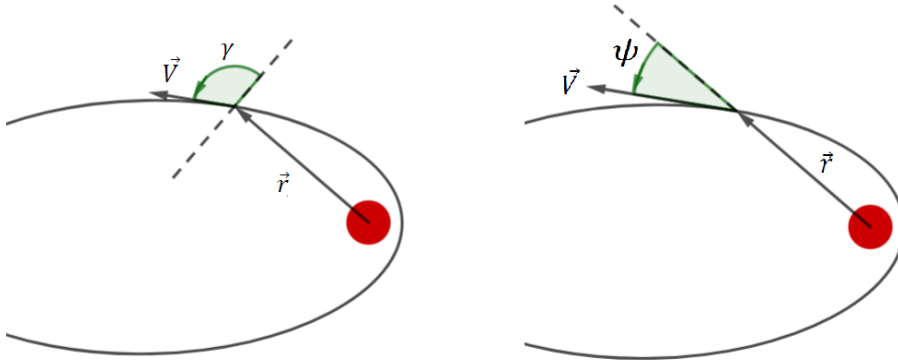
Figure 4.2: (Left) Elliptical orbit and flight path angle γ, as defined by Wakker [25]. (Right) Elliptical orbit and angle ψ as defined by Cornick [2].

This angle serves the same purpose as the flight path angle (γ) in determining the relationship between the direction of the velocity vector and the reference orbit, and can be computed from Equation 4.13.

$$\psi = \arcsin\left(\frac{\sqrt{\mu a_B \left(1 - e_B^2\right)}}{r V_B}\right) \tag{4.13}$$

with the condition:

- $0 \leq \psi \leq \frac{\pi}{2}$ if $0 \leq \theta \leq \pi$
- $\frac{\pi}{2} < \psi < \pi$ if $\pi < \theta < 2\pi$

After having computed the conditions on the first parking orbit (B), one has to compute the velocity on the incoming hyperbolic orbit (A), before the injection maneuver. The quantities necessary for that are the energy integral ($C_{3,A}$), right ascension (α_A) and declination (δ_A) of a position at the edge of the SOI of Mars, which will be an approximation of their values at infinite distance from Mars.

In the problem definition by Cornick [2], in the SOI of Mars, there are two hyperbolas that have the same hyperbolic asymptote direction: one where that direction is the direction of the outgoing asymptote, and one where that direction is the direction of the incoming hyperbolic asymptote. There are only two solutions to the problem because in addition to the conditions at infinity (which define the hyperbolic asymptote direction and the semi-major axis, as will be explained later), there are three conditions determined by the maneuver point (the three components of the $\vec{r}_{capt}$ vector defined in the elliptical problem above).

If one were to look at the two solution hyperbolas in space, without knowing the direction of motion of the spacecraft on such trajectories, the two would be identical since they have the same asymptote and have to go through the same point. However, since they have opposite direction of motion, they will have the same semi-major axis and eccentricity, but different inclination, right ascension of the ascending node and pericenter anomaly.

Before diving in the computation of the results, it is important to look at these two hyperbolas from a geometrical point of view, to derive insight in the expected results. Figures 4.3 and 4.4 show the main angles that will be used for the following analysis.

Three directions are used to define these angles: the direction of the reference hyperbolic asymptote ($\hat{S}$), the direction of the pericenter ($\vec{p}$) and the radial direction indicating the capture position ($\vec{r}_{capt}$).

The angle β is defined as the angle between $\vec{r}_{B,capt}$ and the reference hyperbolic asymptote direction $\hat{S}$. The angle θ is the true anomaly of the maneuver, measured from the pericenter of the hyperbola to the position vector. The angle θ_a is the true anomaly of the hyperbolic asymptote, or the angle between

the pericenter and the hyperbolic asymptote direction ($\hat{S}$). All angles are defined positive in the direction of motion of the hyperbola.

As mentioned before, there are two cases that differ on whether the insertion maneuver happens after pericenter (on the outgoing leg of the hyperbola, $\theta < 180$ deg as in Figure 4.3), or before pericenter (on the incoming leg of the hyperbola, $\theta > 180$ deg, as in Figure 4.4).
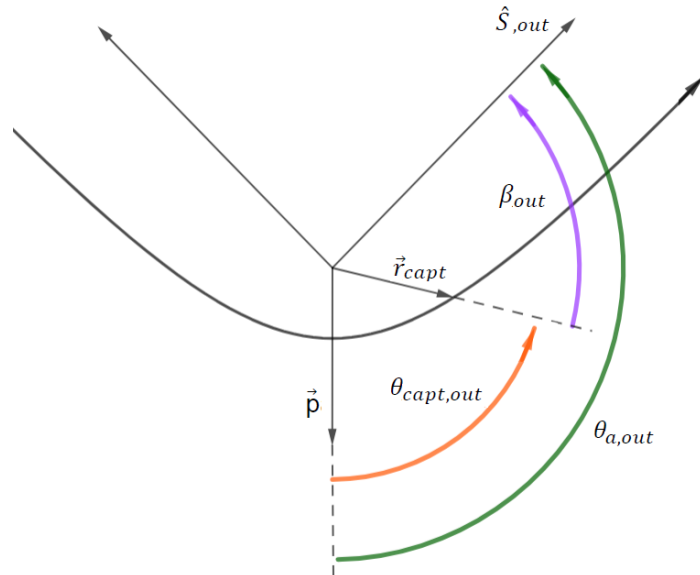
Figure 4.3: Transfer Hyperbola A, highlighted the conditions of an insertion on the outgoing branch. S/C on hyperbola moving in the anti-clockwise direction. $\hat{p}$ is the pericenter direction vector. Figure generated with GeoGebra.
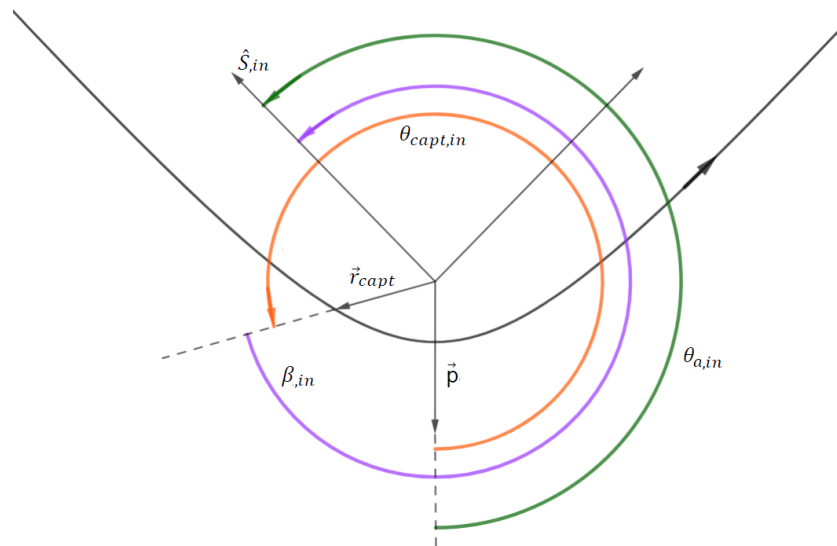
Figure 4.4: Transfer Hyperbola A, highlighted the conditions of an insertion on the incoming branch. S/C on hyperbola moving in the anti-clockwise direction. $\hat{p}$ is the pericenter direction vector. Figure generated with GeoGebra.

From Figures 4.3 and 4.4, the following characteristics can be deduced:

- Outgoing asymptote: $\beta < 180$ deg, $\theta_a < 180$ deg, $\theta < 180$ deg
- Incoming asymptote: $\beta > 180$ deg, $\theta_a > 180$ deg, $\theta > 180$ deg
- In both cases: $\theta_a = \beta + \theta$

- $\theta_{a,in} = -\theta_{a,out}$, $\beta_{in} = -\beta_{out}$, $\theta_{in} = -\theta_{out}$

The right ascension and declination are used to express the direction of the hyperbolic asymptote in the MERF with the following transformation:

$$\hat{S} = [\alpha_A]_3 [-\delta_A]_2 \hat{I} \tag{4.14}$$

The energy integral defines the semi-major axis of Orbit A:

$$a_A = -\frac{\mu}{C_{3,A}} \tag{4.15}$$

with $\mu = 42828 \ \frac{\text{km}^3}{\text{s}^2}$, which is Mars gravitational parameter (see Chapter 3).

To define the true anomaly of the capture on the hyperbola ($\theta_{A,capt}$), it is necessary to to define the orientation of the orbital plane of the hyperbola with respect to the MERF. To do so, first it is necessary to compute β_A (see Equation 4.16). Since the capture can happen on the incoming or outgoing leg of the hyperbola, two values of β_A are possible:

$$\beta_{A,out} = \arccos(\vec{r}_{capt} \cdot \hat{S})$$
$$\beta_{A,in} = 2\pi - \arccos(\vec{r}_{capt} \cdot \hat{S}) \tag{4.16}$$

The hyperbolic angular momentum direction can be defined as:

$$\hat{W} = \hat{r}_{capt} \times \hat{S}/sin(\beta_A) \tag{4.17}$$

In Equation 4.17, only one value of β_A is mentioned, but the study should be carried out for both, to evaluate the most advantageous position to maneuver in terms of ΔV_{capt}.

In order to do so, Cornick [2] provides two different equations to compute the true anomaly of the hyperbolic asymptote for the outgoing and incoming cases. However, only the outgoing case (Equation 4.19) produces results that are consistent with the geometric analysis. The results for the incoming leg will be derived from the ones of the outgoing leg, considering the geometric analysis explained before.

For the outgoing asymptote, the value of β allows to compute $\theta_{A,a}$, (the true anomaly of the hyperbolic asymptote) and $\theta_{A,capt}$ (the true anomaly at the capture location), using the parameter σ to simplify the notation:

$$\sigma = \frac{C_{3,A} r_{capt}}{2\mu} \tag{4.18}$$

$$\tan\left(\theta_{A,a,out}\right) = \sigma \sin \beta_{A,out} + \sqrt{(1 + \sigma)^2 - (1 - \sigma \cos \beta_{A,out})^2} \tag{4.19}$$

$$\theta_{A,capt,out} = \theta_{A,a,out} - \beta_{A,out} \tag{4.20}$$

For the incoming asymptote, as explained before:

$$\theta_{A,a,in} = -\theta_{A,a,out} \tag{4.21}$$

$$\theta_{A,capt,in} = \theta_{A,a,in} - \beta_{A,in} \tag{4.22}$$

Again, for ease of explanation, the following equations refer only to a generic hyperbola A, but should be applied both to the outgoing and the incoming cases separately.

The eccentricity of Orbit A can be computed using:

$$e_A = -\frac{1}{\cos \theta_{A,a}} \tag{4.23}$$

As a sanity check, it is also possible to verify the magnitude of the radial position at capture ($r_{B,capt}$) using the geometric parameters for the hyperbola, to make sure it coincides with the one computed for the elliptical parking orbit:

$$r_{A,capt} = r_{capt} = \frac{a_A \left(1 - e_A^2\right)}{1 + e_A \cos \theta_{A,capt}} \tag{4.24}$$

The hyperbolic velocity is composed of a magnitude and direction (Equation 4.25), the magnitude is computed with Equation 4.26:

$$\vec{V}_A = V_A \hat{V}_A \tag{4.25}$$

$$V_A = \sqrt{C_3 + \frac{2\mu}{r_{capt}}} \tag{4.26}$$

In order to compute the velocity vector direction via the unit vector $\hat{V}_A$, one has to use the angle ψ_A (defined in the same way as for the elliptical case), derived with the use of the hyperbolic angular momentum h_A:

$$h_A = \sqrt{a_A \mu \left(1 - e_A^2\right)} = \mu \sqrt{\frac{e_A^2 - 1}{C_3}} \tag{4.27}$$

$$\psi_A = \arcsin\left(\frac{h_A}{r_{capt} V_A}\right) \tag{4.28}$$

with:

- $0 \leq \psi_A \leq \frac{\pi}{2}$ for $0 \leq \theta_A \leq \pi$

- $\frac{\pi}{2} < \psi_A < \pi$ for $\pi < \theta_A < 2\pi$

from which follows the direction of the velocity vector on hyperbola A:

$$\hat{V}_A = \cos \psi_A \hat{r}_{capt} + \sin \psi_A \left(\hat{W}_A \times \hat{r}_{capt}\right) \tag{4.29}$$

Having defined the velocity vectors before and after the injection maneuver, it is possible to compute the cost of the maneuver as the difference between these vectors:

$$\Delta \vec{V}_1 = \vec{V}_B - \vec{V}_A \tag{4.30}$$

The same equations can be used in the escape scenario, with the only difference of considering the departure orbit as the elliptical orbit I, and the hyperbolic orbit J as the arrival, after the maneuver has been performed (referring to the EMC nomenclature for the bi-elliptic apotwist technique, presented in Chapter 2). However, the project will focus on insertion maneuvers only.

4.3.1. Cornick's problem and insertion conditions

Of the two hyperbolas that are the solutions of the problem, as defined by Cornick [2], one will be optimal in terms of cost (ΔV). However, looking at the problem of a spacecraft transferring from Earth to Mars, and knowing the conditions of one of the asymptotes (α, δ), related to the branch on which the maneuver will be operated, it is clear that only the incoming branch should be used for the Mars insertion problem, and only the outgoing branch should be used for the Mars escape problem, as the input of the problem (presented in Section 4.1) are the coordinates of only one asymptote. If both the asymptotes were known, there would be no freedom of defining the eccentricity and other Keplerian elements of the hyperbola around Mars.

In the computational tool developed in Python for the project (implementing the equations of Section 4.3), this case is selected automatically by verifying the direction of the incoming asymptote of the two solutions, and choosing the one with the correct direction. All the equations employed for this selection will be presented as part of the tests of Cornick's problem in Subsection 4.5.1.

4.3.2. Further analysis on insertion conditions

Insertion maneuvers can be located on either the incoming or outgoing branches of an hyperbola. After testing Cornick's problem for different conditions (part of these tests is presented in Subsection 4.5.1), it was clear that, depending on the input, two kinds of solutions were available.

1. Solutions in which the maneuver point was located on the same branch as the reference asymptote, as presented in Figures 4.3 and 4.4. The reference asymptote ($\hat{S}$) is the asymptote direction given in the input (via α and δ coordinates).
2. Solution in which the maneuver point was located on the opposite branch as the reference asymptote, as presented below in Figures 4.5 and 4.6.

Since the second type of solutions is still a product of Cornick's algorithm (as explained in Section 4.3), the solutions will be two hyperbolas with the same geometrical characteristics, but different orientations in space, such that the intersection with the elliptical parking orbit will be at the same radial distance, once before and once after the pericenter (due to the hyperbola symmetry).

However, this time the angles β and θ_A will not be defined referencing the same asymptote as the branch on which the maneuver is operated, but the opposite. Therefore, the "outgoing" case, identified by the subscript "out" in Section 4.3 will still have the outgoing asymptote as reference asymptote $\hat{S}_{out}$, but the solution will be a maneuver point with $\theta \in [180, 360]$ deg, thus identifying a maneuver on the incoming branch of the hyperbola. This example is presented in Figure 4.5.
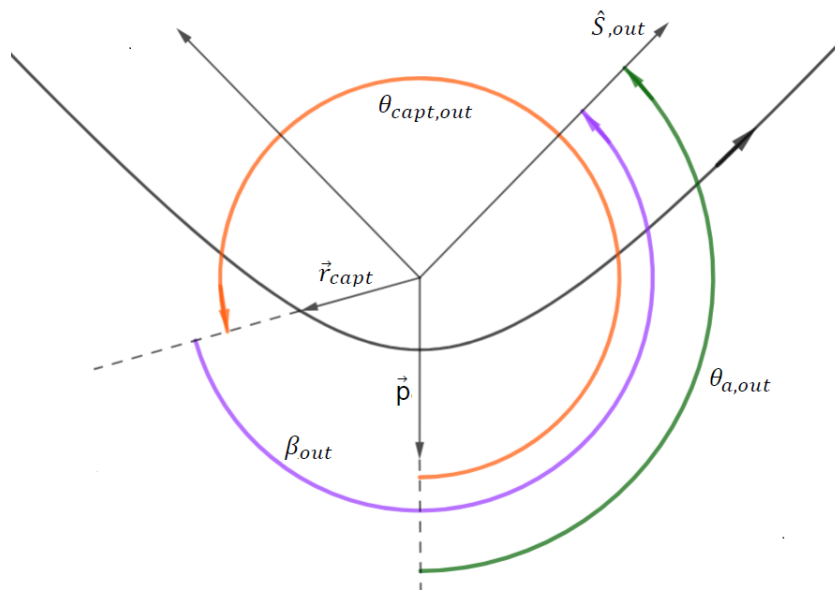
Figure 4.5: Example of the problem 2, outgoing asymptote used as a reference (therefore "out" subscript), solution on the incoming branch. S/C on hyperbola moving in the anti-clockwise direction. $\hat{p}$ is the pericenter direction vector. Figure generated with GeoGebra.

Then, the characteristics of the problem in Figure 4.5:

- Motion of the hyperbola: anti-clockwise (as displayed in the figure)
- Maneuver on the incoming branch, $\theta_{out} \in [180,360]$ deg.
- The outgoing asymptote $\hat{S}_{out}$ is the reference asymptote
- Reference asymptote true anomaly, $\theta_{a,out} < 180$ deg.
- The angle between radial position and reference asymptote is β_{out}
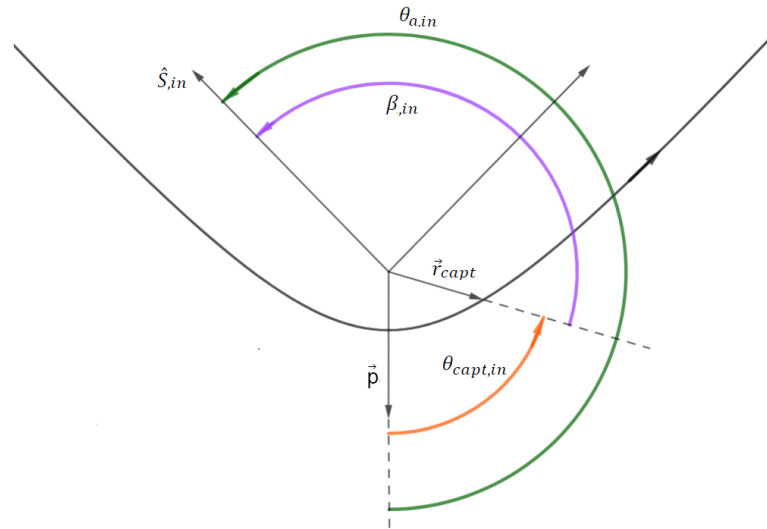
Figure 4.6: Example of the second type of Cornick's solutions. Incoming asymptote used as a reference (therefore "in" subscript), solution on the outgoing branch. Hyperbola moving in the anti-clockwise direction. $\hat{p}$ is the pericenter direction vector. Figure generated with GeoGebra.

The characteristics of the opposite case, in which the reference asymptote is the incoming one ($\hat{S}_{in}$) are presented in Figure 4.6, and are here summarized:

- Motion of the hyperbola: anti-clockwise (as displayed in the figure)
- Maneuver on the outgoing branch, $\theta_{in} \in [0, 180]$ deg.
- The incoming asymptote $\hat{S}_{in}$ is the reference asymptote
- Reference asymptote true anomaly, $\theta_{a,in} > 180$ deg.
- The angle between radial position and reference asymptote is β_{in}

As with problem 1, in Section 4.3, some considerations can be made after examining the figures:

- In both cases: $\theta_a = \beta + \theta$
- $\beta_{in} = - \beta_{out}$, $\theta_{a,in} = - \theta_{a,out}$, $\theta_{in} = - \theta_{out}$

These relationships are the same found in Section 4.3, another proof of how these solutions are indeed related to the same problem.

It is important to make two considerations. The first one is that the equations presented in Section 4.3 identify both solution 1 and solution 2, and therefore there is no way of foreseeing whether the result will be one or the other. Verification can only be made "a posteriori", and that is entirely due to the interplay of the position of the maneuver (defined by $\vec{r}_{capt}$), the hyperbola asymptote direction and its specific energy.

The second consideration comes from a natural follow-up question: is it possible to define an additional equation (different from Equation 4.19) to obtain two additional solutions, and therefore obtain four solutions out of Cornick's algorithm? The simple answer, as it stands, is no.

The reason is that the equation that Cornick suggests for deriving the true anomaly of the hyperbolic asymptote in the case of the incoming branch ($\theta_{A,a,in}$), as mentioned in Section 4.3, gives results that are not consistent for the case of the two identical hyperbolas.

Equation 4.31 consistently outputs values of θ_a outside of the interval [90, 270] deg, which is the standard definition of an hyperbola [25]. The conclusion is that either the values of β_{in} or σ were ill-defined in Cornick's paper, or simply that Equation 4.31 does not define angle $\theta_{a,in}$,in, but some other angle related to the reference directions used in Cornick's problem, different from the interpretation given above. However, it is yet to be understood what that equation (Equation 4.31) should be used for.

$$\tan\left(\theta_{a,in}\right) = -\sigma \sin \beta_{in} - \sqrt{(1+\sigma)^2 - (1 - \sigma \cos \beta_{in})^2} \qquad (4.31)$$

A way of solving a similar problem would be to use as a free parameter the eccentricity of the hyperbola, fixing for example the inclination and right ascension of the hyperbola, and compute for which eccentricity and pericenter anomaly values the resulting hyperbola (that has a defined incoming asymptote) would intersect the target elliptical parking orbit (in random points, as in this case the maneuver point would not be fixed beforehand), and which are the optimal results.

However, that would require to set up a completely different problem, while Cornick's solution does already provide a result. It has been therefore decided to only use the two solutions of the problem deriving from the application of Equation 4.19, and obtain two hyperbolas instead of four.

4.4. Tangential pericenter insertion

Tangential pericenter insertion maneuvers are a very special sub-group of the more generic insertion maneuvers. The maneuver can only be performed under very strict conditions:

- The two orbits are coplanar (identical i and Ω).
- The two orbits have a common orientation in the plane (identical ω).
- The two orbits have the same pericenter radius magnitude.
- As a result, both orbits share the same pericenter vector (same direction, same magnitude).
- As an additional result, the velocities at pericenter on the two orbits are aligned (have the same direction).
- The maneuver can only happen when at the intersection of the two orbits, and therefore can only be performed at pericenter (unless the two orbits have the same shape as well, but in that case the cost of the maneuver would be zero).

Given the characteristics of the maneuver, the pericenter radius will remain the same, while the apocenter radius will change, as well as the semi-major axis and the eccentricity of the orbit. The orientation of the orbit in space does not change (i, Ω, ω remain unchanged).

The cost of the maneuver is derived from Equation 4.32, which can be found in many astrodynamics textbooks such as Wakker's [25].

$$\Delta V = V_{f,p} - V_{i,p} = \sqrt{\frac{-\mu}{a_f} + \frac{2\mu}{r_p}} - \sqrt{\frac{-\mu}{a_i} + \frac{2\mu}{r_p}} \tag{4.32}$$

with:

- $V_{f,p}$ = velocity at pericenter, after maneuver [km/s]

- $V_{i,p}$ = velocity at pericenter, before the maneuver [km/s]

- a_f = semi-major axis of the final orbit [km]

- a_i = semi-major axis of the initial orbit [km]

- r_p = pericenter radius [km]

The eccentricity of the final orbit (e_f) can be found using:

$$e_f = 1 - \frac{r_p}{a_f} \tag{4.33}$$

4.5. Verification of tools

Verification is a step that demonstrates the correct functioning of a model or a tool. This chapter will contain the verification of Cornick's analytical method, and the proof that it indeed is able to make sure the resulting hyperbolic and elliptical orbit intersect, while at the same time being constrained by the input values selected.

4.5.1. Verification of Cornick's method

The first test was implemented to verify that Cornick's method is indeed able to provide, as a result, two trajectories intersecting at the desired maneuver location. The input values used in this example (renamed test T1), are presented in Table 4.2. The maneuver is off-pericenter (θ_e = 10 deg) to verify whether the algorithm can output the correct quantities in this generic case.

Quantity	Input T1
$C_{3,h}$ [km^2/s^2]	20.6
α_h [deg]	138.0
δ_h [deg]	5.9
$r_{p,e}$ [km]	4000
a_e [km]	20000
i_e [deg]	20
Ω_e [deg]	20
ω_e [deg]	50
θ_e [deg]	10

Table 4.2: Input values used for test 1 (T1), h = hyperbola, e = ellipse.

The results of case T1 are shown in Tables 4.3 and 4.4. In Table 4.3 the results for angles β, θ_a, θ show how the result is consistent with the mathematical description in Section 4.3. Since the "out" solution has a true anomaly $\in$ [0, 180], or on the outgoing branch of the hyperbola, this case falls under problem 1, which is the problem in which the position of the maneuver is on the same branch of the reference asymptote (see Figures 4.3 and 4.4 and Subsection 4.3.2).

Quantity	T1 "out" case	T1 "in" case
β_h [deg]	59.2	303.9
$\theta_{a,h}$ [deg]	115	244
θ_h [deg]	56.1	303.9
r_{capt} [km]	4027.2	
$\hat{r}_{capt}$ [km, km, km]	[0.192 0.94 0.30]	
$\vec{v}_e$ [km/s, km/s, km/s]	[-4.18 0.95 0.85]	
$\vec{v}_h$ [km/s, km/s, km/s]	[-4.02 4.97 0.95]	[4.02 -4.97 -0.95]
ΔV [km/s]	4.03	10.28

Table 4.3: Output values of test T1. Pedices h = hyperbola, e = ellipse. The definition of the "out" and "in" cases can be found in Section 4.3.

The results in Table 4.4 are consistent with the method equations: the semi-major axis and eccentricity of the two hyperbolas are the same, while the orientation is "opposite" (one is prograde, one retrograde), as it is also visible from the velocity vectors in Table 4.3, which have the same direction but opposite sign. The Keplerian elements of the elliptical orbit in Table 4.4 have been computed starting from the radial position and velocity of Table 4.3. The elements match those of the input in Table 4.2, and this reverse-engineering experiment is further proof that the result is reliable.

Quantity	Ellipse	Hyperbola "out"	Hyperbola "in"
a [km]	20000	-2079	-2079
e [-]	0.8000	2.3368	2.3368
i [deg]	20.0	17.5	162.44
Ω [deg]	20.0	-22.9	157.08
ω [deg]	50.0	44.7	135.26
θ[deg]	10.0	56.1	303.9

Table 4.4: Resulting trajectories for case T1. The definition of the "out" and "in" cases can be found in Section 4.3

One can apply the following equations to further verify the result, by checking that the asymptote of the hyperbola points in the direction used as an input (α, δ values in Table 4.2).

$$\theta_{\infty} = acos\left[\left(\frac{a - ae^2}{r_{\infty}} - 1\right)\frac{1}{e}\right] \tag{4.34}$$

The equation has two results, both $\theta_{\infty} \in [90,270]$; these results should be the same values of θ_A found in the problem. Knowing the true anomaly at infinite distance (as an approximation), one can compute the radial distance and velocity at infinity as vectors in the MERF; the following equations can be found to derive the direction of the reference asymptote starting from the position at infinite distance (on the outgoing branch for the "out" branch solution, and vice versa for the incoming one).

$$sin\alpha = \frac{r_{\infty,y}}{\sqrt{r_{\infty,x}^2 + r_{\infty,y}^2}} \tag{4.35}$$

$$cos\alpha = \frac{r_{\infty,x}}{\sqrt{r_{\infty,x}^2 + r_{\infty,y}^2}} \tag{4.36}$$

$$\alpha = atan2(sin\alpha, cos\alpha) \tag{4.37}$$

$$\delta = asin\left(\frac{r_{\infty,z}}{\sqrt{r_{\infty,x}^2 + r_{\infty,y}^2 + +r_{\infty,z}^2}}\right) \tag{4.38}$$

In problem 1, case A, both satisfy this condition.

Test T2 will cover an example belonging to problem 2, the problem mentioned in Subsection 4.3.2 and sketched in Figures 4.5 and 4.6. Test T2 will perform verification of the use of Cornick's equation, by applying a reverse engineering experiment. The idea is to start from the solution (the two hyperbolas and their characteristics) to then see if the equations suggested by Cornick are able to guess those solutions, even if the maneuver point is on the opposite branch with respect to the one given by the input asymptote (as per problem 2 definition).

In the next paragraph, the problem of starting from a completely defined hyperbola and finding a random ellipse that intersects it will be described. This problem is used only to generate the input of example T2. The idea is to replicate the example shown in Figure 4.5, but the same procedure is applicable to all the other combinations of true anomaly (of the insertion maneuver) and reference asymptote.

First, plausible values for the problem-specific angles of the hyperbola from Figure 4.5 are presented in Table 4.5. The orientation of the hyperbola is also fixed, and the numbers have been chosen with the only condition of not falling on the cases of a hyperbola with 0 deg inclination (special case for the definition of angles Ω and ω as explained in the Literature Study [22]).

Quantity	Hyperbola
θ_a [deg]	130
β [deg]	140
a [km]	-2300
i [deg]	10
Ω [deg]	20
ω [deg]	30
θ [deg]	350

Table 4.5: Reverse engineering problem to generate input of problem T2, definition of the transfer hyperbola, case based on Figure 4.6.

Then the eccentricity of the hyperbola and its C_3 value can be computed, using the inverse of the equations in Section 4.3.

$$e = -\frac{1}{cos(\theta_A)} = 1.5557 \tag{4.39}$$

$$C_3 = -\frac{\mu}{a} = 18.6\frac{km^2}{s^2} \tag{4.40}$$

Starting from those it is possible to derive the input conditions α, δ for the outgoing and incoming asymptotes, using Equations 4.34, 4.37 and 4.38, results are given in Table 4.6.

Quantity	Incoming asymptote	Outgoing asymptote
α [deg]	279.1	180.2
δ [deg]	3.4	-9.8

Table 4.6: Reverse engineering problem, generation of input for test T2, asymptote direction.

Using θ, it is possible to compute the radial position and velocity at capture on the hyperbola, and generate a random velocity for the same radial position for a parking ellipse (results in Table 4.7).

Quantity	Hyperbola	Ellipse
x [km]	990	990
y [km]	822	822
z [km]	76	76
v_x [km/s]	-6.6	2.5
v_y [km/s]	6.27	2.5
v_z [km/s]	1.43	4.7

Table 4.7: Reverse engineering problem to generate the input of test T2, maneuver point characteristics on the reference hyperbola and parking orbit ellipse.

From position and velocity, it is possible to compute the Keplerian elements of the arrival ellipse, results shown in Table 4.8. It is important to note that a value of 1346 km for the semi-major axis of the orbit would be impossible around Mars, which has a radius of 3389.5 km. However, for the purpose of this test and because of the point mass gravity field assumed in Chapter 3, this value will be considered acceptable.

Quantity	PO Ellipse
a [km]	1346.6
e [-]	0.6457
i [deg]	85.8
Ω [deg]	39.5
ω [deg]	-123.9
θ[deg]	127.3

Table 4.8: Reverse engineering problem to obtain the conditions for problem T2, definition of the elliptical parking orbit

The preparation for test T2 has finished, as a hyperbola and an ellipse intersecting at a specific maneuver point have been defined. Problem T2 has therefore the input values of Table 4.9. The problem uses the outgoing asymptote as an input (therefore the solution to be compared with the input hyperbola will be the "out" solution), while the maneuver point is on the incoming branch, (θ = 350 deg as in Table 4.5), following the example of Figure 4.5.

Quantity	Input test1
$C_{3,h}$ [km^2/s^2]	18.6
α_h [deg]	180.2
δ_h [deg]	-9.8
a_e [km]	1346.6
e_e [-]	0.6457
i_e [deg]	85.8
Ω_e [deg]	39.5
ω_e [deg]	-123.9
θ_e [deg]	127.3

Table 4.9: Input values used for problem T2, subscript h = hyperbola, e = ellipse.

The values of Table 4.9 have been used to generate the results in Table 4.10, which has two solutions, one referring to the outgoing asymtote ("out" solution), and one referring to the incoming asymptote ("in" solution). As expected, it is the "out" solution that replicates the input values for the hyperbola, both for the values of the characteristics angles for Cornick's problem (β, θ_a, θ), and for its Keplerian elements (in Table 4.11).

Quantity	T2 "in"	T2 "out"
β_h [deg]	139.9	220.1
$\theta_{a,h}$ [deg]	130.01	229
θ_h [deg]	350	10
r_{capt} [km]	1290.1	
$\hat{r}_{capt}$ [km, km, km]	[0.76 0.63 0.05]	
$\vec{v}_e$ [km/s, km/s, km/s]	[2.50 2.50 4.70]	
$\vec{v}_h$_vect[km/s, km/s, km/s]	[-6.59 6.28 1.43]	[6.59 -6.28 -1.43]
ΔV [km/s]	10.37	11.46

Table 4.10: Output values of test T2. Pedices h = hyperbola, e = ellipse. The definition of the "out" and "in" cases can be found in Section 4.3.

Quantity	Ellipse	Hyperbola "in"	Hyperbola "out"
a [km]	1346.6	-2300	-2300
e [-]	0.6457	1.5551	1.5551
i [deg]	85.85	10.0	170.0
Ω [deg]	39.5	20.0	200.0
ω [deg]	-123.9	30.0	150.1
θ[deg]	127.3	350.0	10.0

Table 4.11: Resulting trajectories for case T2. The definition of the "out" and "in" cases can be found in Section 4.3.

From these results, it is clear that the problem has correctly identified the hyperbola that intersects the elliptical parking orbit on the incoming branch (the one used as a reference to generate the prob-

lem inputs, and in Figure 4.5), even though the reference asymptote used as input was the outgoing asymptote. As for the second solution, the hyperbola that has a solution on the outgoing branch (see Table 4.11) has an incoming asymptote that points in the input direction (the direction at infinity matches the coordinates given as input at the beginning of the problem). With this reverse-engineering problem it is possible to see that Cornick's problem is able to compute accurately the solution of the insertion maneuver problem, when it comes to correctly identifying the two trajectories (hyperbolic and elliptical orbits).

It is possible to repeat the problem, using as input the values of the incoming asymptote (α, δ of Table 4.6). The results would be the same two hyperbolas, but this time the solution will be on the same side of the reference asymptote (in this case, using the incoming asymptote results in the "in" solution that has the same characteristics of the input, instead of the "out" solution).

After the verification effort, it is possible to consider Cornick's problem (and its implementation in Python for the purpose of the thesis project) fit for the application in the next chapters.

5

Optimization

After having defined the problem and the mathematical model to describe it, it is necessary to introduce the optimization strategy selected for this study. Starting from the results of the literature study and previous chapters, all the elements of the optimization will be defined for the problem of the insertion maneuver in the Mars SOI, with a special focus to the specific conditions of a mission of the EMC frame.

5.1. Analysis of the problem

As mentioned in Chapter 4, this study wants to address the gap between transfer studies and studies focused on orbit repositioning or orbit selection for scientific purposes. The optimization problem stems from the need to not only ensure the continuity between the conditions on the transfer hyperbola and the target elliptical orbit (which has been addressed by adopting Cornick's method) but also look into which are the optimal outcomes for an insertion maneuver, or what is the best possible maneuver that can be achieved under certain conditions.

It is therefore useful to remind the reader of the parameters that mission designers provide as an output of preliminary studies on transfer and parking orbits, as discussed in Section 4.1. These parameters are key quantities in the insertion problem, a fact that has to be considered before choosing the problem variables and constraints of the optimization in the following sections.

Symbol	Hyperbola characteristics	Symbol	Ellipse characteristics
α_h	Right ascension of hyperbola	$r_{p,e}$	Pericenter radius
δ_h	Declination of hyperbola	T_e	Orbital period
$C_{3,h}$	Energy Integral of hyperbola	i_e	Inclination

Table 5.1: Overview of the result from transfer studies (impacting the hyperbola characteristics) and the parking orbit studies (impacting the arrival ellipse characteristics), which inform the insertion problem definition.

5.2. Variables

Optimization variables are the quantities that are varied in order to find the combination that yields the optimal result. Starting from all the input variables necessary for the model (in Section 4.1), those have been restricted to select a number of variables for the optimization problem, highlighted among the other input quantities in Table 5.2. The remaining input quantities will be mentioned in Section 5.4, as part of the equality constraints, also referred to as the fixed parameters of the problem.

Symbol	INPUT
α_h	**Right ascension of hyperbola**
δ_h	**Declination of hyperbola**
$C_{3,h}$	**Energy Integral of hyperbola**
a_e	Semi-major axis of ellipse
e_e	Eccentricity of ellipse
i_e	**Inclination of ellipse**
Ω_e	**RAAN of ellipse**
ω_e	**Anomaly of Pericenter of ellipse**
θ_e	**True Anomaly of ellipse**

Table 5.2: Input quantities for Cornick's analytical method, highlighted in bold the selected optimization variables (Orbit inclination variable only in A1 and A2 cases) [2]

The chosen optimization variables are:

- **Hyperbola asymptote conditions (α, δ):** the idea is to test multiple available options instead only the one considered optimal on the transfer trajectory side. The objective of the study is to not only achieve a result on the optimal insertion maneuver for a single mission (like the EMC campaign) but to also gain further insight into how the conditions of the arrival hyperbola itself can influence the propellant budget of an insertion maneuver.
- **Hyperbola energy integral C_3:** the hyperbola energy integral, together with the asymptote angles, defines the Earth-Mars transfer when outside of the SOI of Mars. The reasoning for choosing a range of values instead of a specific one is similar to the reasoning for the quantities above.
- **Parking orbit inclination i:** will be used as a variable only in the case studies concerning arrival elliptical orbits (A1 and A2, presented in Section 3.2), as there is not a specific orientation to be targeted by the insertion (it will be changed as part of the repositioning strategy).
- **RAAN Ω and anomaly of pericenter ω of the elliptical PO**: part of the orientation of the PO is left as a free variable, as it plays a slightly less important role than the inclination of the orbit. The orientation plays a role in some missions (for example, reaching a specific spot on the surface of the planet), but can generally be adjusted with less expensive maneuvers than inclination changes.
- **True anomaly θ of the maneuver point on the elliptical PO**: to allow the maneuver to be located off-pericenter. The idea is to identify the best spot for the maneuver, which may not be pericenter as the hyperbola may intersect the PO at any point, and not have the same orientation of the PO (to investigate further the results by Desai mentioned in Chapter 2).

The chosen variables and ranges on which to perform the optimization will be presented in Section 5.6, as to constrain the optimization and perform a more focused study, which should yield clearer results on the research questions.

5.3. Objectives

The objective of an optimization is the quantity that is intended to be minimized or maximized (depending on the problem definition) via the process. This quantity is therefore the main metric used to evaluate the result of each step of the optimization, and derive information on how the algorithm should proceed to converge. A discussion of the chosen convergence criteria will follow in Section 5.5.

The optimization will be a single-objective optimization, with the propellant budget (ΔV) as objective. Considering the insertion maneuver alone, this is the main metric to be minimized, as can be seen in similar studies on the topic such as Merrill [15], and Landau [13], in their studies on the insertion and repositioning strategy in the SOI of Mars.

Other metrics, such as the time-of-flight are not as critical if the insertion maneuver is considered alone, instead of as part of the complete mission profile. The accuracy of the maneuver (whether it is able to target the desired PO or not) could be better examined in a sensitivity study than as part of the first global optimization, as it is customary to first derive information on the problem as a whole, before examining specific cases in detail.

5.4. Constraints

Constraints are necessary to make sure that the results of the optimization are realistic and feasible in the context of the EMC frame.

The equality constraints, or fixed quantities used as inputs for the problem are:

- **Orbital period of the elliptical orbit (T_e)**: from this information it is possible to compute the semi-major axis of the elliptical orbit using the third of Kepler's laws [25] as in Equation 5.1

$$a_e = \left(\frac{\mu T_e^2}{4\pi^2} \right)^{\frac{1}{3}}$$

(5.1)

- **Radius of pericenter of the elliptical orbit ($r_{p,e}$)**: from this value it is possible to compute the eccentricity of the elliptical orbit using Equation 4.33.

- **Elliptical orbit inclination (i_e)**: will be used for the parking orbit scenarios (P1 and P2), as the parking orbit selected is tied to the mission objectives, and has therefore a specific inclination required, as explained in Section 3.2.

The quantities that are fixed for the problem, with the special case of the PO inclination, are presented in Table 5.3, while numerical values of these constraints are mentioned in Section 5.6.

Symbol	INPUT
α_h	Right ascension of hyperbola
δ_h	Declination of hyperbola
$C_{3,h}$	Energy Integral of hyperbola
a_e	**Semi-major axis of ellipse**
e_e	**Eccentricity of ellipse**
i_e	**Inclination of ellipse**
Ω_e	RAAN of ellipse
ω_e	Anomaly of Pericenter of ellipse
θ_e	True Anomaly of ellipse

Table 5.3: Input quantities for Cornick's analytical method, highlighted in bold the equality constraints introduced (Orbit inclination only for P1 and P2 cases) [2].

The output of the algorithm implementation is a full characterization of the incoming hyperbola and parking orbit ellipse (via Keplerian elements), as well as the state of the spacecraft at the maneuver point and the ΔV of the insertion maneuver (the objective of the optimization). One can rank the solutions based only on the results of the objective. On the other hand, one can use fitness functions, a combination of objective function and penalization functions, which are the product of a fitness factor and the constraint parameter, computed as in Equation 5.2 (see [22] for more information on that).

$$F = O + \sum_{i=1}^{N} C_i f_i$$

(5.2)

F = fitness function
O = objective function
N = number of constraints
C = constrained parameter
f = fitness factor

Fitness functions are a valid option when there is a single-objective optimization, but there is at the same time the need for the solution to respect some additional requirements or to avoid infeasible solutions (under aspects that are not directly tied with the minimization of the objective).

In our problem case, the following constraints have been identified, which could be added as part of the fitness function:

- Maximum ΔV, based on the propellant budget, which according to Merrill [15] should be between 1.7 -2.5 km/s for the combined arrival and departure ΔV, which makes the expected ΔV of an optimal insertion between 0.8-1.25 km/s approximately [15]. It could be possible to penalize higher ΔV solutions.

- Penalization for true anomaly of the maneuver point (on the hyperbola side) that are "far" from the pericenter: first, because a solution that is far from pericenter is automatically also far from Mars. In addition to this, in case of emergencies and if the insertion was operated on the outgoing branch of the hyperbola, it would be more difficult to recover as the spacecraft travels farther away from the target PO.

- Penalization for a large change in orbit inclination between hyperbola and ellipse, as changes in inclination are usually the most expensive maneuver category in terms of propellant.

It is clear how all of these constraints are related to the propellant budget of the insertion maneuver, which is already minimized by the objective function alone. It is possible to assume that at the end of the optimization, the constraints will be met or at least be redundant. That is the reason why the tuning of the optimizer has been performed using the objective (minimize ΔV) without implementing the use of a more complex fitness function (the use of penalties related to additional constraints).

However, during the optimization it was ensured that some solutions were to be rejected due to the properties that made them infeasible. The reasoning can be traced back to geometrical considerations or to simple practical limitations:

- Only values of θ_A that were in the [90, 270] interval were accepted, otherwise it would not have been an hyperbola. The constraint was implemented directly in the formulation of Cornick's problem in Chapter 4.

- Only solutions that reference the incoming asymptote for insertion maneuvers are selected, also explained in Chapter 4.

- The radius of pericenter of the hyperbola must be higher than the radius of Mars(r_{MARS} = 3389 km, [14]), with an additional safety altitude (h = 100 km), in order to avoid impact with the planet (in case of failed insertion maneuver or post-pericenter maneuver). However, this constraint was never active in the whole optimization process, due to the choice of appropriate ranges for the input variables in Section 5.6.

As explained, such constraints were either embedded in the formulation of the analytical method, or were never active in the optimization and therefore had no influence on the result.

5.5. Stopping criteria

The convergence criteria is a limit imposed on the optimization problem once the result is deemed "good enough" to satisfy some accuracy and stability requirements. Adding a convergence criteria is necessary for optimization problems, as most of them are based on iterative processes that would otherwise continue to try to improve on a solution way beyond a realistic result for a preliminary study. Another strategy is to demand a fixed maximum number of iterations of the algorithm, however this method would not ensure convergence at each optimization run. Another problem to avoid is premature convergence, which means that the optimizer has converged to a local optimum. A proper set of convergence criteria should check that the optimum should not change significantly over several successive iterations of the optimization algorithm, to reduce the possibilities of identifying a local optimum instead of the intended global optimum.

The convergence and stability requirements suggested for the optimization problem are:

- **The result of the optimization should be accurate to up to 0.01 m/s.**
  The study is a preliminary study, based on an analytical model and the two-body problem. Similar studies mentioned before report their ΔV budget with an accuracy of 1 m/s [15], [21]. In order to

grant the same accuracy for the final result, the numerical model (which the optimization is part of) should yield an even more accurate result. In this case, we have chosen to achieve a result that is stable up to 0.01 m/s on the optimization objective. The idea is to compare the results of the current optimization output with those of previous iterations, and verify that the change in result is less than 0.01 m/s; when this condition is achieved, the process can stop.

- **The convergence will be evaluated on the total population.**
  Usually, the accuracy mentioned above is evaluated by comparing the current best solution (best individual in the population) with the best solution of a previous iteration. However, global optimizers do have a large exploratory phase, in which they keep generating new solutions in order to explore the largest number of solutions possible, so as to exclude premature convergence. The idea for this criteria is to evaluate the average of the solutions; once that has converged (according to the criteria above) it means that all the individuals in the final population have converged to the same solution (considering the required accuracy) and therefore the optimization algorithm has ended its "exploratory phase", and therefore the optimization can be considered finished.

- **The algorithm should at least examine 2000 different scenarios.**
  The smallest number of different scenarios (i.e. combination of input values) that have to be examined is added as a criterion to avoid premature convergence. The number chosen is based on the number of scenarios considered by Merril [15] as initial guesses, though it must be pointed out that their paper employs a very different model and optimization strategy. It is a ballpark figure, but it ensures that the optimizer does not stop prematurely. It means that the accuracy criterion is activated only after 2000 different scenarios have been examined by the algorithm. The number of scenarios can be computed by multiplying the population size by the number of generations of the optimization. For a definition of such quantities, refer to Section 5.8.

- **The result should be stable for at least 50 iterations.**
  The condition refers to the accuracy criterion; the average of the current population is compared with the accuracy of a population that is 50 generations in the past. That is to ensure the robustness of the result, and make sure that the optimizer algorithm is not coming up with radically different solutions in the final population.

The list above can be converted in the following convergence criteria:

$$\text{If } k > 2000 \text{ and } \Delta\bar{V}_i - \Delta\bar{V}_{(i-50)} < 0.01 \text{ m/s} : \rightarrow \text{stop optimization}$$

k = cumulative number of scenarios used for the whole optimization
$\Delta\bar{V}$ = average cost of the insertion over the results of the whole population
i = number of iterations of the process

On the other hand, convergence does not mean automatically that the algorithm has found the global optimum of the problem, as complex problem usually have multiple local optima. In order to avoid local optima, and investigate more options, the use of different randomizer seeds for the sampling of the input values is adopted. By starting with different populations, the idea is to achieve a more consistent result, which should provide a better assessment of whether or not the global optimum has been identified correctly. The seeds chosen will be reported to allow these experiments to be replicated.

5.6. Design Space Exploration

The Design Space Exploration (DSE) is the phase of the study in which the input variables are reviewed to determine meaningful ranges for their optimization. It is possible to apply the largest range possible for all the variables (for example as done by Nervo [17]) but it is not recommended, as the Design Space of a real space mission does have some limitations. In addition to this, it is helpful to identify regions of such space in which the optimum is more likely to be located, to expedite the optimization process.

5.6.1. Free parameters ranges

First, the free variables ranges will be established by looking at studies of the EMC frame and Mars missions, to derive insight in what is feasible for a crewed Martian mission.

The values of the transfer hyperbolas selected by Qu [21] for their EMC study refer to three mission windows in the years 2037, 2041 and 2045, and have been presented in Section 3.3, Table 3.2. However, Qu reports the transfer hyperbola values for a single mission scenario instead of ranges.

Merrill's study on the EMC parking orbit reorientation [15] constrains the arrival declination δ of the hyperbolas between -33 and 38 degrees. It also mentions a range of v_∞ values between 2.6 and 4.8 km/s for chemical propulsion missions.

More values for transfer trajectories between Earth and Mars can be found in the NASA Interplanetary Mission Handbook, for missions between 2026 and 2045 [1]. Two transfer types are considered in this study, type I (characterized by shorter trip times but higher cost of the injection maneuver towards Mars) and type II (characterized by longer trip times but lower cost of the injection maneuver). In addition to this, both ballistic trajectories (defined as direct-to-Mars transfers, with no maneuvers in between launch and insertion in the Mars orbit) and DSM trajectories, characterized by the use of one or more DSMs during the transfer.

Contour plots for the optimization of such transfers are reported in the Handbook, as well as tables with optimal v_∞, RA α and declination δ of the hyperbolic asymptote. However, it is important to note that those refer to the launch hyperbola, and do vary if DSMs are applied. Since it is not clear from the tables whether the optimal solutions reported employ DSMs or not, it is assumed that they do not.

It is also important to note that the assumptions of the EMC study consider a launch from a lunar-distance orbit, while the NASA Handbook considers transfers from a 407 km circular parking orbit around Earth. The conclusion is that optimal launch conditions could vary between the two environments, therefore it has been decided to consider ranges for the hyperbola conditions at infinite distance from Mars as a guideline, rather than a definitive source.

Both from the tables and the contour plots referring to the ballistic trajectories, as well as the results of EMC papers mentioned before, the resulting ranges of input data chosen for each mission window are presented in Table 5.4.

Launch Year	Mars Arrival	v_∞ [km/s]	α [deg]	δ [deg]
2037	2037-2038	2.0 - 3.5	20 - 60	0 - 40
2041	2042	2.3 - 4.2	90 - 130	10 - 40
2045	2046	3.0 - 5.6	160 - 230	-35 - +25

Table 5.4: Selected Earth-Mars transfer input conditions (ranges) for chemical propulsion, missions between 2037 and 2045.

As mentioned before, the 2041 mission window has been selected, but the other ranges are reported for future developments or validation of the method.

The insertion maneuver targets an elliptical orbit. Many studies have been performed on how to select specific elliptical orbits in order to perform flyby missions of the Martian moons, or observe a specific side of the planet, or even land on its surface.

In preliminary studies, often only one parking orbit is considered, similarly to what is mentioned in lunar missions, without the need of repositioning (as explained in Chapter 2). However, the EMC differs in that multiple orbits around Mars are employed in a "repositioning strategy" to rendez-vous with additional modules, allow for the crew to transfer and achieve an overall lower propellant budget.

Two main orbits are mentioned by Merrill in their study on the EMC on parking orbit reorientation:

- **1-sol parking orbit**, defined as the target parking orbit for the scientific objectives of the mission, with pericenter altitude (h_p) of 250 km, which is going to be considered for the mission scenario P1.

- **10-sol parking orbit**, defined as the arrival and departure parking orbit, chosen because it would be less expensive to later on perform a plane change at apoapsis at a larger distance, which is going to be considered for the mission scenarios A1 and A2.

Additional constraints on the parking orbits are based on the following considerations:

- Parking orbit P2 is a parking orbit for an observation mission; therefore, a circular or near-circular orbit is recommended (e ≈ 0) to stay close to the planet for the full orbit, as well as a polar orbit to make sure to cover most of its surface (at different latitudes). Polar orbits have ≈ 90 deg inclination.
- Parking orbit P1 is the target orbit for a landing mission. According to Merril's study [15], the parking orbit inclination and periapsis argument are both constrained by the landing location and latitude. For a mission targeting the Jezero Crater as landing spot, for the 2041 EMC mission, Merril suggests a 18.8 deg inclination (i) and a periapsis argument (ω) of 86 deg.
- The optimal arrival parking orbits can be both prograde (A1) and retrograde (A2), according to Qu [21]; all the other parameters are the same for these two cases, in order to compare whether prograde or retrograde orbits are more advantegeous for the insertion problem defined.
- Retrograde parking orbits (inclination larger than 90 deg) should be avoided for missions that want to target Phobos or Deimos (transferring the crew to a separate taxi vehicle), as the ΔV budget of the taxi vehicle is clearly penalized in those cases, according to Qu [21].
- A range for the true anomaly values on the elliptical orbit (θ_e) is suggested in order not to drift too much away from a pericenter insertion (considered often the optimal insertion point). This will only be applied to the elliptical orbits (A1, A2, P1) and not to the circular PO of case P2. The recommended range is between -20 and +20 deg.

The parking orbit parameters that will be used in the optimization are summarized in Table 5.5.

Orbit Name	A1 Prograde	A2 Retrograde	P1 Landing	P2 Polar
h_p [km]	250	250	250	250
T [sol]	10	10	1	0.075
a [km]	94911	94911	20448	3643
e [-]	0.9616	0.9616	0.8220	0.001
i [deg]	14 - 24	157 - 167	18.8	88
Ω [deg]	0 - 360	0 - 360	0 - 360	0 - 360
ω [deg]	0 - 360	0 - 360	70 - 90	0 - 360
θ [deg]	-20 - +20	-20 - +20	-20 - +20	0 - 360

Table 5.5: Preliminary free parameters selected for elliptical orbits around Mars, insertion problem optimization. The true anomaly is the true anomaly of the insertion maneuver.

The idea is to explore four different cases, corresponding to each mission (A1, A2, P1, P2) each paired with the hyperbolic transfer for the 2041 mission. After having completed this preliminary selection of the free variables ranges, a Monte Carlo analysis was performed in order to better understand the effect of the input variables on the objective value and possibly further restrict the search space.

5.6.2. Monte Carlo analysis

The Monte Carlo analysis was made for 1000 samples, with the all-at-once method, meaning that all the input variables were sampled at the same time, and varying for each individual case analyzed. The summary of the settings used in the Monte Carlo analysis is presented in Table 5.6. The computations are repeated for three seed numbers, but unless stated the discussion below will refer to one case (seed 1728) and the conclusions that have been made can be applicable to the other seeds as well (all the results are included in Appendix A).

Sobol sampling has been chosen, with a higher number of generated individuals (1048576) with respect to the number of samples, because the number of samples (1000) was not a power of 2. As explained in the scipy implementation of the method (see [23]), it is therefore necessary to employ a higher number of samples. A Sobol sequence that is not scrambled will always be characterized by exactly the same numbers, regardless of the seed choice. That is why the scrambling has been added as a setting, as well as a much higher number of generated individuals (with respect to the sample size N) from which the parameters can be selected from (after scrambling it), to increase diversity in the results across different seeds.

DSE method	N = Number of samples	Core random generator algorithm	Seeds used
Monte Carlo all at once	1000	Sobol sequences, dimensionality = 7	1728, 2358, 3682

Table 5.6: Settings for the Monte Carlo analysis used in the DSE for the insertion problem, with scrambling and a total generation of 1048576 individuals, of which only the first N were used.

Case A1 has been chosen for the MC analysis, as it has the additional free parameter of the inclination of the orbit (P1 and P2 only have six free variables instead).

The results of the MC sampling for the hyperbolic transfer quantities (α, δ and C_3) are shown in Figure 5.1. First, it is clear how for the entire range of α values it is possible to find a variety of results, as the minima do not seem to be located in one specific sector. On the other hand, for values of δ greater than 30 deg the cost of the maneuver is clearly higher, as there are no results under 2 km/s. This could have to do with the inclination range selected for the elliptical orbit, as the same is verified for the two other seeds. The decision is to therefore reduce the range for the declination of the hyperbolic asymptote. The same stands for the value of the orbital energy C_3; it would make sense that, as hyperbolas have a higher energetic content than ellipses, in order to reduce the cost of an insertion maneuver it is more advantegeous to adopt a lower-energy hyperbola, and the trend is reflected in the Monte Carlo results. It is therefore decided to leave the lower bound of energy content for the hyperbola, and modify the upper bound to 12 km^2/s^2.
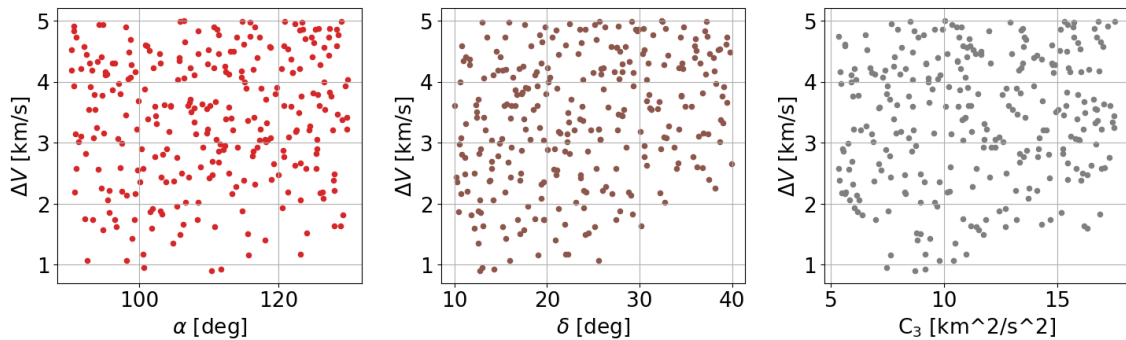
Figure 5.1: Monte Carlo analysis results, hyperbolic transfer free parameters and objective function results (ΔV), seed 1728. Results shown are filtered, only results with ΔV < 5 km/s.

The results of the Monte Carlo sampling of the elliptical orbit free parameters are shown in Figure 5.2. The ranges of θ_{el} and i_{el} generate results that are scattered across the entire range of the free parameter considered. It would be possible to highlight a small reduction in the range of the inclination, maybe between 15 and 22 degrees instead of the [14,24] deg interval, but the conclusion is that it would not be a meaningful reduction, and the range is kept as is.

It is interesting how the results for the RAAN Ω and argument of pericenter ω seem to be somehow related. The initial range selected for these quantities was [0,360] deg, but there is a clear gap for both quantities for which there are no optimal solutions. In order to investigate the issue, the sum of Ω and ω was plotted in Figure 5.3. From this plot, it is clear how the behaviour of the cost of the maneuver, as a function of the sum of the two quantities, is periodic (following a cosine function).

This is probably due to the orientation of the elliptical orbit with respect to the orientation of the incoming hyperbola, constrained since it is still coming from a specific direction (represented by the α and δ values) and how the best solutions can probably be achieved when they both have a similar orientation, therefore pericenter positions that are close to each other.
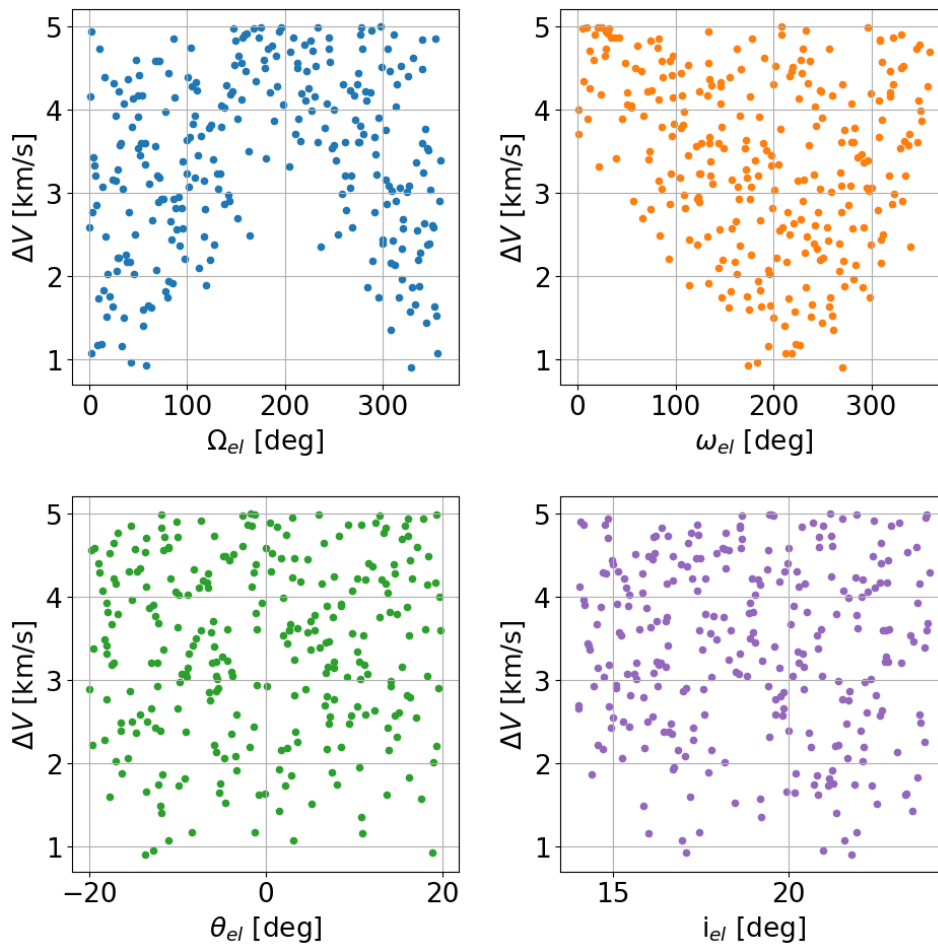
Figure 5.2: Monte Carlo analysis results, elliptical arrival orbit free parameters, case A1, and objective function results (ΔV), seed 1728. Results shown are filtered, only results with ΔV < 5 km/s.

The two quantities (Ω and ω) are therefore tied to each other, at least for cases A1, A2, P1 with elliptical orbits and a selected range of true anomaly values, and that the best decision would be to split each scenario in two, one to ensure that the sum of the Ω and ω (called S=Ω + ω) was in the interval [150, 300] deg, and another to ensure that the sum was in the [525, 675] deg interval.
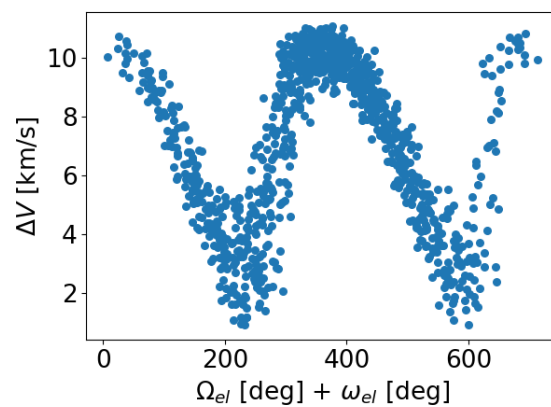
Figure 5.3: Monte Carlo analysis results, elliptical arrival orbit free parameters, case A1, and objective function results (ΔV), seed 1728. Results shown are unfiltered.

The split has been performed in the following way:

- For cases A1, and A2 the range for ω is selected to be between 150 deg and 300 deg for the case A-left, or 525 deg and 675 deg for the scenario A-right, similar to the desired ranges for the sum of the two variables (S). The range for a new free variable, that substitutes the RAAN so it will be called $\tilde{\Omega}$, will be between [-75, 75] deg, to make sure that the sum $\Omega + \omega$ is in range. In the optimization process, it is then possible to compute the value of Ω starting from the random value of ω and $\tilde{\Omega}$ as presented in Equation 5.3

$$\Omega = \left(\frac{S_{UP} + S_{DOWN}}{2} \right) - \omega + \tilde{\Omega} \tag{5.3}$$

S_{UP} = upper bound of the range for the sum of Ω and ω
S_{DOWN} = lower bound of the range for the sum of Ω and ω

- For case P1, the argument of pericenter is constrained in order to target a specific landing position. Therefore, the same procedure as for A1 and A2 is applied, only the range of ω is reduced to be between [70, 90] deg. Equation 5.3 is applied to compute Ω and obtain the P1-left and P1-right cases.
- Case P2 considers a circular PO and therefore the range of true anomaly is left as open as possible (between 0 and 360 deg); it has therefore been decided to not apply the split to this last scenario.

The new ranges selected for the problem are presented in Table 5.7. Cases A1, A2 and P1 are split into a left and right case, due to the discovery of the relationship between Ω and ω. The two problems will be optimized independently, to avoid dealing with discontinuities in the optimization.

Orbit Name	A1 Prograde		A2 Retrograde		P1 Landing		P2 Polar
h_p [km]	250		250		250		250
T [sol]	10		10		1		0.075
a [km]	94911		94911		20448		3643
e [-]	0.9616		0.9616		0.8220		0.001
i [deg]	14/24		156 - 166		18.8		90
Ω [deg]	Used $\tilde{\Omega}$		Used $\tilde{\Omega}$		Used $\tilde{\Omega}$		0 - 360
$\tilde{\Omega}$ [deg]	-75 - +75		-75 - +75		-75 - +75		Not used
ω [deg]	150 - 300	525 - 675	150 - 300	525 - 675	70 - 90		0 - 360
S ($\Omega + \omega$) [deg]	225	600	225	600	225	600	Not used
θ [deg]	-20 - +20		-20 - +20		-20 - +20		0 - 360

Table 5.7: Final selected free parameters for elliptical orbits around Mars, insertion problem optimization, after Monte Carlo study.

5.7. Optimizer selection

The selection of the optimizer algorithm has been led by two references: the literature study [22], and the availability of optimization tools. As explained in the literature study, Pygmo is the suite of tools for optimization that will be used for the optimization problem. The most versatile and approachable single-objective optimizers available in Pygmo were the Bee Colony (BC) and Differential Evolution (DE), both for their stability and ease of tuning, due to the limited number of tuning parameters. The stability of the result concerns how these algorithms have been proven to be able to solve complex problems in a contained number of repetitions, converging in most of the tested cases.

The final choice has been to apply the DE algorithm to be problem. Hrstka [10] in a comparison between different evolutionary algorithms mentions that DE is a good tool for problems with less than ten free variables, and the reference paper for the algorithm implementation in Pygmo, authored by Storn [24] shows how competitive it can be against other optimization strategies, especially for its robustness under a wide range of settings.

The DE algorithm is a heuristic approach part of the Evolutionary Algorithms family. Without going into too much detail (a more thorough description can be found in Storn's paper [24]), the main steps of the optimization will be presented:

- **Initial population**
  A population is a group of size NP (an integer) of individuals $\vec{x}_i$, which are D-dimensional vectors (D is the number of free parameters of the optimization problem). The initial population is chosen by randomly sampling the design space, and a uniform distribution is used for the randomizer.

- **Mutation**
  The initial population is, at the moment, the current generation (G) of individuals. In order to create the next generation, new individuals must be created. A mutated individual is created by computing the difference of two individuals of the current generation ($x_{1,G}$ and $x_{2,G}$), multiply the result by a factor F and then combine it with a vector of the current generation that is subject to mutation ($x_{i,G}$). The result is the so-called "mutated" vector. Mutation is controlled, in the algorithm implementation in Pygmo, by the parameter F, with F $\in$ [0,2].

- **Crossover**
  Crossover is the operation by which only some parameters of the mutated vector ($\vec{v}_i$) get substituted with the parameters of another vector from the current generation ($\vec{x}_j$), to form the "trial" vector. It is different from mutation as not all parameters of the mutated vector may get changed at the same time, and also because the parameters of the mutated vector $\vec{v}_i$ are substituted, not combined with those of the additional vector $\vec{x}_j$. Crossover is controlled, in the algorithm implementation in Pygmo, by the parameter CR, with CR $\in$ [0,1].

- **Selection**
  Selection of the new population is made with a greedy criterion: the newly generated vector $x_{i,G+1}$ and current vector $x_{i,G}$ are used as input in the cost function, and the one that yields the lowest result is added to the new population (G+1).

The selected version of DE is rand/1/bin, which is cited by Storn [24] as the one used in the study with all the test functions. In the definition, "rand" stands by the selection method of the vector to be mutated (x_i, G) which in this case is random from the current population G; "1" stands for the number of difference vector couples ($x_{1,G}$ and $x_{2,G}$ in this case, therefore one couple) used in the method; "bin" stands for the way the crossover is applied, which in this case is by performing independent binomial experiments (related to the way the parameters to be changed are selected).

The algorithm will be tuned in the next section in order to gain familiarity both with the problem and with the DE optimizer, and perform the most efficient optimization.

5.8. Tuning
The following parameters are used to tune the DE rand/1/bin algorithm:

- **F**: F influences how much the mutation will affect the selected vector, with higher values of F generating mutated vectors that are (on average) more distant from the initial one. This means that, as a rule of thumb, lower values of F will result in a faster convergence, as the individuals of the population look more and more similar to each other between generations (they do not mutate that much between generations). Storn [24] suggests F=0.5 as a reference value to begin the tuning, and to not go below F=0.4 or higher than F=1.0.
  The three values of F chosen for the tuning are: 0.4, 0.5, 1.0.

- **CR**: CR influences how many parameters will be interested by the crossover process. A higher value of CR corresponds to (on average) more parameters being interested by crossover for each individual. Higher values of CR correspond to a faster convergence, as noted by Storn [24], whose study suggests to test CR=0.1 and CR= 0.9, the latter to see if convergence can be sped up. A possible explanation for this behaviour is that by having a high crossover rate the individuals in the population begin to be more and more homogeneous, with a runaway effect that keeps generating more uniformity inside the population itself, therefore between populations as well, which leads to converging to a minimum (if convergence is possible).
  The three values of CR chosen for the tuning are: 0.1, 0.5, 0.9.

- **NP, or population size**: The population size is the number of individuals for which the cost function is evaluated at each generation. A lower number of individuals speeds up convergence, as there is a smaller number of vectors with which the algorithm can perform mutation and crossover. Storn [24] recommends as a rule of thumb to employ a population size between 5D and 10D (D is the number of free parameters in the optimization). However, in the verification steps with test functions, Storn often employs NP = 20 even for problems with six or seven parameters.
  The three values of NP chosen for the tuning are: 20, 35, 50.

All the considerations above are a trend more than a strict rule applicable to any and all cases, since the random nature of the process allows for instances in which the behaviour is not foreseen correctly by simply applying those conclusions. That is why the tuning process has been repeated over three different seed numbers (1728, 2358, 3682), which generate different series of (quasi) random numbers. The results across different seed numbers can be found in Tables 5.8 to 5.10 and in Appendix B.

The tuning has been performed using the "A1-left" problem, as defined in Section 5.6. Usually tuning has to balance two sides: a slow convergence could be the sign that the optimizer is covering multiple solutions, therefore having a better chance of finding the global optimum instead of a local one; on the other hand, more generations equal a higher number of function evaluations, and therefore cpu time employed. The insertion problem has an analytical solution (i.e. lengthy numerical processes such as integrations are absent), and by performing the tuning of the optimizer it has become apparent that the maximum cpu time, in the worst-case scenario, still amounted to less than one minute. The cpu time (represented by the number of function evaluations in the tables below) is therefore a less important metric, compared to trying to avoid premature convergence and achieving a robust result over different seed numbers.

Different seed numbers all seem to yield the same solution in terms of ΔV budget, which indicates that for whatever value of the settings, the optimizer is able to find the same optimum; however, a discussion on whether this is the global optimum is premature, as the DE algorithm is theoretically not tuned yet. The optimization results will be discussed in Chapter 6.

The following conclusions on tuning have been drawn:

- **F:** F = 0.5 has been selected. For this parameter, in Table 5.8 the number of function evaluations does not vary that much across different values of F per seed, compared to the tuning of CR (Table 5.9) and NP (Table 5.10). It is necessary then to evaluate the behaviour of the best fit, average of the population and standard deviation of the population across different generations. Across different seeds, F=0.4 provided the steepest and fastest convergence, while F=1.0 had a more gentle slope, especially considering the standard deviation. The results are slightly contradictory between different seeds, with F=1.0 sometimes achieving a faster convergence than F = 0.4. It has therefore been decided to select F=0.5 in order to stay in the middle of the two recommended boundaries.

Seed	1721		2358		3682	
F	ΔV [km/s]	Func. eval.[-]	ΔV [km/s]	Func. eval.[-]	ΔV [km/s]	Func. eval.[-]
0.5	0.564336	6880	0.564398	10180	0.564345	9160
0.4	0,564346	6780	0.564386	8200	0.56434	7800
1	0.56441	6480	0.564353	9160	0,564348	10460

Table 5.8: Tuning of DE optimizer, under different settings of parameter F. A1-left insertion problem, CR = 0.1, NP = 20 for all cases.

- **CR:** CR = 0.5 has been chosen as the result in Table 5.9 that is the most consistent across different seeds (in terms of number of function evaluations and of result) while at the same time trying to avoid premature convergence with a higher setting like 0.9, as can be seen in the resulting number of function evaluations.

Seed	1721		2358		3682	
CR	ΔV [km/s]	Func. eval.[-]	ΔV [km/s]	Func. eval.[-]	ΔV [km/s]	Func. eval.[-]
0.1	0.56434	6880	0.56440	10180	0.56435	9160
0.5	0.56435	5260	0.56435	4920	0.56434	4360
0.9	0.56440	3840	0.56433	2740	0.56433	2820

Table 5.9: Tuning of DE optimizer, under different settings of parameter CR. A1-left insertion problem, F = 0.5, NP = 20 for all cases.

- **NP:** NP = 50 has been selected. It is the largest value for population size, which yields the highest number of function evaluations per seed number in Table 5.10. However, this is a global optimization on a preliminary study, and the exploratory phase of the optimizer should be facilitated, since the cpu time is not a limiting factor.

Seed	1721		2358		3682	
NP	ΔV [km/s]	Func. eval.[-]	ΔV [km/s]	Func. eval.[-]	ΔV [km/s]	Func. eval.[-]
20	0.564336	6880	0.564398	10180	0.564345	9160
35	0.564338	13650	0.564343	19110	0.564336	12950
50	0.564334	24450	0.564336	26400	0.564337	24000

Table 5.10: Tuning of DE optimizer, under different settings of parameter NP. A1-left insertion problem, F = 0.5, CR = 0.1 for all cases.

Having performed the tuning, the summary of the characteristics of the chosen DE algorithm for the optimization of the insertion maneuver problem are presented in Table 5.11. In the next chapter, these settings will be applied to all the mission scenarios and the results of the optimization will be discussed.

Name	Setting
DE method	rand/1/bin
F	0.5
CR	0.5
NP	50

Table 5.11: Tuning of the DE optimizer for the insertion problem, final settings chosen for the optimization in Chapter 6.

Results

This chapter will cover the results of the optimization strategy defined in Chapter 5. The results will be presented first divided by case study (A1, A2, P1, P2), and will serve as a starting point to draw general conclusions on the insertion maneuver problem.

6.1. Optimization results

The optimization has been repeated across three seed numbers (1728, 2358, 3682) achieving consistent results. The following discussion will present such results employing figures obtained all using the same seed number (1728) in order to avoid repetitions. However, a complete set of all the figures generated across different seed numbers can be found in Appendix C.

All the case studies converged to a solution, under the criteria mentioned in Chapter 5. As an example and proof of this statement, the statistical data on the best individual, average fitness and standard deviation of the population at different generations has been plotted for case A1-left in Figure 6.1. Instead of plotting the best individual value, the plot presents the difference between the best individual at generation "i" and the best individual of the complete optimization, meaning the best individual of the final generation. This difference shows how the method does not only converge in terms of average of the whole population, but that the choice of this convergence criterium also means that the best individual has reached the desired accuracy.

The "vertical" line at the end of the graph showing the difference between the best individual of the current and final generation is due to the choice of adopting the logarithmic scale; once the best solution is found, the quantity (a difference between two theoretically identical numbers) should drop to zero, which would mean an infinite y-axis in logarithmic form.
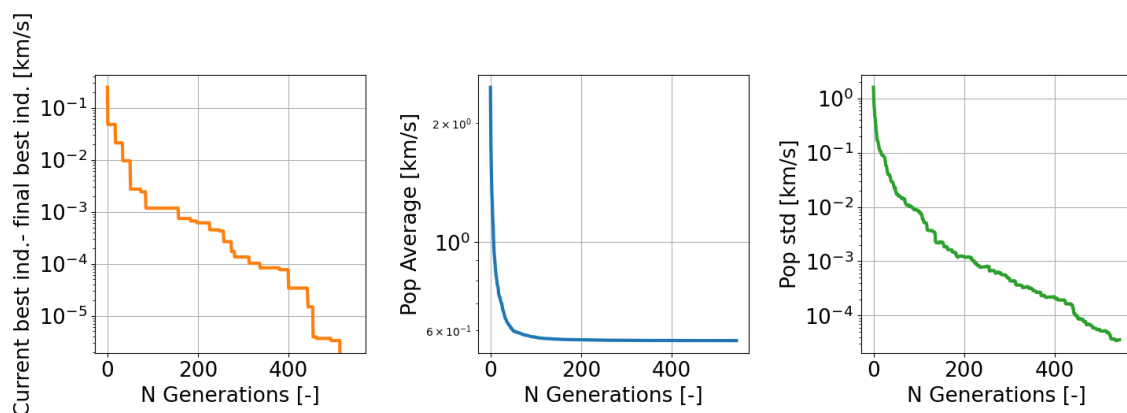
Figure 6.1: Statistical data on the ΔV values of the population over the complete optimization of the A1-left insertion problem, seed number = 1721

6.1.1. Case A1

Case A1 was divided in a "A1-left" and "A1-right" problem as explained in Chapter 5, and the optimization of the two cases has been carried out independently. Both optimizations have converged under the criteria mentioned in Chapter 5.

The results for case study A1 are reported in Tables 6.1 and 6.2. The optimum ΔV is extremely low, even lower than the expected values according to Merril (see Section 5.4). The relative geometry between the hyperbolic and elliptical orbit make it an almost perfect coplanar tangential periapsis insertion (see definition in Chapter 4), thus granting the lowest ΔV budget possible as expected. Another result that was confirmed from an hypothesis made in the Monte Carlo analysis is that the best result is paired with the lowest value of C_3, or hyperbolic energy, available based on the input range selected.

However the result is far from redundant, as the algorithm is able to find the best orientation (for hyperbola and ellipse) based on the given direction of the transfer hyperbola asymptotes.

The result is so close to the pericenter of the hyperbolic and elliptical orbits, for both the left and right case, that any discussion on whether it would be more advantageous to adopt the solution placed on the incoming branch or outgoing branch is not relevant.

Quantity	Transf. hyperbola (L)	Elliptical orbit (L)	Transf. hyperbola (R)	Elliptical orbit (R)
a [km]	-8095.955	94911.256	-8095.856	94911.2563
e [-]	1.4495	0.9616	1.4495	0.9616
i [deg]	19.694	19.680	17.987	17.992
Ω [deg]	28.428	28.376	18.005	18.029
ω [deg]	-128.147	231.955	-122.403	237.497
θ [deg]	359.951	-0.094	0.573	0.648

Table 6.1: Characteristics of the best individual, hyperbolic transfer and elliptical orbit Keplerian elements, A1-left (L) and A1-right (R) cases. The true anomaly is that of the insertion maneuver location. Seed number = 1721.

Trajectory	α_h [deg]	δ_h [deg]	$C_{3,h}$ [km^2/s^2]	ΔV insertion [km/s]
Transfer hyperbola (left)	127.164	19.482	5.29009	0.56434
Transfer hyperbola (right)	122.669	17.437	5.29015	0.56435

Table 6.2: Characteristics of the best individual, hyperbolic transfer input values and cost of the insertion maneuver, A1-left and A1-right cases. Seed number = 1721.

In Table 6.1 it is clear that the A1-left and A1-right problems do not converge to the same optimum. That can be explained by the input values for the hyperbola asymptote direction in Table 6.2, as the two hyperbolas have clearly different orientation. Even though the "true" optimum should be the one from the A1-left problem, by examining the entire population of both cases it is clear that the insertion problem does not only yield one optimum results, but identifies a larger area in the design space were optimal maneuvers can be located. The analysis therefore continues by looking at the entire population of the final generation, starting by the elliptical PO results.

The elliptical parking orbit had fixed semi-major axis and eccentricity, with the other Keplerian elements variable within a range and used as input in the optimization problem. The results in Figure 6.2 show a reduction in the range of the Keplerian elements for the final population, even though the values still range over more than 10-15 deg (for i, Ω and ω), while still maintaining a very low cost of the maneuver. This result shows how the method has converged to a minimum that is quite robust, since for a set of different orientations of the parking orbit the insertion cost does not change drastically.
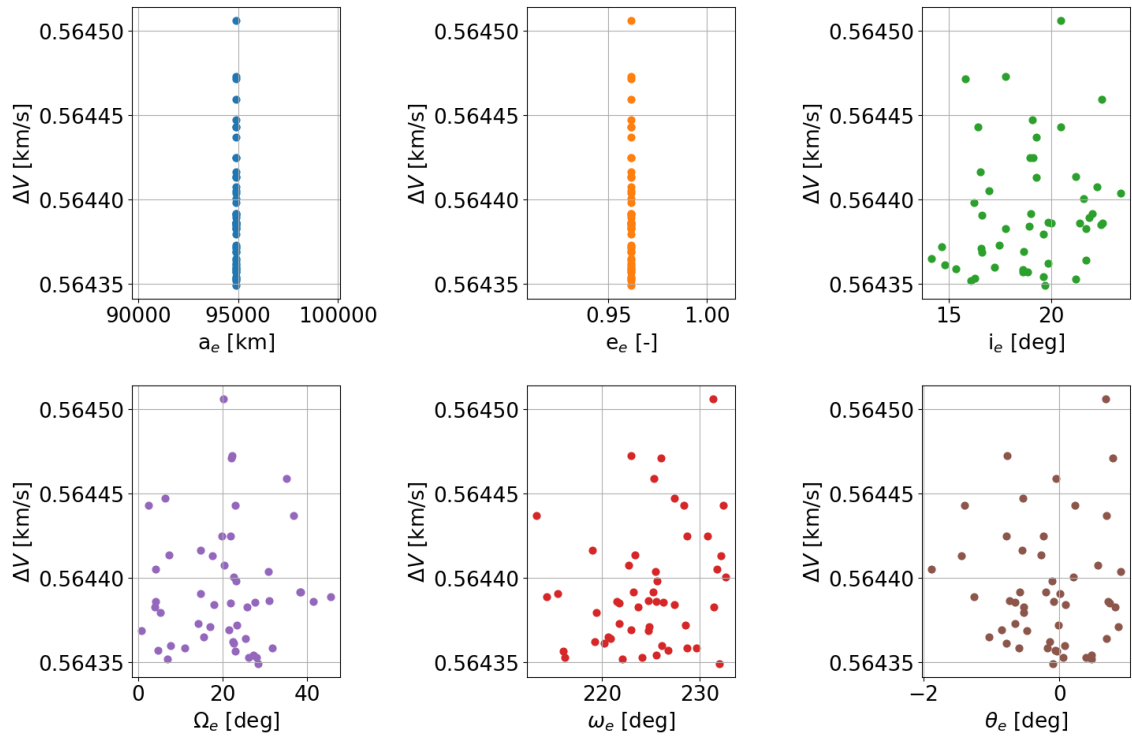
Figure 6.2: Results from the final population, elliptical parking orbit Keplerian elements, A1-left insertion problem, seed number=1721.

The Keplerian elements of the hyperbolic transfer maneuver are all results of the optimization problem, as there was no range set from the beginning. The final population is characterized by values of C_3 that are close to the minimum (due to the range), as explained above; this, in return, yields results that have virtually the same semi-major axis value (all the results are between -8097 km and -8094 km). The same goes for the eccentricity; all the individuals of the final population have similar eccentricity (up to 1e-4). This is due to two effects of the optimization: the semi-major axis value gets flattened towards the same value, corresponding to min(C_3), and the true anomaly of the solution becomes very close to pericenter, both for hyperbola and ellipse. Since the pericenter radius is fixed for the elliptical PO, if it becomes the maneuver location it will also be fixed for the hyperbolic orbit, therefore determining the eccentricity.

The optimal results in Figure 6.3 show the remaining Keplerian elements for the transfer hyperbola. In the initial population (top row of the figure) the values of Ω and ω are conditioned by the values on the elliptical parking orbit (the ranges presented in Section 5.6). This effect has a simple explanation: Cornick's method always guarantees the intersection between the two orbits, therefore their orientation in space must be similar.

As explained for the best individual of the final population in Table 6.1, the hyperbolas in the final population are very close in orientation to their respective elliptical orbits, in order to achieve insertion close to pericenter and tangentially. The values of true anomaly (not shown in the figure) confirm this as well, with all the results clearly grouped close to θ = 0 deg.
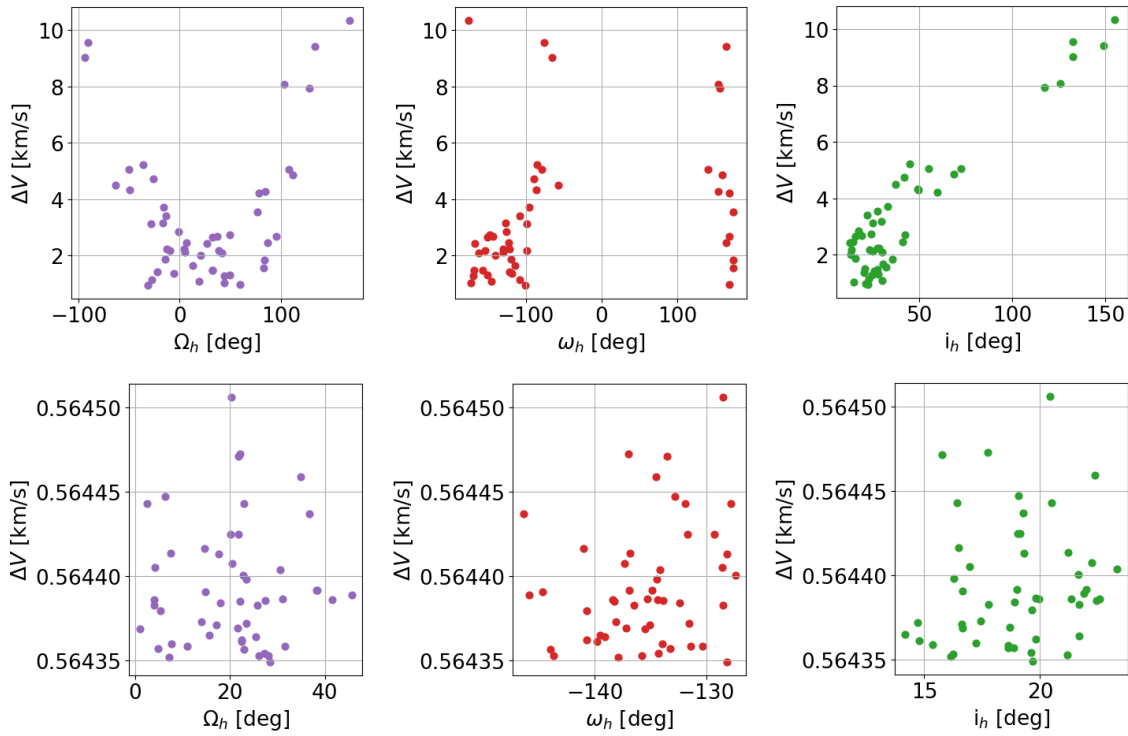
Figure 6.3: Results from the initial (top row) and final (bottom row) populations, A1-left insertion problem, seed number=1721

6.1.2. Case A2

Case A2 was separated in cases A2-left and A2-right, in a similar way as A1, and their optimization was carried out independently. The optimization converged to two best individuals, presented in Tables 6.3 and 6.4.

The conclusions made for case A1 are applicable to A2 as well: both results are almost a perfect coplanar tangential insertion at pericenter, with very low values for the cost of insertion ΔV. The two solutions, this time, are extremely similar to each other, and it is possible to conclude that the results of the optimization of the left and right cases found the same minimum (at least in terms of location of the minimum considering the complete search space as a whole).

Quantity	Transf. hyperbola (L)	Elliptical orbit (L)	Transf. hyperbola (R)	Elliptical orbit (R)
a [km]	-8096.081	94911.256	-8095.995	94911.256
e [-]	1.4495	0.9616	1.4495	0.9616
i [deg]	162.793	162.793	162.088	162.088
Ω [deg]	-94.813	265.220	-95.330	264.651
ω [deg]	-89.223	270.921	-83.613	276.349
θ [deg]	359.509	-0.602	359.972	-0.007

Table 6.3: Characteristics of the best individual, hyperbolic transfer and elliptical orbit Keplerian elements, A2-left (L) and A2-right (R) cases. The true anomaly is that of the insertion maneuver location. Seed number = 1721.

Trajectory	α_h [deg]	δ_h [deg]	$C_{3,h}$ [km^2/s^2]	ΔV insertion [km/s]
Transfer hyperbola (left)	126.724	11.604	5.2900	0.56434
Transfer hyperbola (right)	120.540	10.724	5.2900	0.56434

Table 6.4: Characteristics of the best individual, hyperbolic transfer input values and cost of the insertion maneuver, A2-left and A2-right cases. Seed number = 1721.

The selection of case study A2 was originated by Merril's and Desai's studies (see Section 5.6) and their use or retrograde PO for missions to Mars. It is known from Cornick's problem (presented in

Chapter 4) that the problem always has two solutions, that are two identical hyperbolas from a geo-
metrical standpoint, though one is prograde and the other one is retrograde. Case A2 is therefore also
a sanity check, to see whether the optimization is able to identify those two hyperbolas independently
(not as part of the same solution of the analytical insertion problem) by forcing one solution space to
investigate only prograde parking orbits (A1) and one only retrograde parking orbits (A2).

However, there is no constraint on the hyperbola inclination, and in the initial population the orbits are
free to adopt both prograde and retrograde inclinations (see Figure 5.1), both in the A1 and A2 cases.
How would one be sure that the optimization of case A1 would not yield both of Cornick's solutions by
itself (without the need of problem A2)? According to astrodynamics, moving from an orbit with opposite
orientation (prograde vs retrograde) will result in a very high insertion ΔV. Therefore, the results for
the inclination range of the hyperbolas of the final population will automatically act accordingly, only
containing prograde or retrograde orbits according to what was imposed on the elliptical PO.

Both case A2-left and A2-right have results that are very close to those of case A1-right, due to the
inclination of the elliptical parking orbit, which is ≈ 18 deg in all three scenarios. This proves that the
optimizer is identifying the same region dense in local minima in the design space, that contains case
A1-left and case A2, even if the results are not perfectly coinciding.

6.1.3. Case P1

Case P1 has been divided in P1-left and P1-right in a similar way as it was done for A1 and A2, and
the optimization of the two cases has been performed independently. For both P1 and P2, conver-
gence has been achieved much faster than for A1 and A2, as shown in Figure 6.4. While case A1
and A2 converged (on average) after 400-500 generations, cases P1-left and P1-right converged (on
average) after 200-300 generations. That is probably related to the lower number of free parameters
(the inclination of the elliptical PO is fixed in cases P1 and P2).
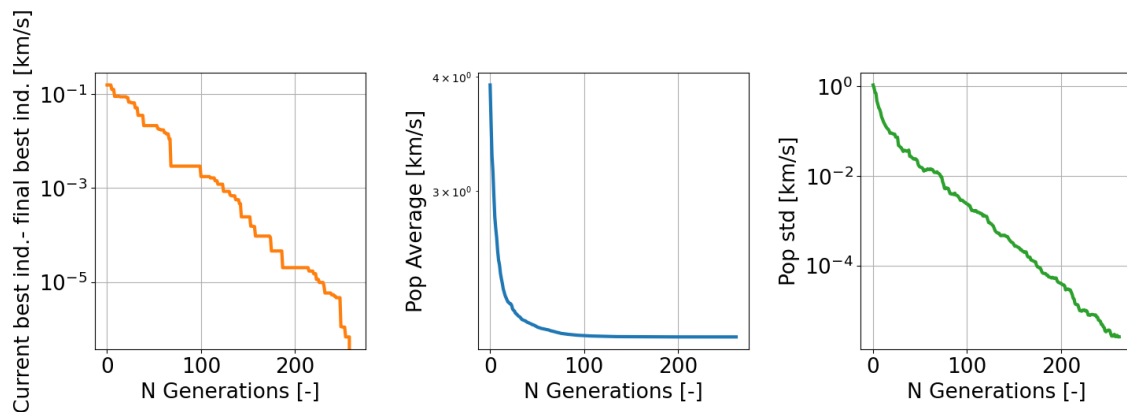
Figure 6.4: Statistical data on the ΔV values of the population over the complete optimization of the P1-left insertion problem,
seed number = 1721

The results of the optimization are presented in Tables 6.5 and 6.6. The ΔV is around 1.5 km/s higher
than the result for the insertion on an arrival orbit (A1 and A2). This is probably due to the restriction
of the search space, both considering the fixed inclination and the reduced range of the pericenter
anomaly.

It is also worth pointing out how the inclination of the hyperbola and the inclination of the ellipse
are quite different, making the resulting insertion non-coplanar. In addition to this, the true anomaly of
the maneuver is ≈ 20 deg on the ellipse, and ≈ 353 deg on the hyperbola, which is further away from
pericenter than in the first scenarios. This would confirm what Desai had postulated in his study on PO
[4], which is that in certain conditions pericenter insertions are either not available (due to the geometry
of the problem), or simply not the optimal solution.

The true anomaly on the ellipse is also the upper boundary on the range imposed for this input
variable (in the DSE of Section 5.6). This would suggest that opening up the search space (with a
wider range) may yield a more optimal solution to the problem.

The results of the left and right problem yield similar results in terms of ΔV, but once again differ in

the orientation of the hyperbolic transfer. It is interesting how, in this scenario, only the Ω differs between P1-left and P1-right, both in the hyperbolic and elliptical orbits. This is mirrored by the asymptote right ascension α in Table 6.6, which differs between the two cases, while the declination and value of C_3 are approximately the same. In order to investigate this characteristic of the problem, the entire final population has been analyzed.

Quantity	Transf. hyperbola (L)	Elliptical orbit (L)	Transf. hyperbola (R)	Elliptical orbit (R)
a [km]	-4863.224	20448.010	-4869.655	20448.0103
e [-]	1.7662	0.82209	1.7651	0.8220
i [deg]	27.968	18.800	27.975	18.800
Ω [deg]	93.966	126.1803	76.319	108.547
ω [deg]	146.216	89.999	146.233	89.999
θ [deg]	353.563	19.999	353.559	19.999

Table 6.5: Characteristics of the best individual, hyperbolic transfer and elliptical orbit Keplerian elements, P1-left (L) and P1-right (R) cases. The true anomaly is that of the insertion maneuver location. Seed number = 1721.

Trajectory	α_h [deg]	δ_h [deg]	$C_{3,h}$ [km^2/s^2]	ΔV insertion [km/s]
Transfer hyperbola (left)	113.361	10.000	8.8065	2.07578
Transfer hyperbola (right)	95.707	10.000	8.7949	2.07578

Table 6.6: Characteristics of the best individual, hyperbolic transfer input values and cost of the insertion maneuver, P1-left and P1-right cases. Seed number = 1721.

The final population of elliptical POs is characterized by orbits that all share the same semi-major axis, eccentricity, inclination. The results of the optimization show that these individuals also have (approximately) the same argument of pericenter ω and true anomaly θ of maneuver (the standard deviation for both is < 10^{-3} deg).
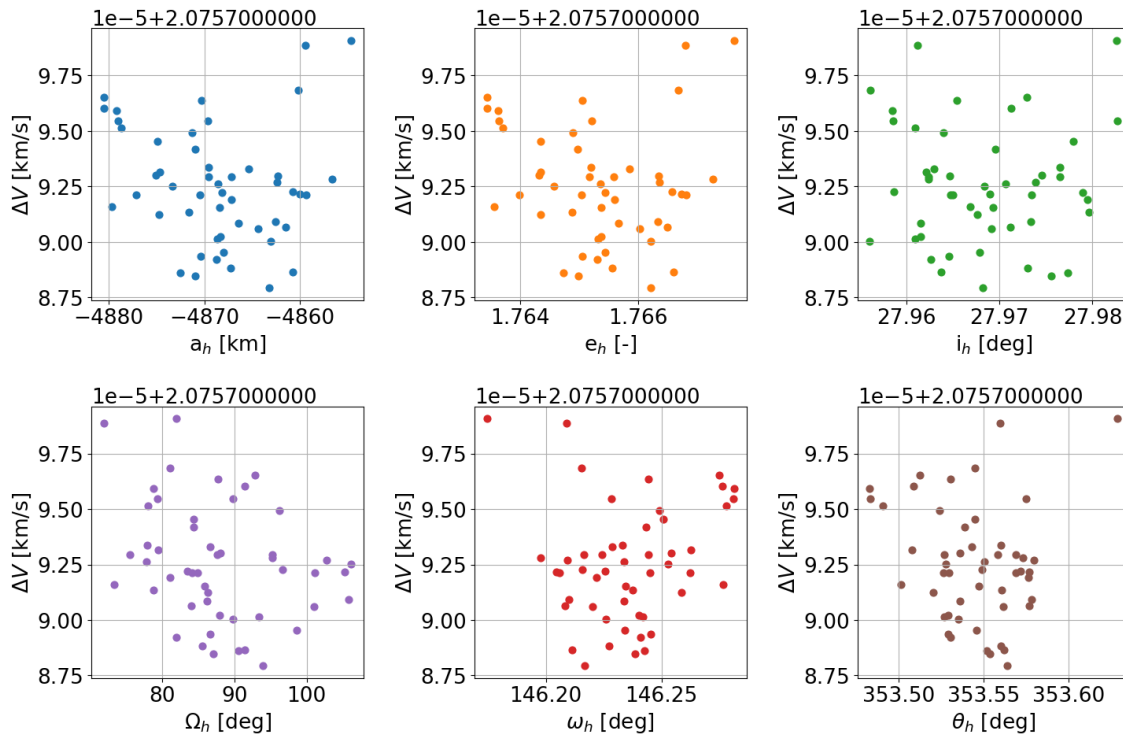
Figure 6.5: Results from the final population of hyperbolic transfer orbits, P1-left insertion problem, seed number=1721.

The entire final population, for the hyperbolic transfer, has been presented in Figure 6.5. All the Keplerian elements are characterized by a small range, and all the individuals have approximately the same cost of insertion. The only exception is the RAAN Ω, which ranges in the interval [75, 105] deg. It is possible to conclude that the optimization has resulted in a very tight locus of optimum solutions, all similar except for the values of Ω.

An interesting conclusion is that in order to target a PO with specific inclination and a small range of argument of pericenter acceptable, one must identify a highly specific combination of conditions on the ellipse and hyperbola, but still has some freedom via the RAAN.

6.1.4. Case P2

Case study P2 has not been separated into two separate cases, due to the adoption of a circular parking orbit (as explained in Section 5.6). The optimization converges but requires more generations than all the previous cases (Figure 6.6), on average (averaged across different seed numbers) about 200 generations more than cases A1 and A2. This is probably due to the adoption of the largest search space possible ([0, 360] deg) for three free variables (i, Ω, ω), since the orbit is circular. Results for all seed numbers can be found in Appendix C.
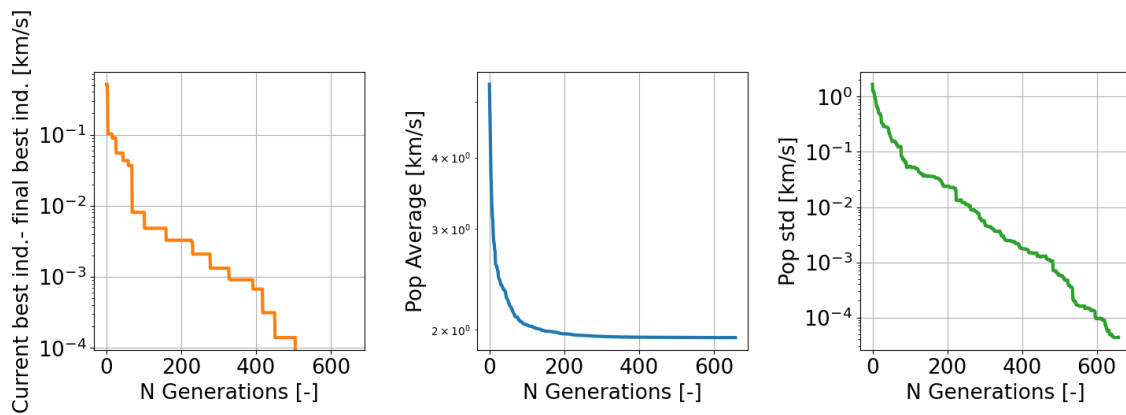
Figure 6.6: Statistical data on the ΔV values of the population over the complete optimization of the P2 insertion problem, seed number = 1721

The result of the optimization is presented in Tables 6.7 and 6.8. The optimum result for an insertion in a polar orbit corresponds to an approximation of a pericenter, coplanar, tangential insertion. The inclination of the hyperbolic and elliptical orbit is, in first-order approximation, the same, and since the eccentricity of the orbit is very low, the condition for θ = 354 deg can be approximated with those at pericenter. In fact, the difference between the true anomaly of the ellipse and that of the hyperbola is compensated by the difference in argument of pericenter ω between the two trajectories, thus aligning the velocity vectors.

The cost of the maneuver, though minimum due to the pericenter insertion, is still much higher than that of case A1 and A2, and closer to the result found for P1, even with a larger range of input for the orientation of the ellipse.

The semi-major axis of the hyperbola is determined by the value of C_3 which, like in case A1 and A2 is the lowest value possible according to the ranges selected for the input variables.

Trajectory	Transfer hyperbola	Elliptical orbit
a [km]	3643.143	-8095.930
e [-]	0.0010	1.4495
i [deg]	88.000	87.981
Ω [deg]	98.198	98.204
ω [deg]	167.238	161.946
θ [deg]	354.708	0.000

Table 6.7: Characteristics of the best individual, hyperbolic transfer and elliptical orbit Keplerian elements, P2 case. The true anomaly is that of the insertion maneuver location. Seed number = 1721.

Trajectory	α_h [deg]	δ_h [deg]	$C_{3,h}$ [km^2/s^2]	ΔV insertion [km/s]
Transfer hyperbola (left)	99.291	28.293	5.2901	1.93682

Table 6.8: Characteristics of the best individual, hyperbolic transfer input values and cost of the insertion maneuver, P2 case. Seed number = 1721.

All the elliptical parking orbits in problem P2 share the same semi-major axis, eccentricity and inclination. Results in Figure 6.7 show that, while reduced, the range for Ω and ω that correspond nearly to the same cost of insertion maneuver is quite large (around 30-40 deg). On the other hand, even though the orbit has a very low eccentricity, the values of θ still group around $\approx$0 and $\approx$360 deg (with approximately +/- 3 deg of standard deviation).
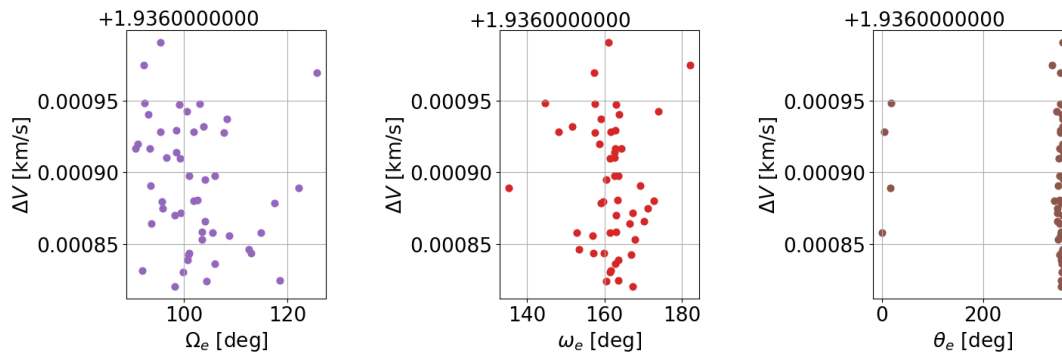
Figure 6.7: Results from the final population of elliptical orbits, P2 insertion problem, seed number=1721.

The hyperbola has the same trends for the values of Ω, ω and θ as the elliptical PO, as it is clear from Figure 6.8, when comparing it with Figure 6.7. However, the values of true anomaly are much closer to the pericenter than for the ellipse, since the latter is almost circular and the true anomaly value holds a smaller influence on the result.
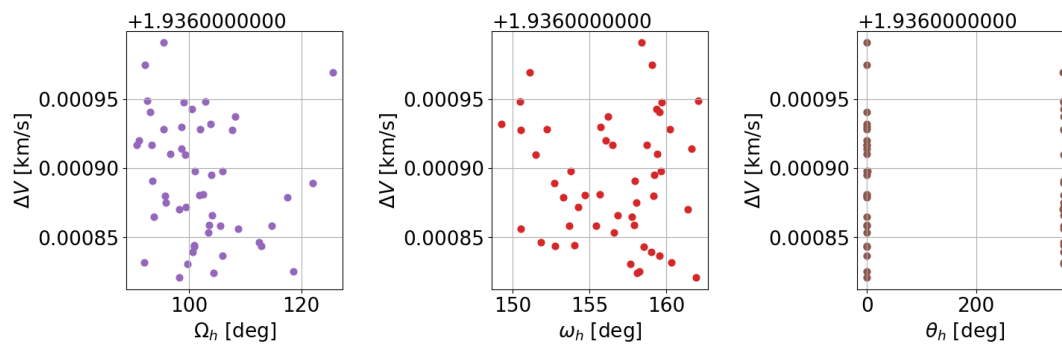
Figure 6.8: Results from the final population of hyperbolic transfer orbits, P2 insertion problem, seed number=1721.

6.2. Validation and lessons learned

Given the results of the optimization, a summary of useful deductions on the insertion maneuver problem, solved via Cornick's method and a DE optimizer, is presented:

- In case A1 and A2 the optimizer did not converge to a single solution, a single pairing between an hyperbolic orbit and a target elliptical orbit. The result was a larger and more flexible set of solutions, all with minimal ΔV, which could be a useful tool for mission designers.
- If one wanted to obtain a single solution, defined more strictly, two ways are possible. The first one is to constrain the target PO, such as in the P1 example. The second one would be to select a specific transfer hyperbola, rather than a range of values for its energy and especially its asymptote direction. In this way, it would be possible to understand which elliptical PO are more advantageous for a given launch schedule.

- The results of cases A1 and A2 in terms of ΔV were even lower than expected. Percy, in an overview of the EMC mission [20], computes the cost of the Trans Mars Injection maneuver (TMI, to move the spacecraft on the hyperbolic transfer trajectory from Earth to Mars) and Mars Orbit Insertion maneuver (MOI, the insertion problem). The ΔV results by Percy for both the TMI and MOI, shown in Figure 6.9, are higher than the optimal insertion maneuver computed in cases A1 and A2. It would then be an idea to perform an iteration of transfer and parking orbit studies, to achieve a compromise between conditions that have lower cost of the TMI, and those that have the lowest MOI cost.
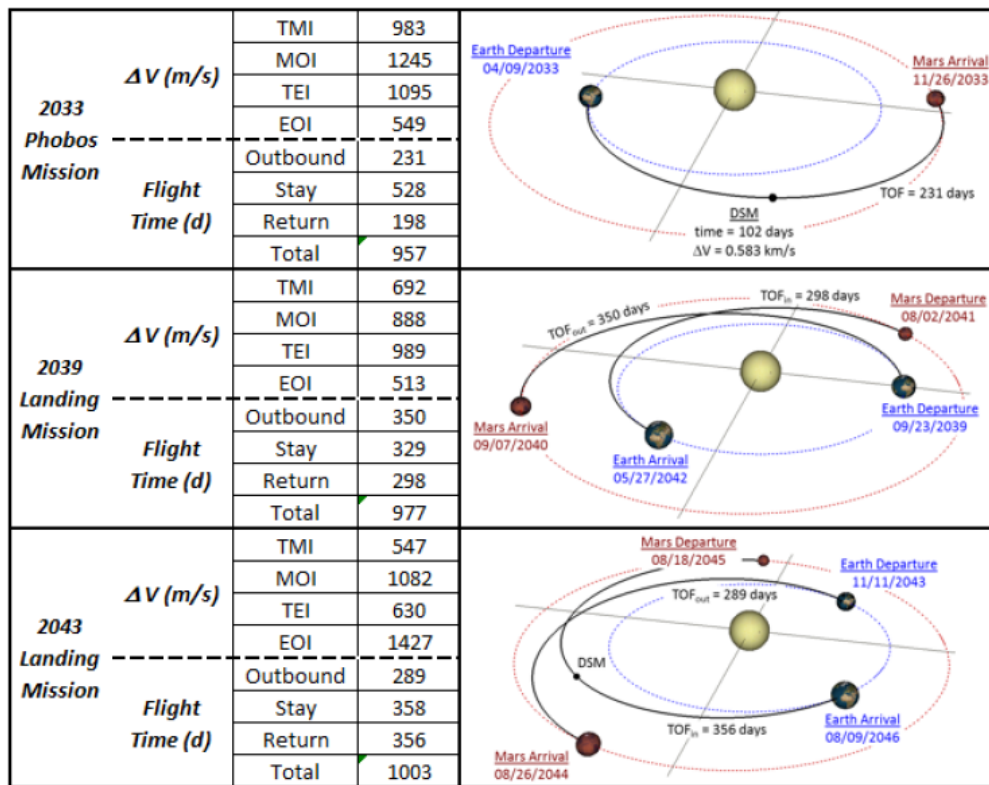
Figure 6.9: Overview of propellant and TOF budget for the EMC missions. [20]

- Qu, in a study on the EMC frame, makes a preliminary assessment of the total cost of the repositioning maneuvers, which should be approximately 0.05 km/s for cases A1 and A2, and around 0.20 to 0.30 km/s for case P2 [21]. The budget for the insertion, repositioning and escape maneuvers is set by Qu to 2.3 km/s. If one were to consider the direct insertion in a PO, as exemplified in cases P1 and P2, it is clear how those strategies would be too expensive, since the insertion alone would amount to $\approx$ 2 km/s. This is a confirmation that repositioning strategies are advantageous from the standpoint of the propellant budget.
- The division between a "left" and "right" problem is not recommended for future applications of the problem. The results were either very similar, or almost identical. It is simply recommended to perform the optimization on the "left" side alone, since the input selection process of the "right" side uses basically the same range for ω of the "left" side (only with a 360 deg difference).
- The use of different seeds has been implemented in the problem. However, since the result of the optimization, more often than not, highlighted a pool of options with minimal ΔV, it is possible to compare the size and shape of such pool with that generated by a different seed, but no conclusions should be made by simply comparing the best individual trajectory pairs (hyperbolic and elliptical orbit) out of the optimization process. In terms of ΔV, the use of different seeds always yielded the same result (up to the desired accuracy). In order to not repeat the same conclusions at each case study, the proof of this will be presented in Appendix C. The use of different seeds is evidence of the robustness of the solutions.

7

Conclusions and recommendations

This study has focused on insertion maneuvers, in the context of crewed missions to Mars. First, an overview of previous studies on maneuvers in the context of Mars missions has been given in Chapter 2, as well as the presentation of the EMC, the NASA set of missions used as a reference for this project. Then, all the assumptions necessary to create a model of the problem were presented in Chapter 3. The chapter also presented the different case studies selected as good candidates for further analysis. These cases all had specific characteristics that made them relevant either under the EMC frame (cases A1, A2 and P1) or for an optional exploration mission (case P2). An analytical method to solve the insertion maneuver problem, by Cornick [2], was presented in Chapter 4.

After the insertion problem and model have been defined, as well as the case studies to be optimized, the optimization problem had to be defined with the introduction of the variables, objectives, constraints and the choice and tuning of an optimizer in Chapter 5. The choice of the optimizer landed on the Differential Evolution, for its limited number of settings and efficiency on a wide set of problems.

Chapter 6 presented the results of the optimization problems. Via these results, the research question has been answered. The research question was: *"What are the optimal conditions for an insertion in an operational orbit around Mars in terms of cost of the maneuver and characteristics of the trajectories involved, ensuring the compatibility of the maneuver with the transfer trajectory and resulting parking orbit, and considering a single maneuver?"*.

The answer of the research question is obtained by answering the sub-questions mentioned in Chapter 2:

- **What is the smallest ΔV achievable?**
  The smallest ΔV achievable via insertion, for the EMC frame, have been summarized in Table 7.1.

Case	ΔV insertion [km/s]
A1-left	0.56434
A1-right	0.56435
A2-left	0.56434
A2-right	0.56434
P1-left	2.07578
P1-right	2.07578
P2	1.93682

Table 7.1: Characteristics of the best individual, cost of the insertion maneuver. Seed number = 1721.

- **What is the optimal pairing of transfer hyperbola conditions and target PO?**
  The pairing of hyperbolic and elliptical orbits is a complex problem. It is clear how certain values are more affected by the problem definition, resulting in a very narrow range of optimal solutions (for example, the semi-major axis of the hyperbola in all cases, or its inclination in case P1). The insertion problem is very robust to other quantities, such as part of the orientation of the hyperbola

(especially its Ω), which in all problems could be varied by 10-20 deg without impacting majorly the objective result.

- **What is the difference in ΔV between insertion in the target PO, and insertion in a preliminary PO, which is later modified (as defined by the EMC)?**
  As explained in Chapter 6, the insertion directly in the target PO (cases P1 and P2) is a very expensive maneuver, especially if the target PO has a specific inclination which is relevant to the scientific objectives of the mission. The conclusion is that the repositioning strategy by Merril [15] is indeed the best way of tackling the problem, by first performing an insertion in an arrival orbit (A1, A2) which can lower significantly the cost of insertion, and then perform less expensive repositioning maneuvers.

- **How robust are the resulting optimal insertion conditions? What is the sensitivity of the solution to a variation in the input conditions (the relative geometry between the transfer and parking orbits)?.**
  The optimization problem is quite robust to changes in seed number, but it is recommended to perform a separate sensitivity study in the future, to assess further the behaviour of the solution under perturbations. The results of Chapter 6 highlight a difference in sensitivity between cases A1 and A2 and cases P1 and P2. Cases A1 and A2 identified areas of optimum conditions that allowed to vary the free variables of the problem around a wide range, between 10 and 20 deg for Ω and ω and around 5 deg for i and θ (both for the elliptical and hyperbolic orbits) and still obtain optimum results. Problems P1 and P2 have less free variables. Problem P1 sees a reduction in the size of the optimum solution ranges, with a very small range in the elliptical PO orbit characteristics (around 10^{-3} deg) and ≈ 25 deg in Ω and 0.05 deg for both ω and θ for the hyperbolic orbit. The results for case P2 show how optimum solutions can be found for a range of around 20 deg for Ω, 10 deg for ω and around 2-3 deg for θ. However, this study varies both elliptical and hyperbolic orbit conditions at the same time; it would be interesting, once a solution is selected, to see the sensitivity of the result to changes in the characteristics of one of the trajectories instead of both at the same time.

The insertion problem is a fundamental link between the Earth-to-Mars transfer and the repositioning techniques inside the SOI of Mars. This study has proven that an analytical method can provide solutions quite quickly while ensuring the continuity of the conditions between the different phases of a mission. The optimization tool can be used in future preliminary mission studies, as its flexibility (can be adapted for different free parameters and constraints very easily) and computational speed make it a desirable candidate.

Bibliography

[1] Laura M Burke, Robert D Falck, and Melissa L McGuire. *Interplanetary mission design handbook: Earth-to-mars mission opportunities 2026 to 2045*. Tech. rep. 2010.

[2] DE Cornick and LK Seversike. "Optimum parking orbit orientation for a three-dimensional capture-escape mission". In: *Journal of Spacecraft and Rockets* 7.7 (1970), pp. 808–813.

[3] Howard D Curtis. *Orbital mechanics for engineering students*. Butterworth-Heinemann, 2013.

[4] Prasun N Desai. *Aspects of parking orbit selection in a manned Mars mission*. Vol. 3256. National Aeronautics and Space Administration, Office of Management …, 1992.

[5] Prasun N Desai and James J Buglia. "Arrival and departure impulsive Delta V determination for precessing Mars parking orbits". In: *AAS and AIAA* (1992).

[6] Prasun N Desai and James J Buglia. "Determining Mars parking orbits that ensure tangential periapsis burns at arrival and departure". In: *Journal of Spacecraft and Rockets* 30.4 (1993), pp. 414–419.

[7] L Diamant et al. *Abort planning for Apollo missions*. 1970, p. 94.

[8] Kandyce E Goodliff et al. "Comparison of Human Exploration Architecture and Campaign Approaches". In: *AIAA SPACE 2015 Conference and Exposition*. 2015, p. 4413.

[9] Gerald R Hintz. *Orbital mechanics and astrodynamics*. Springer, 2015.

[10] O Hrstka et al. "A competitive comparison of different types of evolutionary algorithms". In: *Computers & Structures* 81.18-19 (2003), pp. 1979–1990.

[11] Claude R Joyner et al. *Earth to Mars abort analysis for human Mars missions*. 2018.

[12] Claude R Joyner et al. "Enabling multiple abort strategies using the NTP approach for human Mars missions". In: *AIAA Space and Astronautics Forum and Exposition*. 2017, p. 5273.

[13] Damon F Landau, James M Longuski, and Paul A Penzo. "Method for parking-orbit reorientation for human missions to mars". In: *Journal of spacecraft and rockets* 42.3 (2005), pp. 517–522.

[14] Jack J Lissauer and Imke De Pater. *Fundamental planetary science: physics, chemistry and habitability*. Cambridge University Press, 2013.

[15] Raymond G Merrill et al. "Mars Sphere of Influence Maneuvers for NASA's Evolvable Mars Campaign". In: *AIAA/AAS Astrodynamics Specialist Conference*. 2016, p. 5210.

[16] NASA. *NASA ARTEMIS official website*. 2017. URL: `https://www.nasa.gov/specials/artemis/` (visited on 06/24/2022).

[17] Alice Nervo. *"Analysis of parking orbits for round-trip Mars missions"*. Politecnico di Torino, 2020.

[18] Palash Patole. "Propulsive abort trajectory options for a reconnaissance human Mars mission". In: *MSc thesis repository* TU Delft (2020).

[19] Thomas Percy, Melissa McGuire, and Tara Polsgrove. "Combining solar electric propulsion and chemical propulsion for crewed missions to Mars". In: *2015 IEEE Aerospace Conference*. IEEE. 2015, pp. 1–10.

[20] Thomas Percy, Melissa McGuire, and Tara Polsgrove. "In-space transportation for NASA's Evolvable Mars Campaign". In: *AIAA Space 2015 Conference and Exposition*. 2015, p. 4519.

[21] Min Qu et al. "Optimizing parking orbits for roundtrip Mars missions". In: *2017 AAS/AIAA Astrodynamics Specialist Conference*. NF1676L-26982. 2017.

[22] Cristina Riti. *Literature Study, Premature End-Of-Life Maneuvers*. 2022, TU Delft.

[23] SCIPY. *Sobol Sampling class, scipy.stats.qmc.Sobol*. 2023. URL: `https://docs.scipy.org/doc/scipy/reference/generated/scipy.stats.qmc.Sobol.html` (visited on 07/01/2023).

[24]   Rainer Storn and Kenneth Price. "Differential evolution–a simple and efficient heuristic for global optimization over continuous spaces". In: *Journal of global optimization* 11 (1997), pp. 341–359.

[25]   Karel F Wakker. *Fundamentals of astrodynamics*. TU Delft, 2015.

[26]   James Richard Wertz. *Mission geometry; orbit and constellation design and management*. Space Technology Library, 2001.

[27]   Greg Williams and Jason Crusan. "Pioneering space–the evolvable mars campaign". In: *NASA Headquarters, Washington* (2015).

[28]   Paul Wooster et al. "Trajectory options for human Mars missions". In: *AIAA/AAS Astrodynamics Specialist Conference and Exhibit*. 2006, p. 6308.

$\huge A$
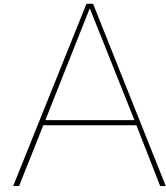
Appendix A

The following appendix is dedicated to showing all the results of the Monte Carlo analysis discussed in Section 5.6. The analysis has been repeated using three different seed numbers in order to ensure that a single randomized sample did not condition too heavily the choice of variable ranges of the DSE. The results are presented in the following graphs:

- ΔV results plotted against the initial conditions of the hyperbolic orbit (α, δ, C_3).
- ΔV results plotted against the free variables belonging to the elliptical POs.
- ΔV results plotted against the sum of Ω and ω of the elliptical POs.

A.1. Seed 1728
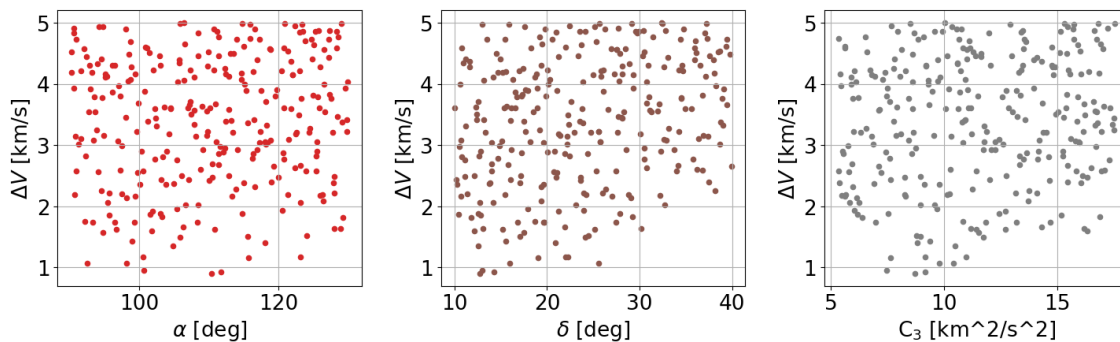
Figure A.1: Monte Carlo analysis results, hyperbolic transfer free parameters and objective function results (ΔV), seed 1728. Results shown are filtered, only results with ΔV < 5 km/s.
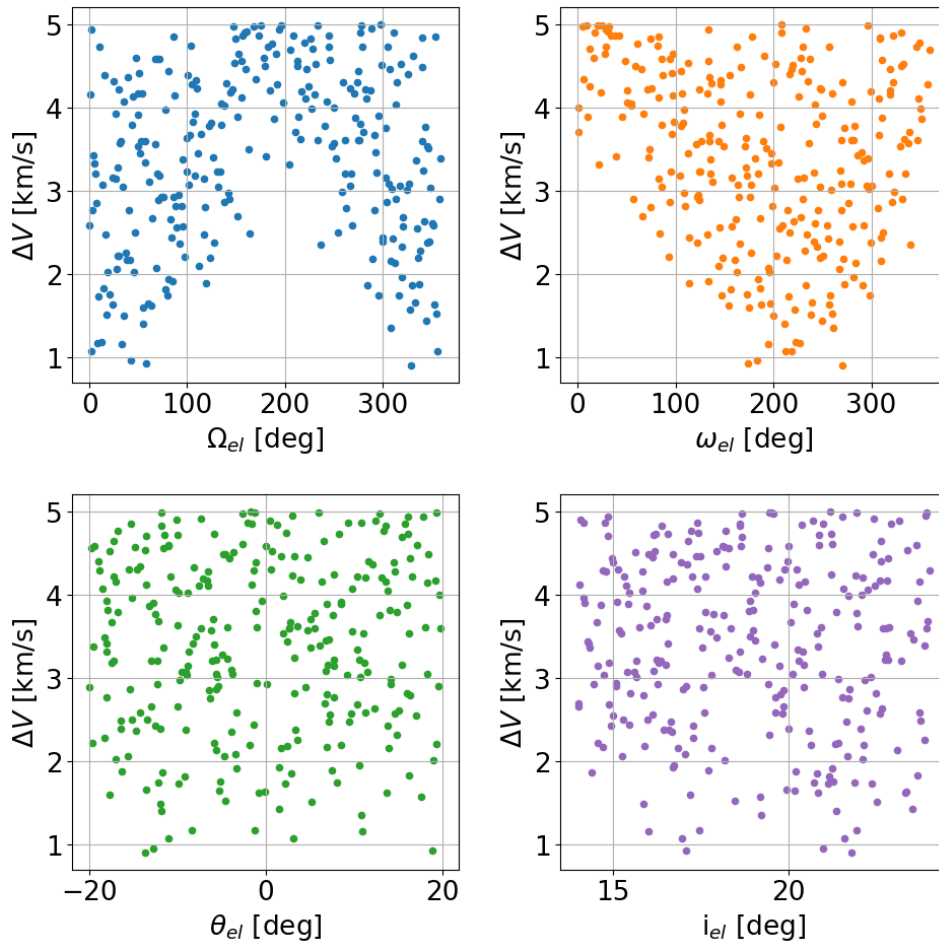
Figure A.2: Monte Carlo analysis results, elliptical arrival orbit free parameters, case A1, and objective function results (ΔV), seed 1728. Results shown are filtered, only results with ΔV < 5 km/s.
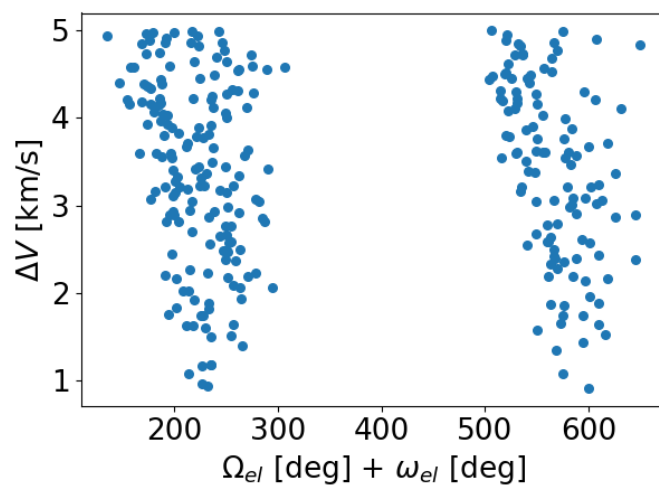
Figure A.3: Monte Carlo analysis results, elliptical arrival orbit free parameters, case A1, and objective function results (ΔV), seed 1728. Results shown are filtered, only results with ΔV < 5 km/s.

A.2. Seed 2368
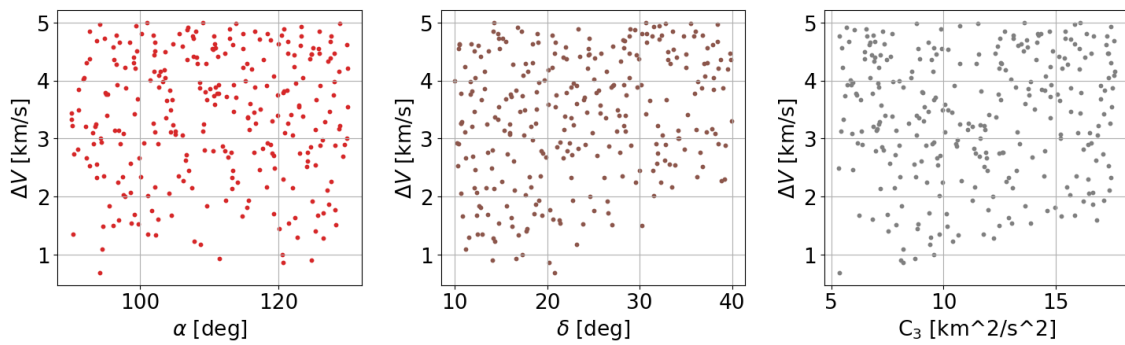
Figure A.4: Monte Carlo analysis results, hyperbolic transfer free parameters and objective function results (ΔV), seed 2358. Results shown are filtered, only results with ΔV < 5 km/s.
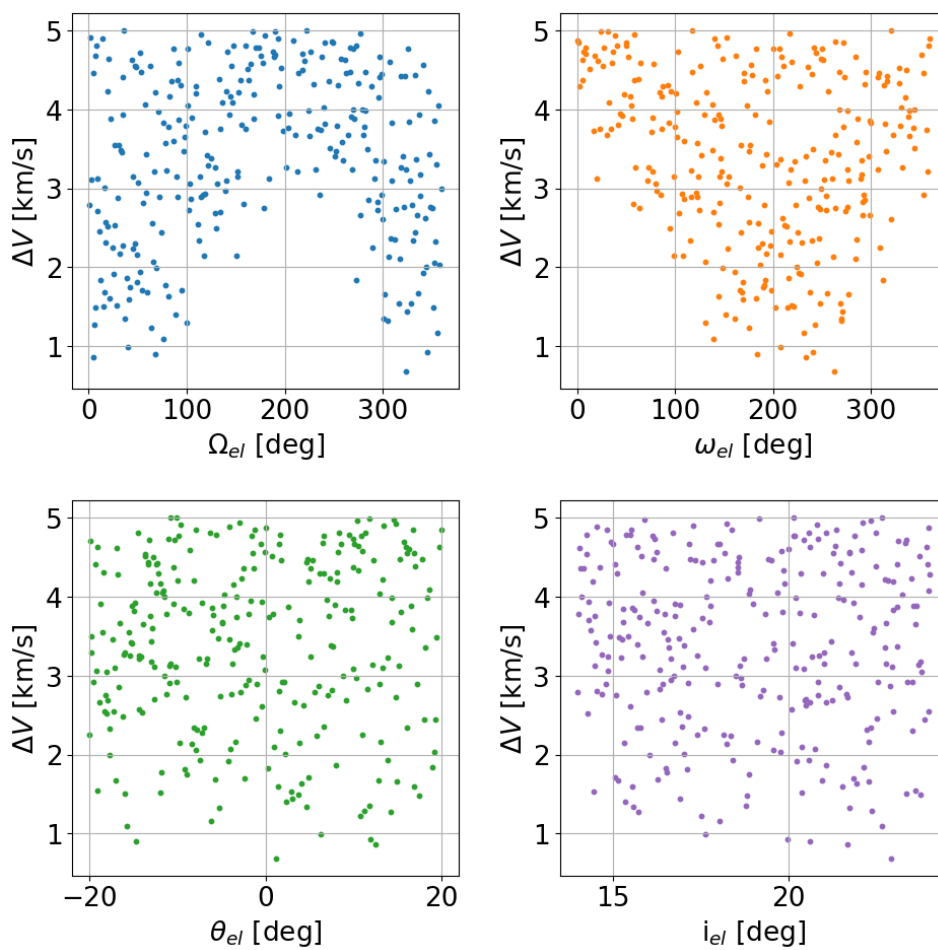
Figure A.5: Monte Carlo analysis results, elliptical arrival orbit free parameters, case A1, and objective function results (ΔV), seed 2358. Results shown are filtered, only results with ΔV < 5 km/s.
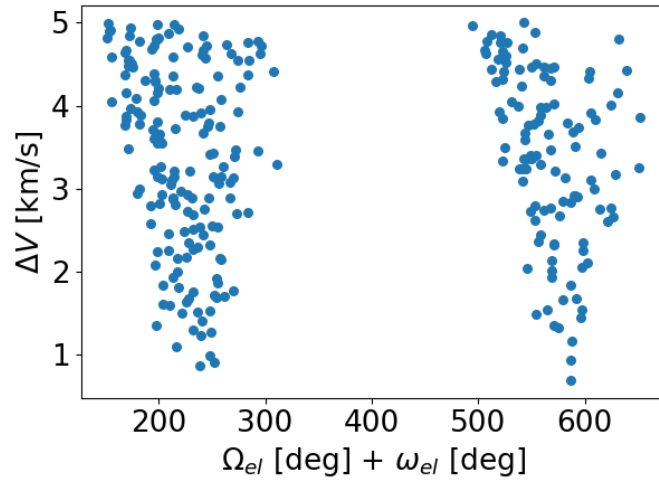
Figure A.6: Monte Carlo analysis results, elliptical arrival orbit free parameters, case A1, and objective function results (ΔV), seed 2358. Results shown are filtered, only results with ΔV < 5 km/s.
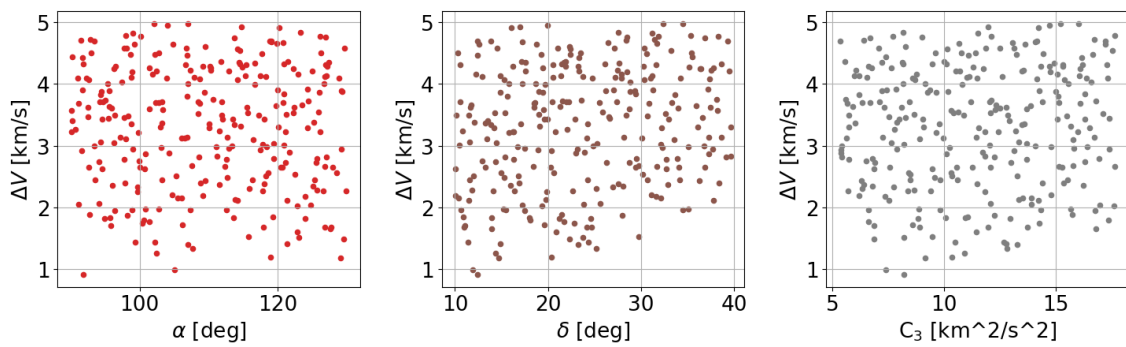
A.3. Seed 3682

Figure A.7: Monte Carlo analysis results, hyperbolic transfer free parameters and objective function results (ΔV), seed 3682. Results shown are filtered, only results with ΔV < 5 km/s.
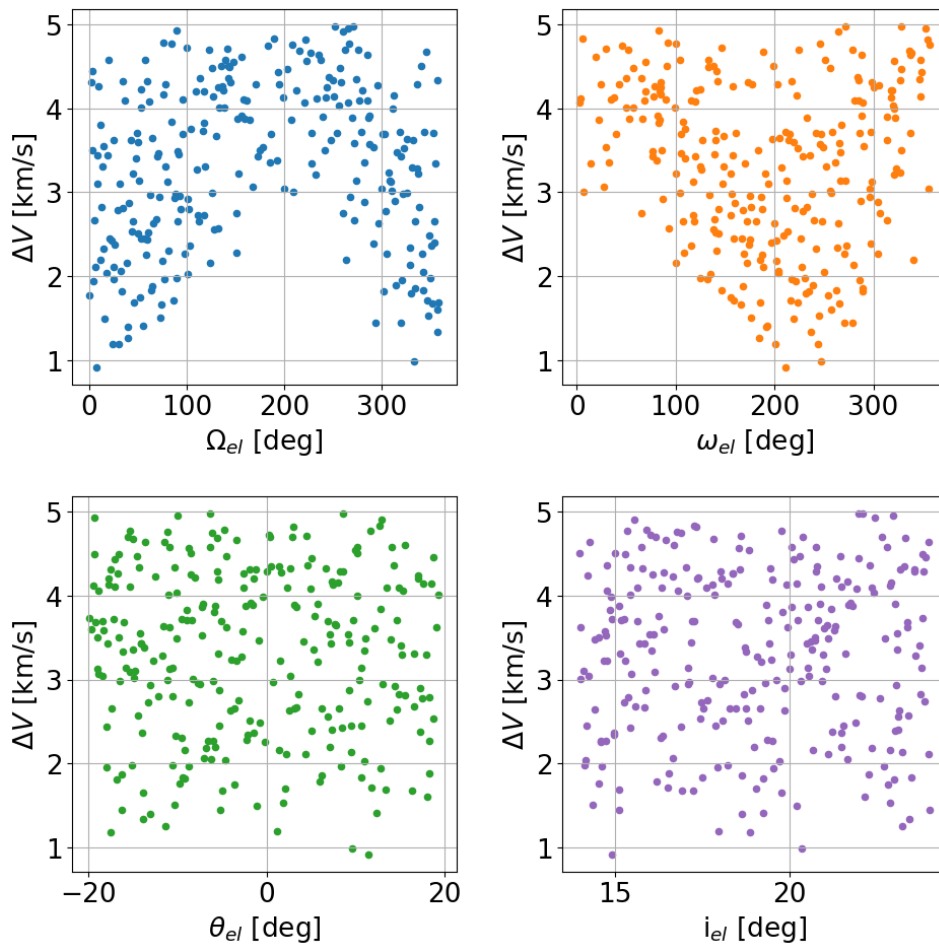
Figure A.8: Monte Carlo analysis results, elliptical arrival orbit free parameters, case A1, and objective function results (ΔV), seed 3682. Results shown are filtered, only results with ΔV < 5 km/s.
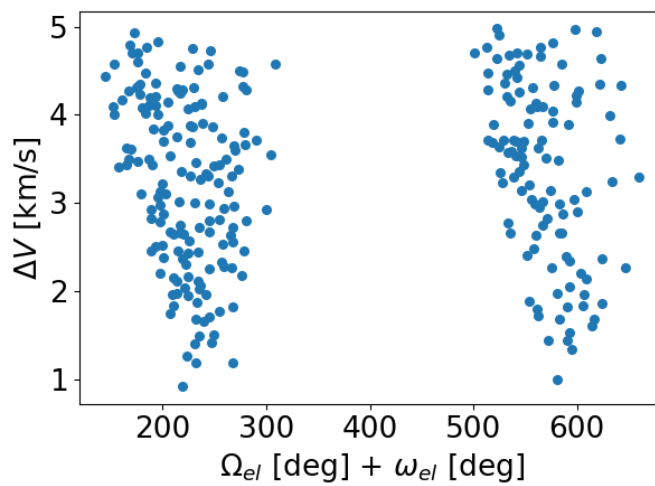
Figure A.9: Monte Carlo analysis results, elliptical arrival orbit free parameters, case A1, and objective function results (ΔV), seed 3682. Results shown are filtered, only results with ΔV < 5 km/s.

B

Appendix B

The following appendix is dedicated to showing all the results of the optimizer tuning process discussed in Section 5.8. The analysis has been repeated across multiple seeds to ensure the most reliable tuning of the DE optimizer. For each parameter (F, CR, NP) the optimization has been run till convergence (according to the criteria mentioned in Chapter 5). For each generation, three metrics have been computed and shown in the graphs:

- Result of the optimization objective of the best individual (minimum ΔV of that generation).

- Average of the population objective values (ΔV).

- Standard deviation of the population objective values (ΔV).

B.1. Seed 1728
Tuning F
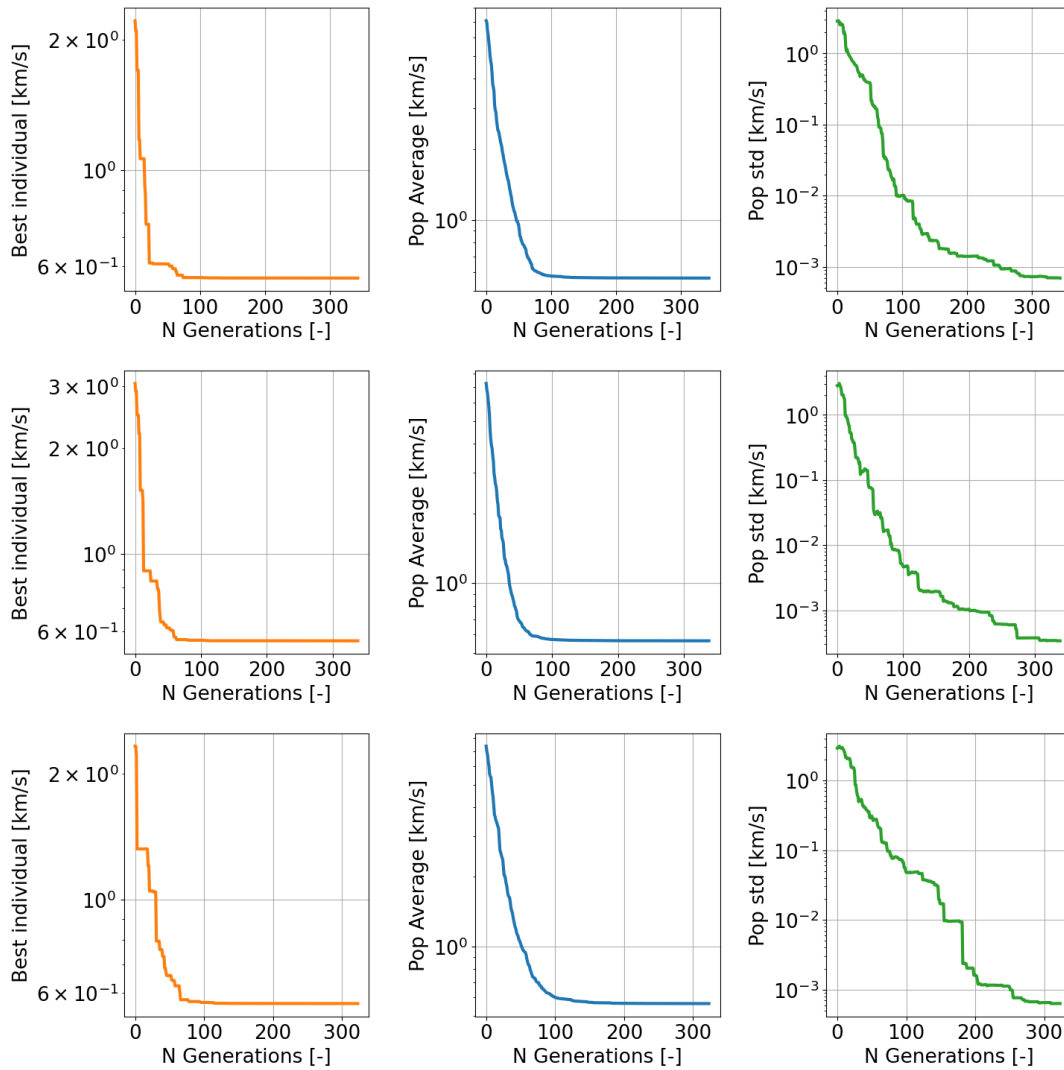
Figure B.1: Statistical data on the ΔV values of the A1-left insertion problem, seed number = 1721. F = 0.5 (top), F = 0.4 (center), F = 1.0 (bottom). For all: CR = 0.1 , NP = 20.
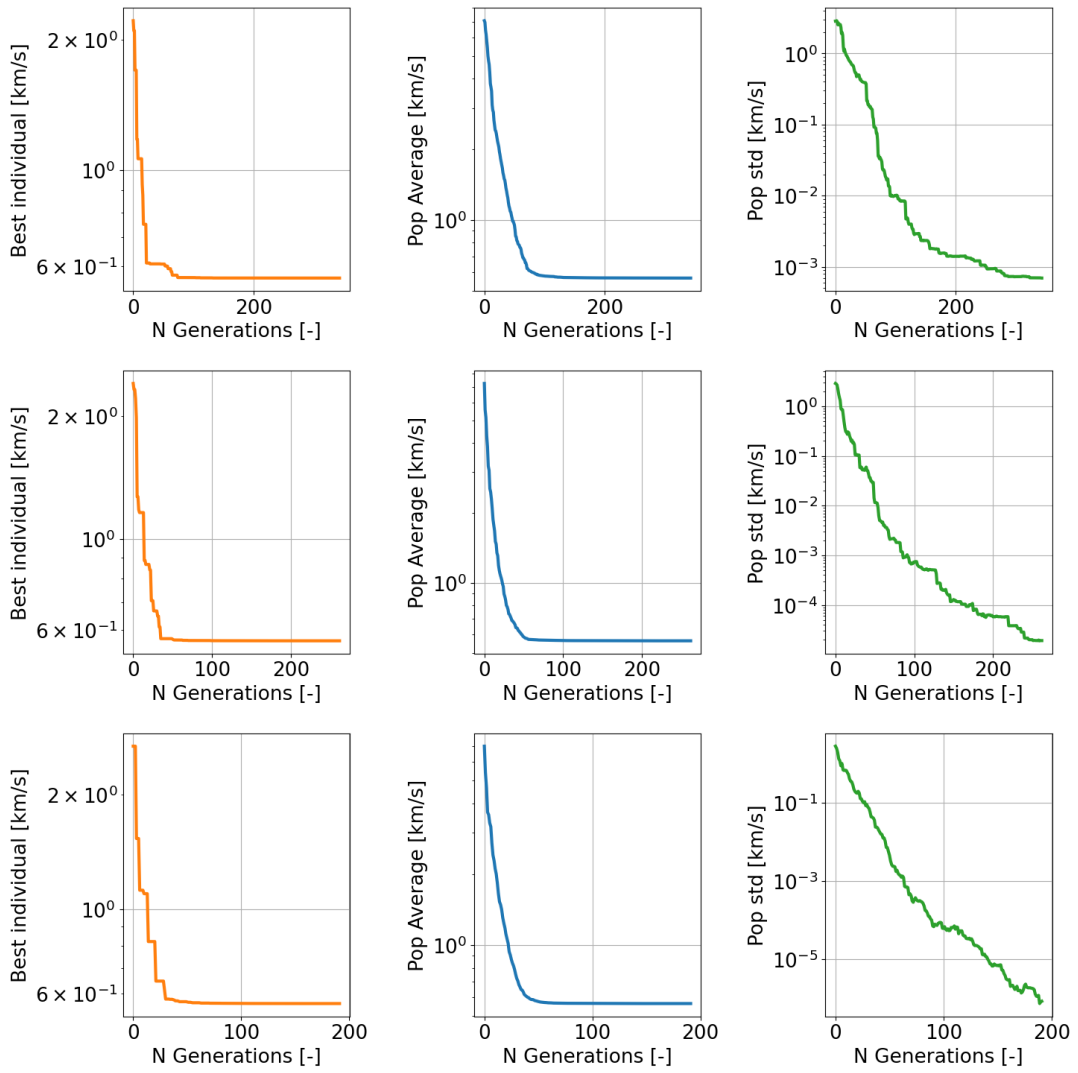
Tuning CR

Figure B.2: Statistical data on the ΔV values of the A1-left insertion problem, seed number = 1721. CR = 0.1 (top), CR = 0.5 (center), CR = 0.9 (bottom). For all: F = 0.5, NP = 20.
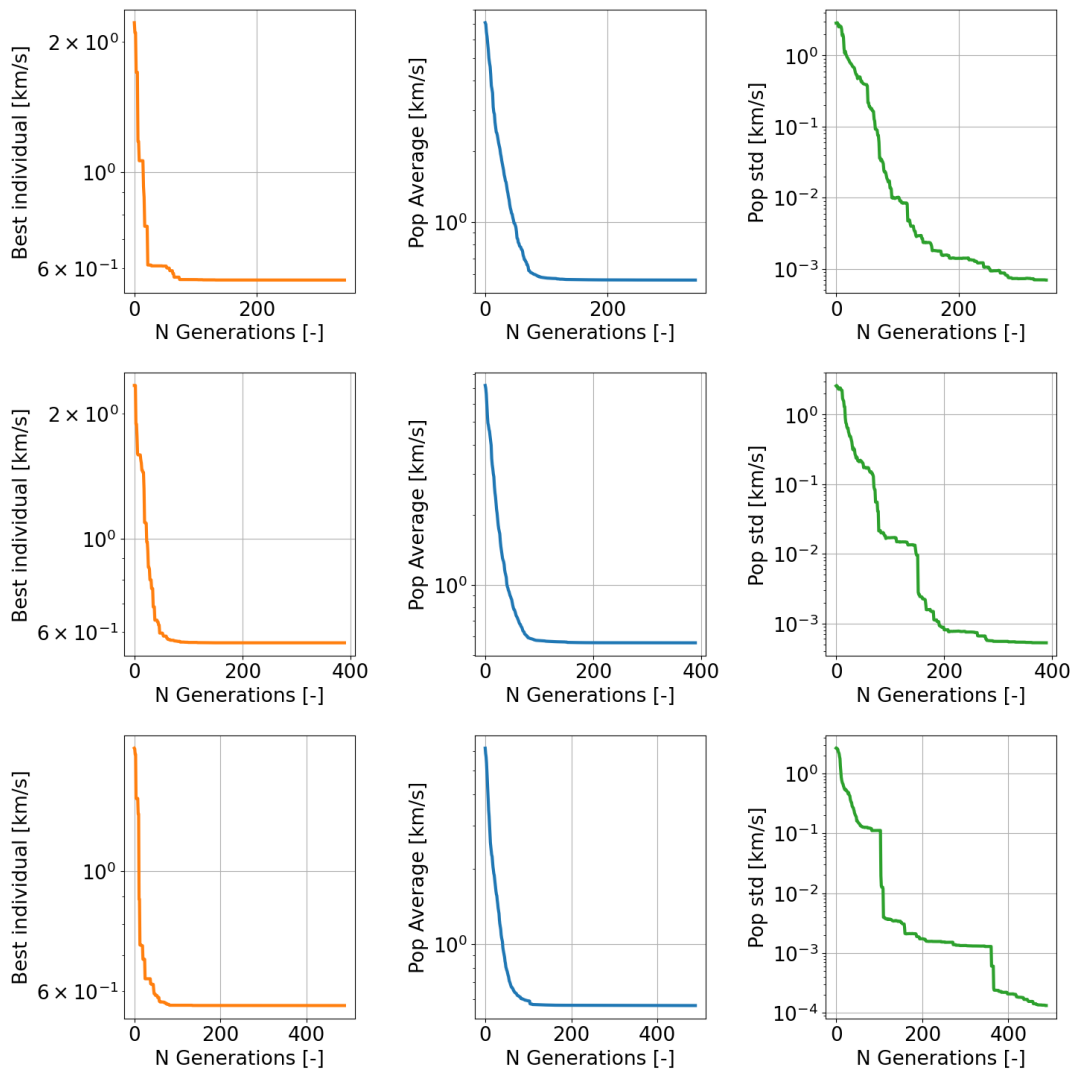
Tuning NP

Figure B.3: Statistical data on the ΔV values of the A1-left insertion problem, seed number = 1721. NP = 20 (top), NP = 35 (center), NP = 50 (bottom). For all: F = 0.5, CR = 0.1.

B.2. Seed 2358
Tuning F
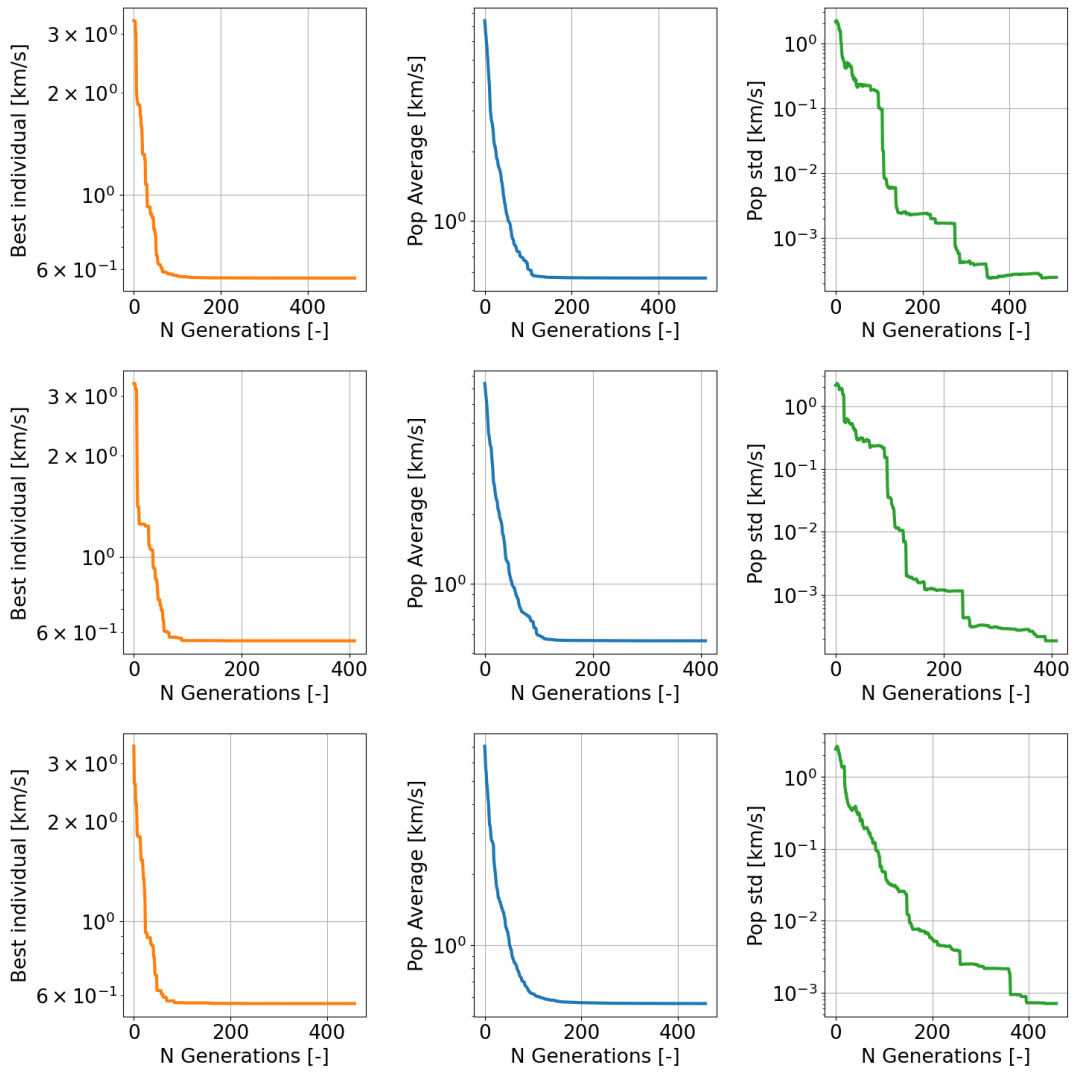
Figure B.4: Statistical data on the ΔV values of the A1-left insertion problem, seed number = 2358. F = 0.5 (top), F = 0.4 (center), F = 1.0 (bottom). For all: CR = 0.1 , NP = 20.
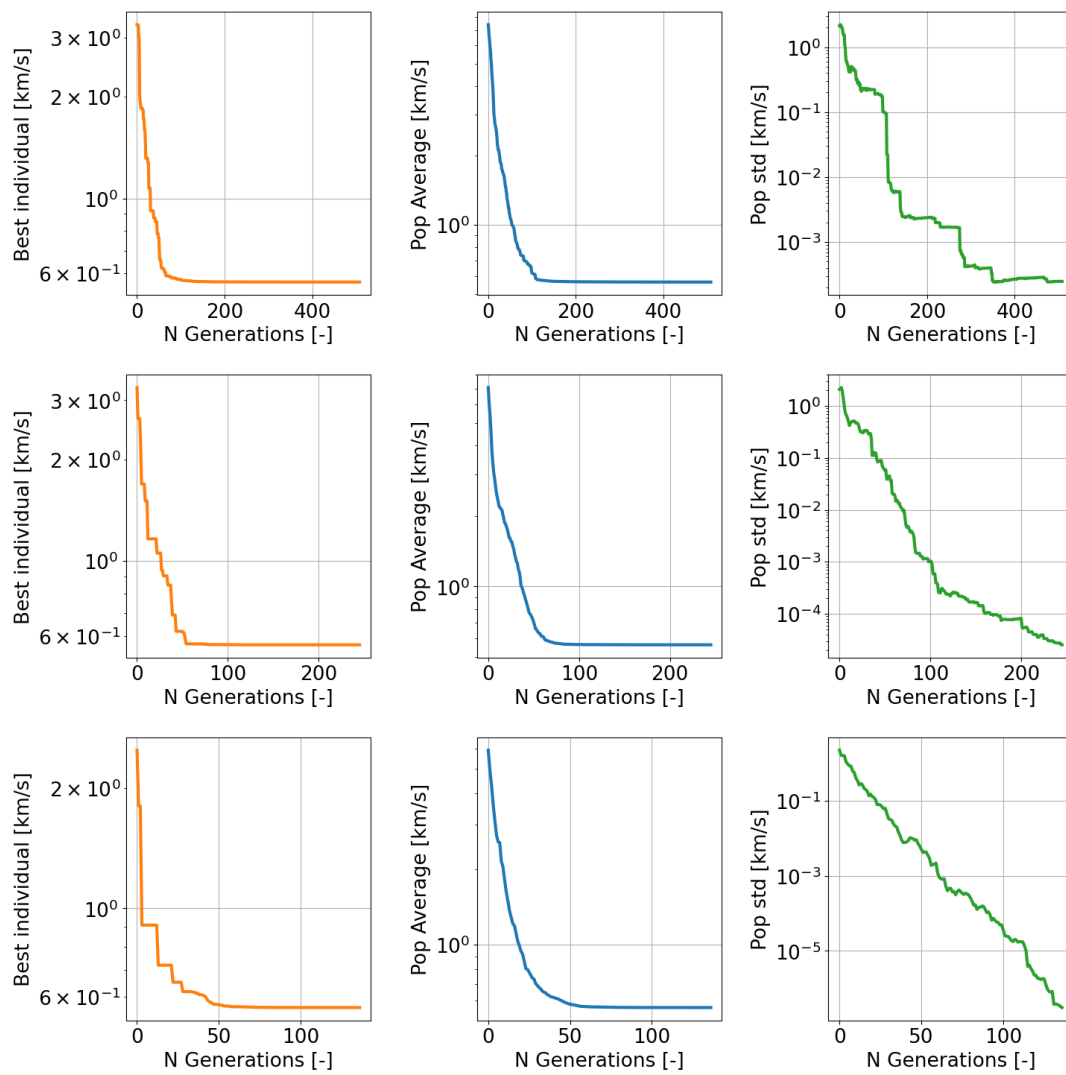
Tuning CR

Figure B.5: Statistical data on the ΔV values of the A1-left insertion problem, seed number = 2358. CR = 0.1 (top), CR = 0.5 (center), CR = 0.9 (bottom). For all: F = 0.5, NP = 20.
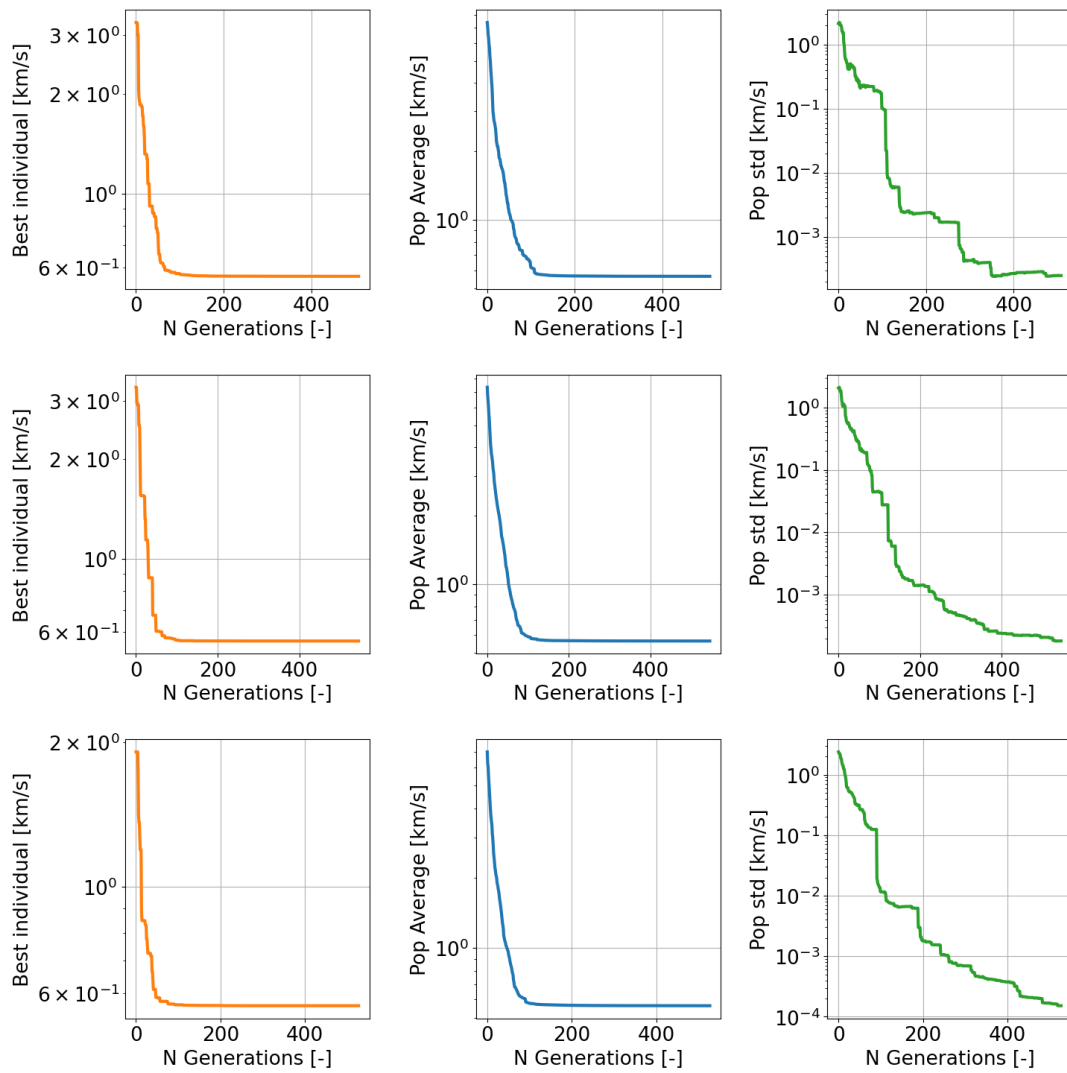
Tuning NP

Figure B.6: Statistical data on the ΔV values of the A1-left insertion problem, seed number = 2358. NP = 20 (top), NP = 35 (center), NP = 50 (bottom). For all: F = 0.5, CR = 0.1.

B.3. Seed 3682
Tuning F
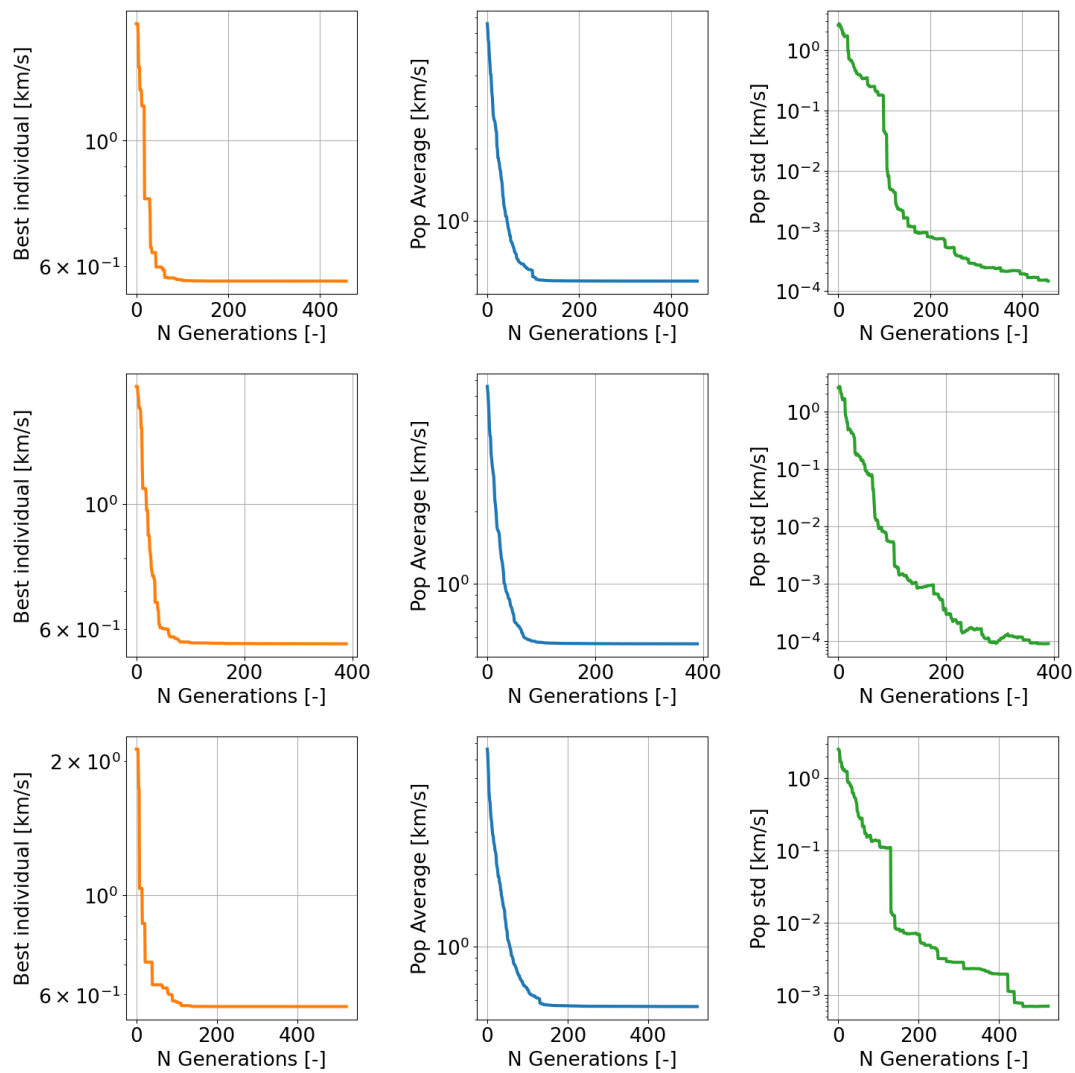
Figure B.7: Statistical data on the ΔV values of the A1-left insertion problem, seed number = 3682. F = 0.5 (top), F = 0.4 (center), F = 1.0 (bottom). For all: CR = 0.1 , NP = 20.
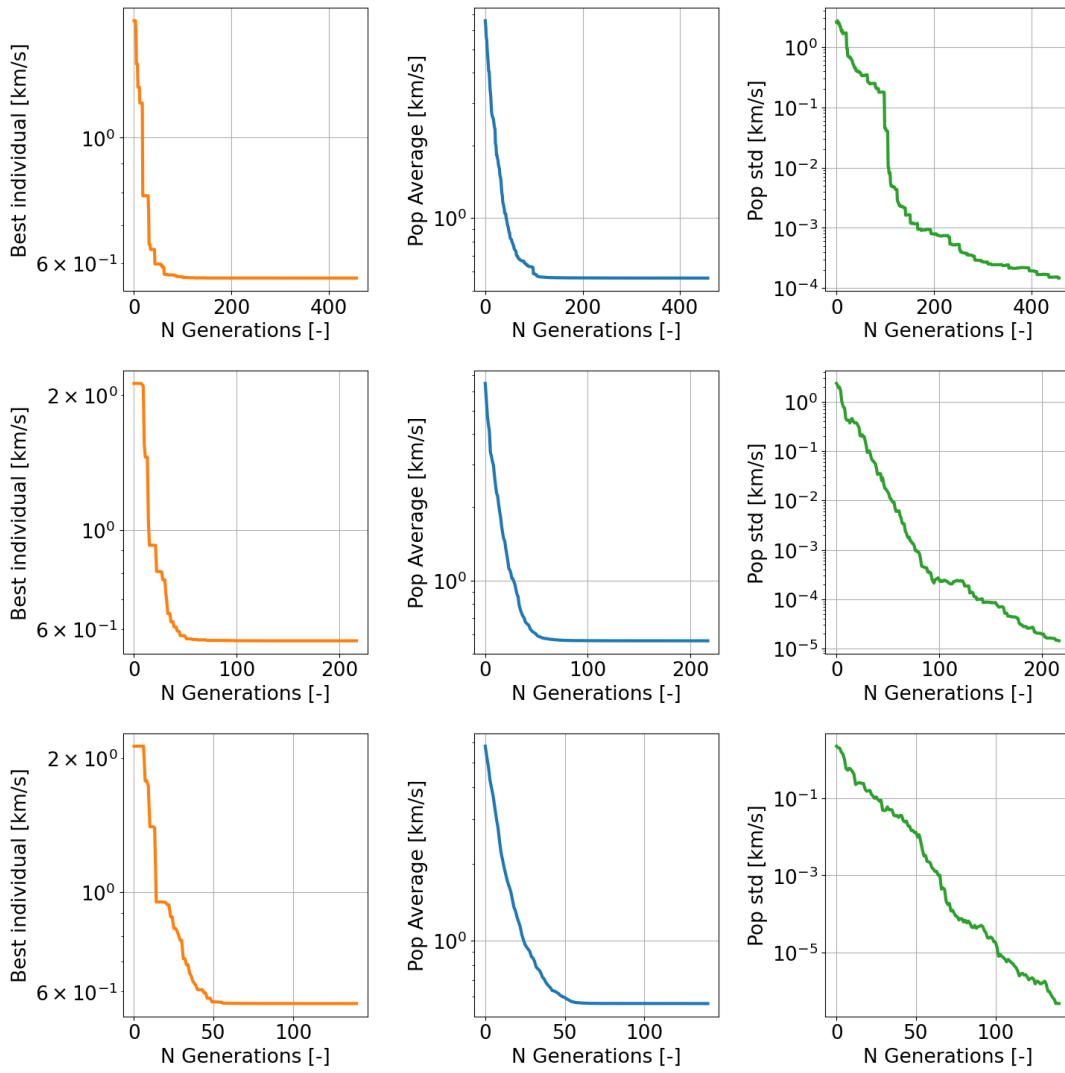
Tuning CR

Figure B.8: Statistical data on the ΔV values of the A1-left insertion problem, seed number = 3682. CR = 0.1 (top), CR = 0.5 (center), CR = 0.9 (bottom). For all: F = 0.5, NP = 20.

Tuning NP
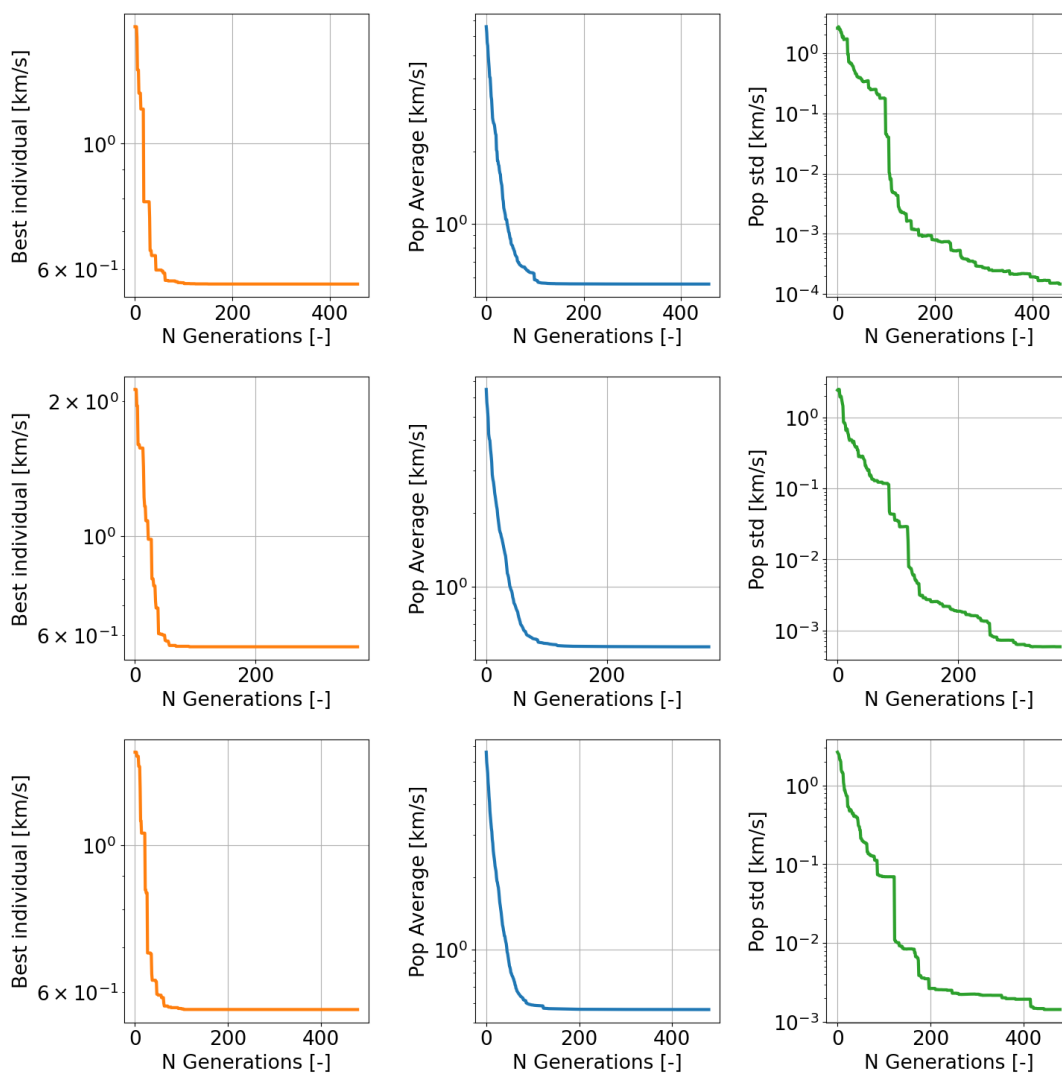
Figure B.9: Statistical data on the ΔV values of the A1-left insertion problem, seed number = 3682. NP = 20 (top), NP = 35 (center), NP = 50 (bottom). For all: F = 0.5, CR = 0.1.

C
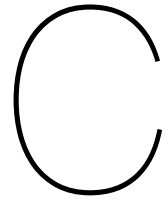
Appendix C

The following appendix is dedicated to the optimization results across multiple seeds. For all cases (A1, A2, P1, P2) the optimization has been repeated for three different seeds, with the same optimizer settings mentioned in Chapter 5. Only the results of the final population are included. The results are presented in the following graphs:

- Initial conditions of the hyperbolic orbit (α, δ, C_3), and hyperbolic asymptote influence on the ΔV.
- Keplerian elements of the final elliptical POs.
- Keplerian elements of the final hyperbolic orbits.

These graphs have been included as proof of the conclusions made in Chapter 6 and Chapter 7.

C.1. Case A1-left
Seed 1721
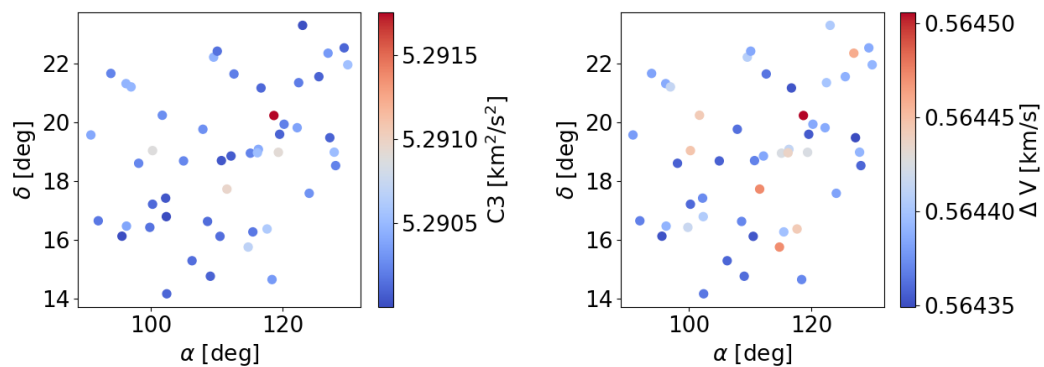
Figure C.1: Results from the final population of hyperbolic orbits, (left) conditions at infinite distance, (right) asymptote angles vs ΔV. A1-left insertion problem, seed number=1721.
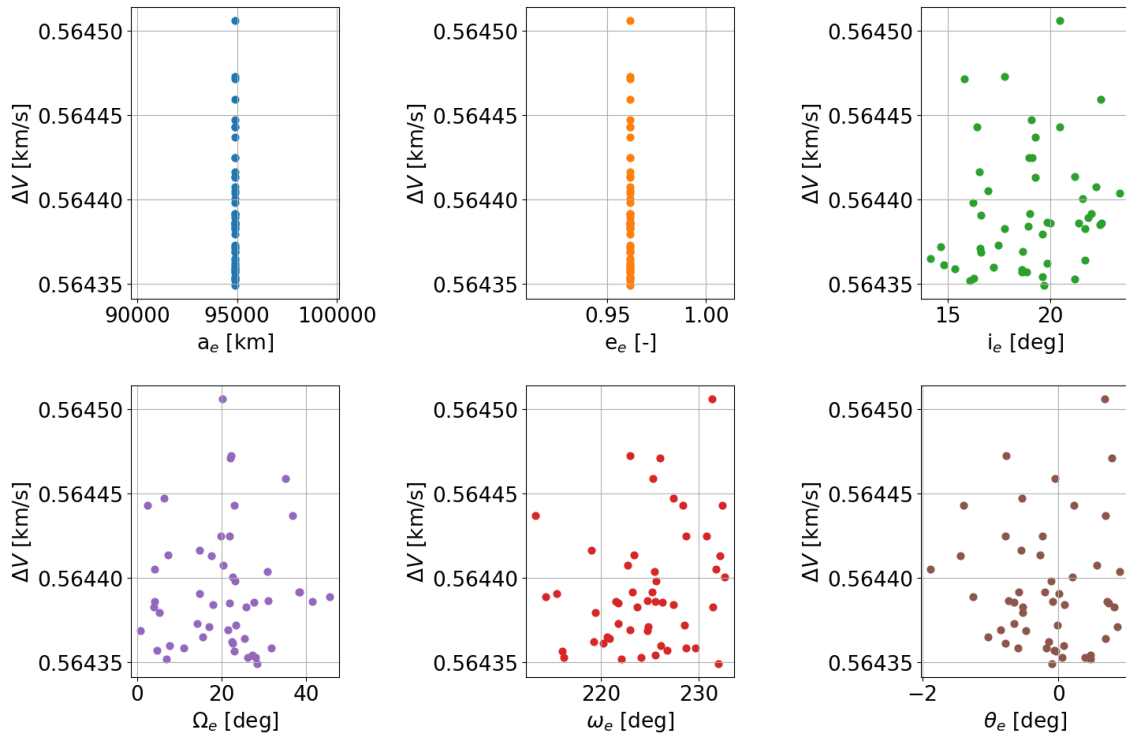
Figure C.2: Results from the final population of elliptical parking orbits, A1-left insertion problem, seed number=1721.
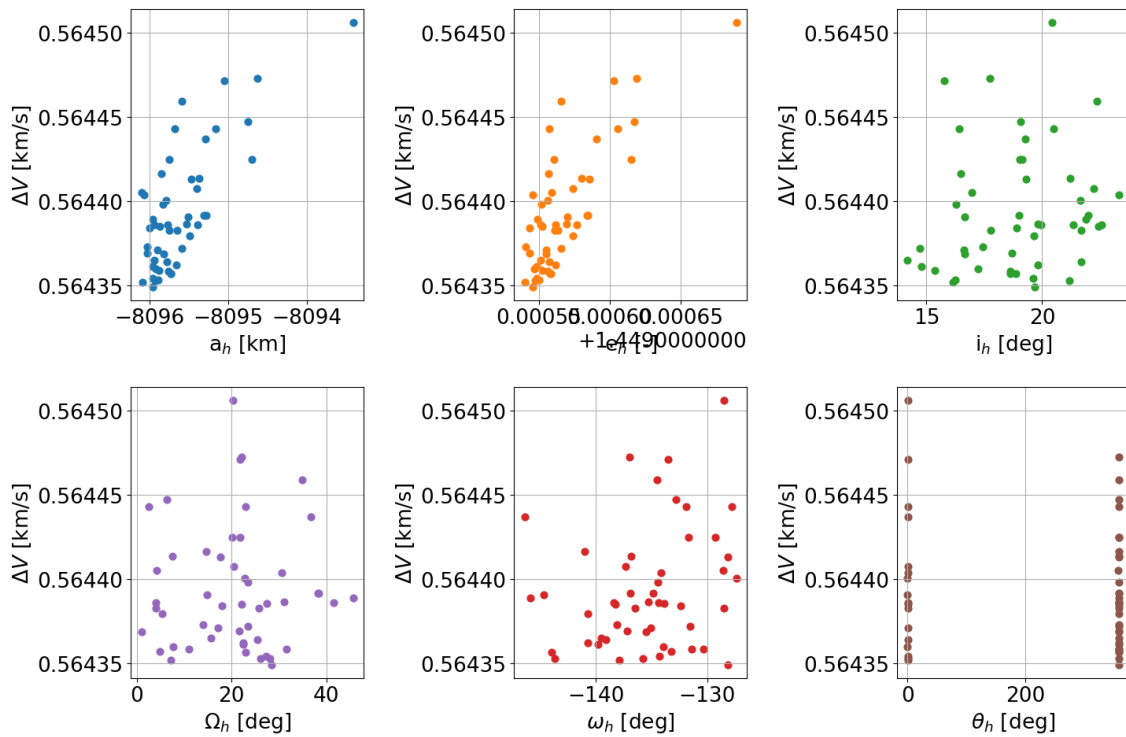
Figure C.3: Results from the final population of hyperbolic orbits, A1-left insertion problem, seed number=1721.

Seed 2358
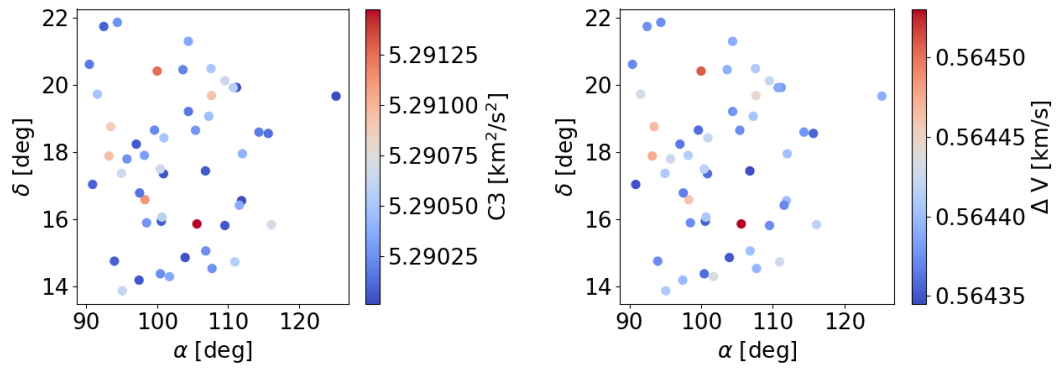
Figure C.4: Results from the final population of hyperbolic orbits, (left) conditions at infinite distance, (right) asymptote angles vs ΔV. A1-left insertion problem, seed number=2358
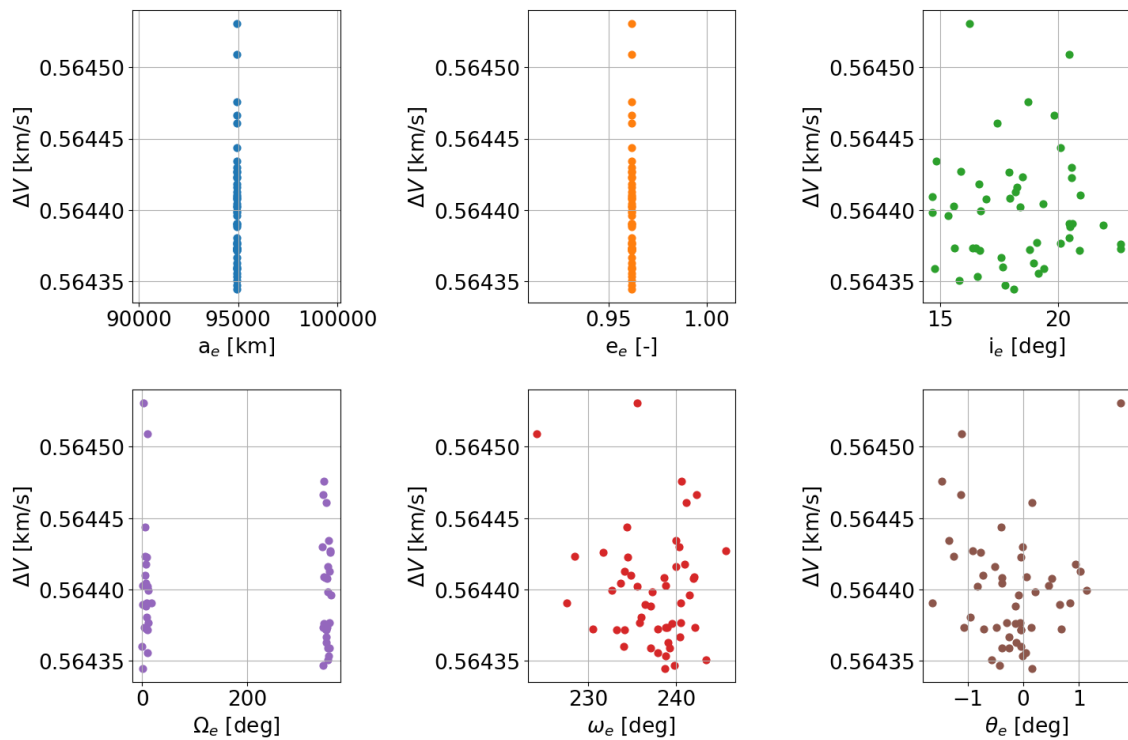
Figure C.5: Results from the final population of elliptical parking orbits, A1-left insertion problem, seed number=2358.
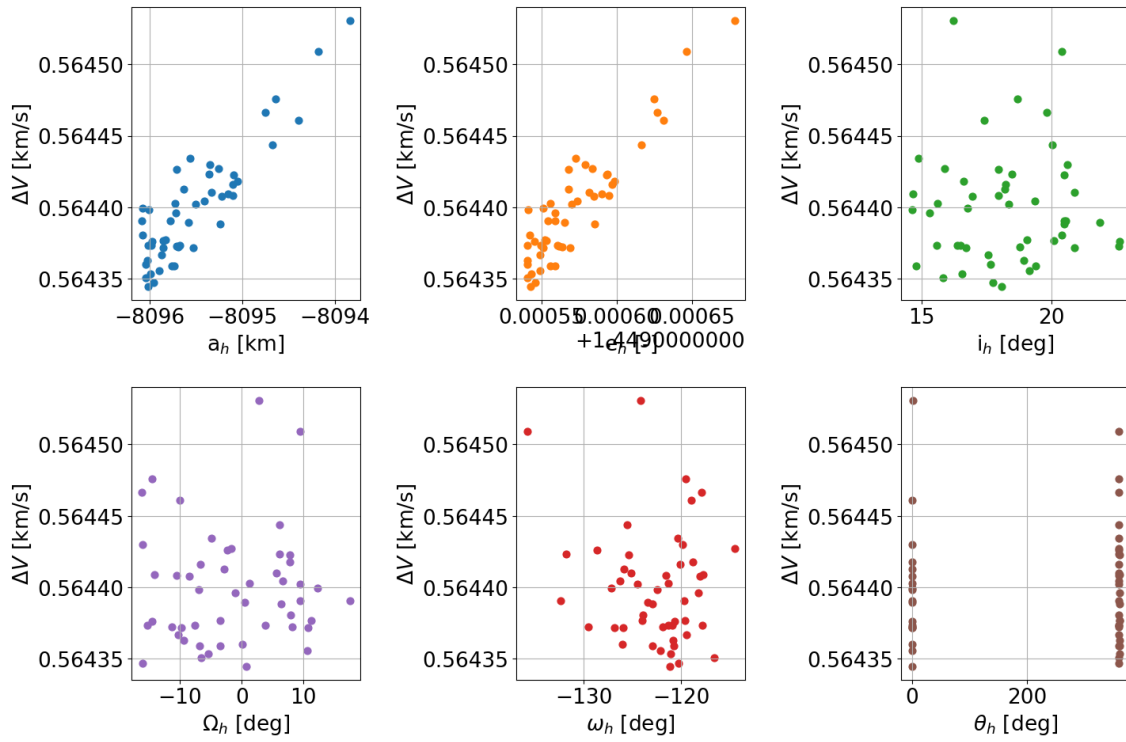
Figure C.6: Results from the final population of hyperbolic orbits, A1-left insertion problem, seed number=2358.

Seed 3682
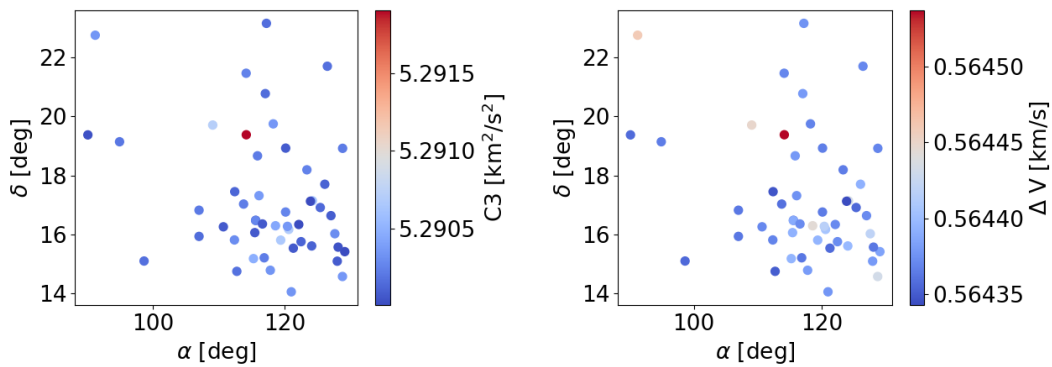
Figure C.7: Results from the final population of hyperbolic orbits, (left) conditions at infinite distance, (right) asymptote angles vs ΔV. A1-left insertion problem, seed number=3682
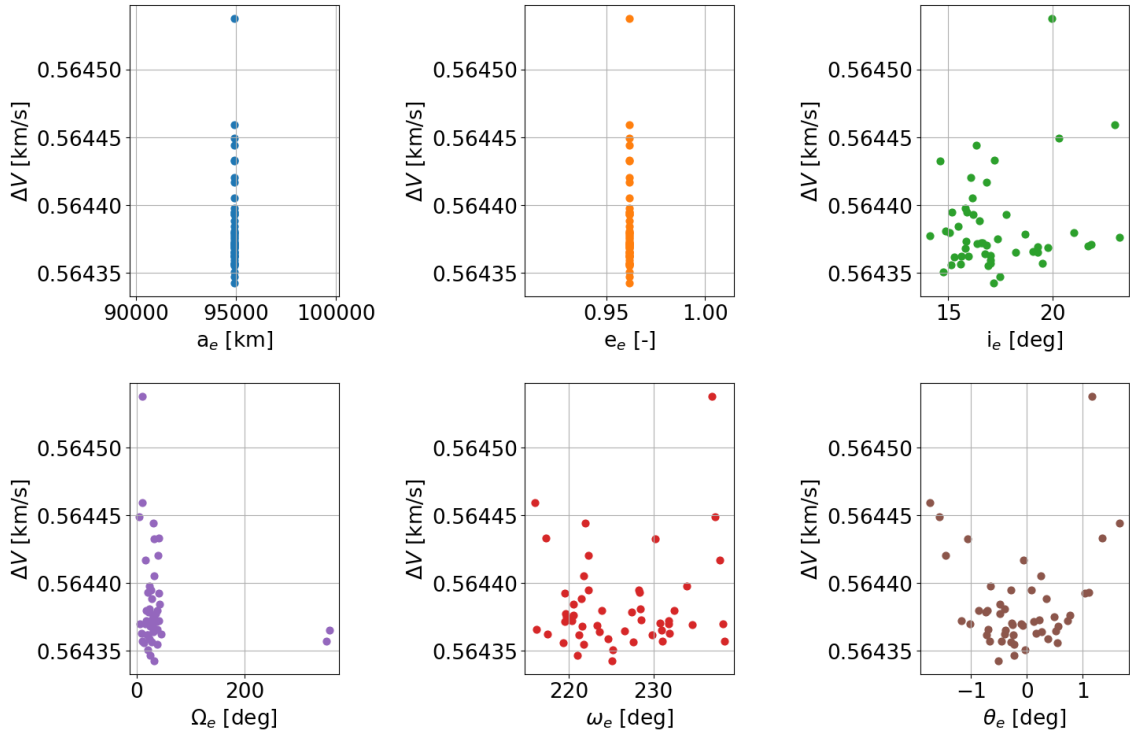
Figure C.8: Results from the final population of elliptical parking orbits, A1-left insertion problem, seed number=3682.
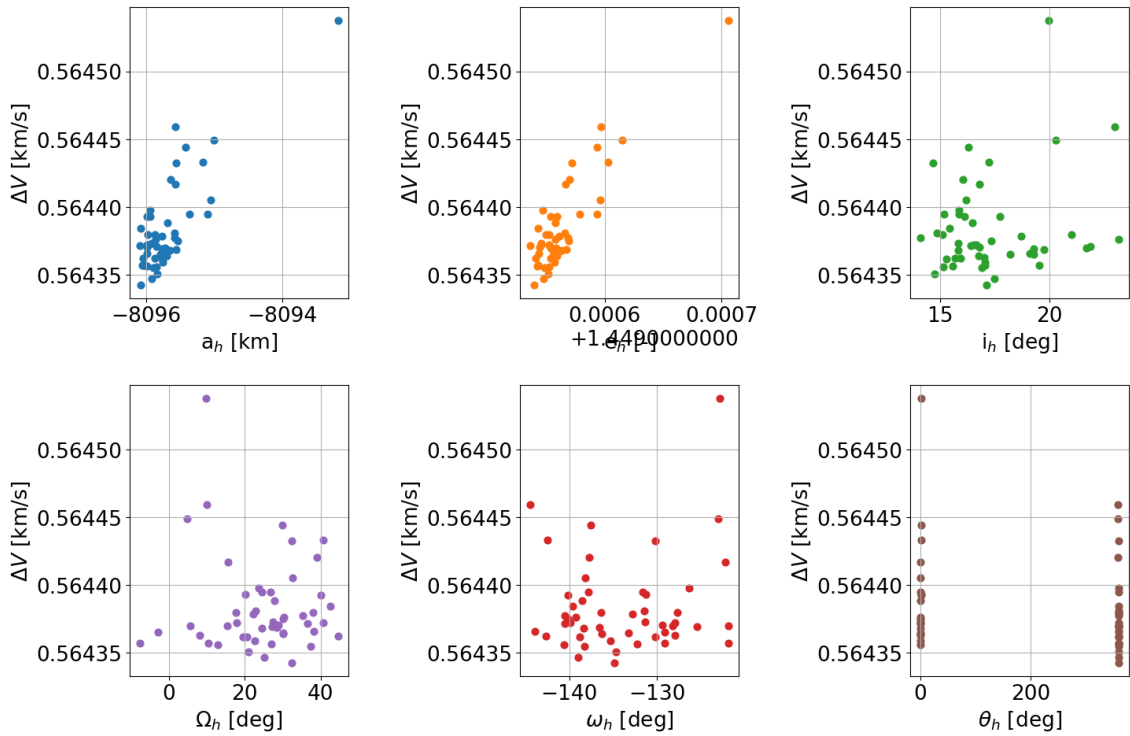
Figure C.9: Results from the final population of hyperbolic orbits, A1-left insertion problem, seed number=3682.

C.2. Case A1-right
Seed 1721
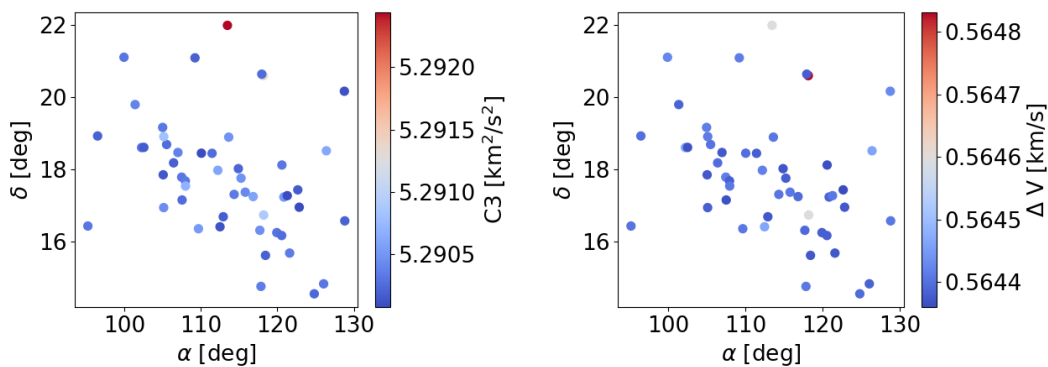
Figure C.10: Results from the final population of hyperbolic orbits, (left) conditions at infinite distance, (right) asymptote angles vs ΔV. A1-right insertion problem, seed number=1721.
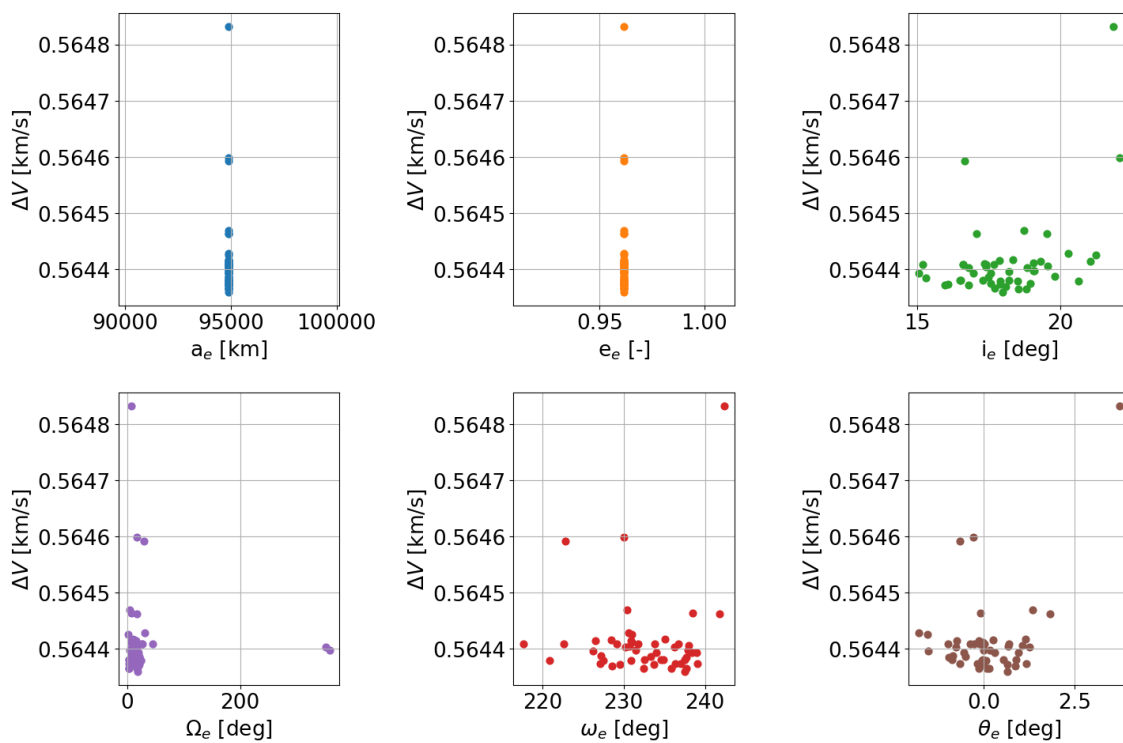
Figure C.11: Results from the final population of elliptical parking orbits, A1-right insertion problem, seed number=1721.
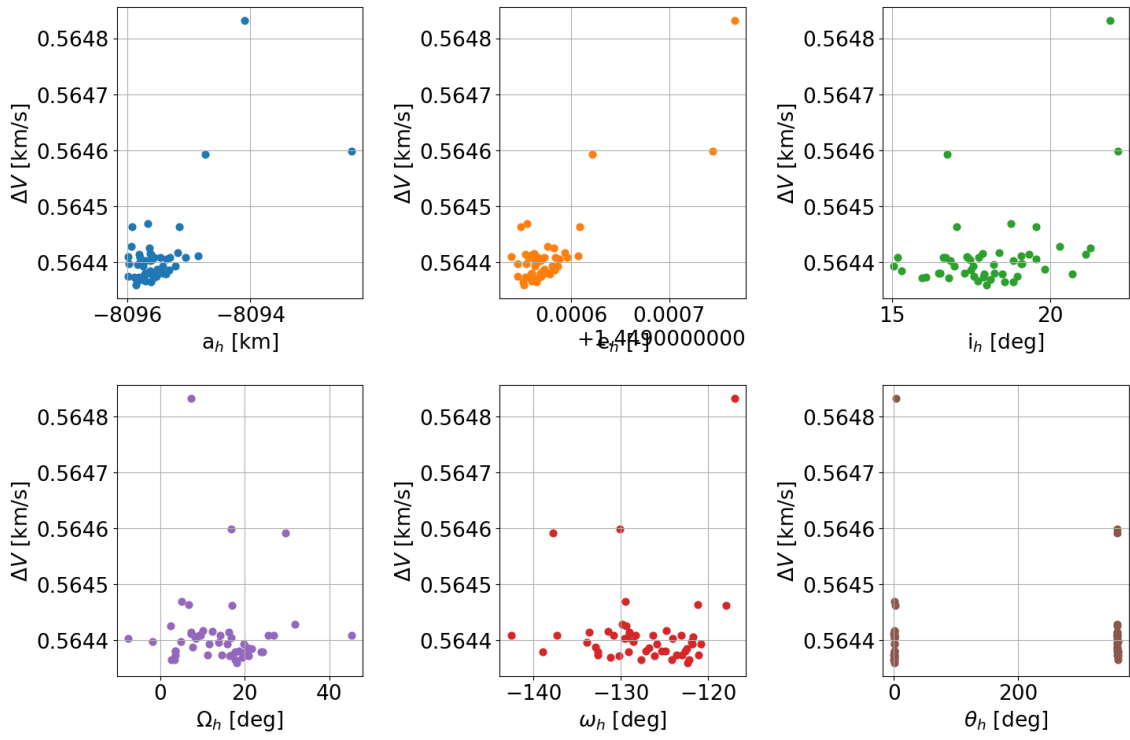
Figure C.12: Results from the final population of hyperbolic orbits, A1-right insertion problem, seed number=1721.

Seed 2358
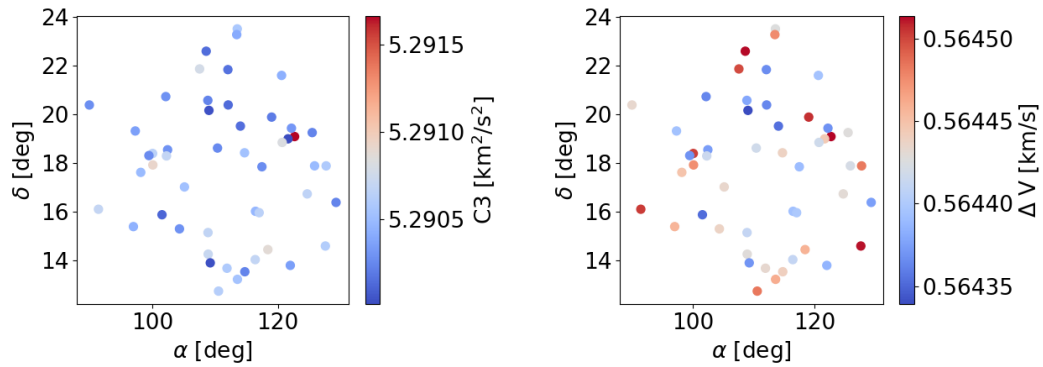
Figure C.13: Results from the final population of hyperbolic orbits, (left) conditions at infinite distance, (right) asymptote angles vs ΔV. A1-right insertion problem, seed number=2358
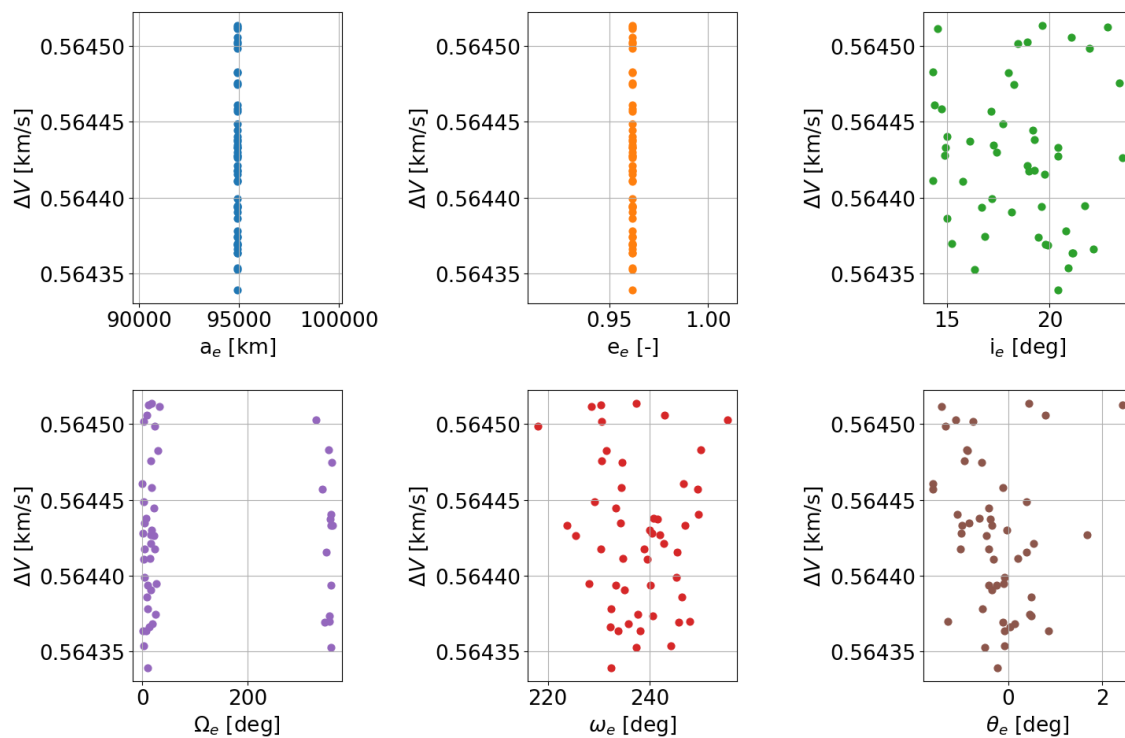
Figure C.14: Results from the final population of elliptical parking orbits, A1-right insertion problem, seed number=2358.
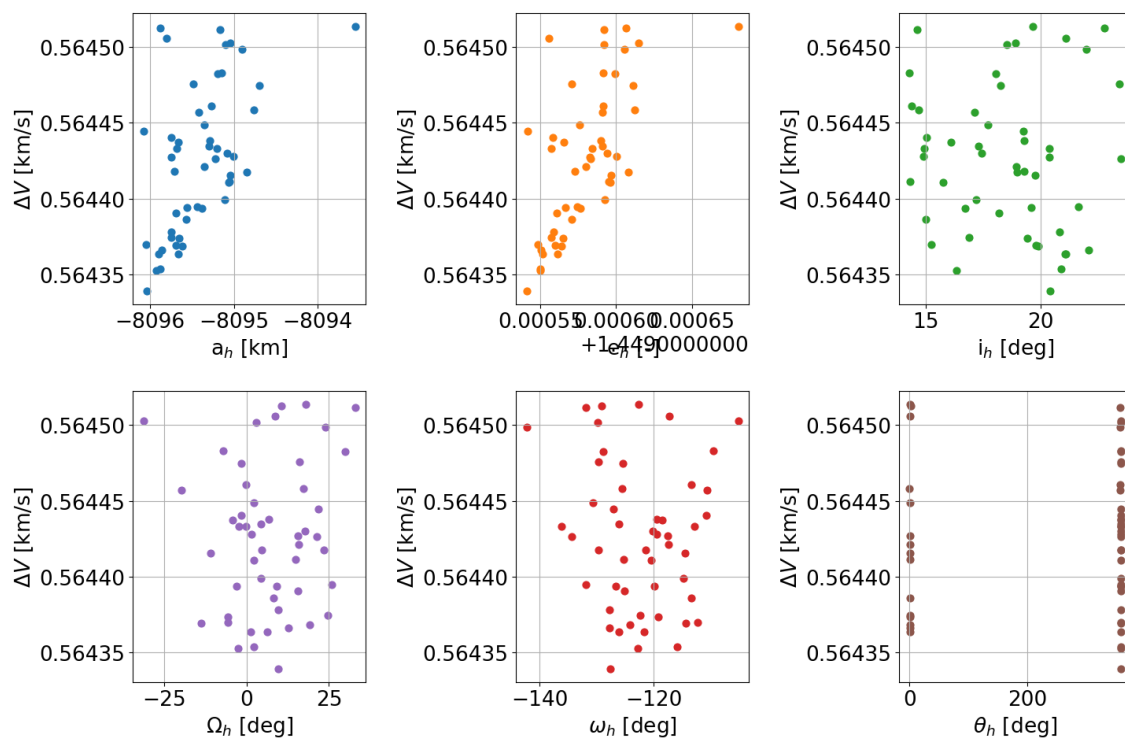
Figure C.15: Results from the final population of hyperbolic orbits, A1-right insertion problem, seed number=2358.

Seed 3682
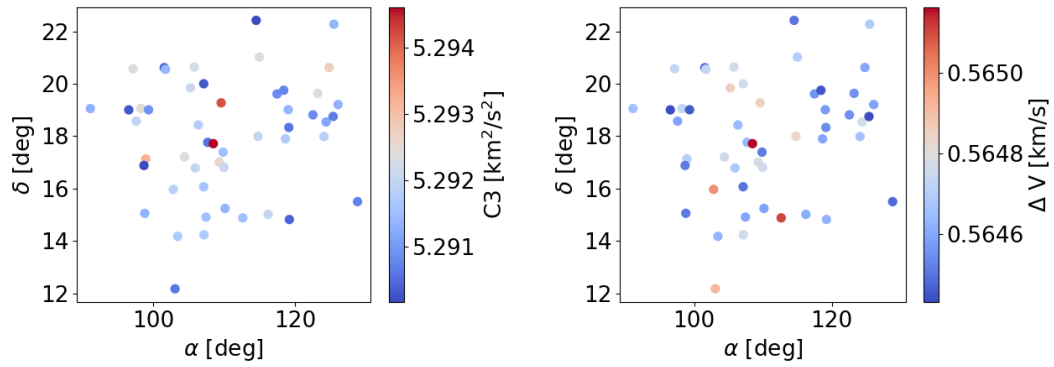
Figure C.16: Results from the final population of hyperbolic orbits, (left) conditions at infinite distance, (right) asymptote angles vs ΔV. A1-right insertion problem, seed number=3682
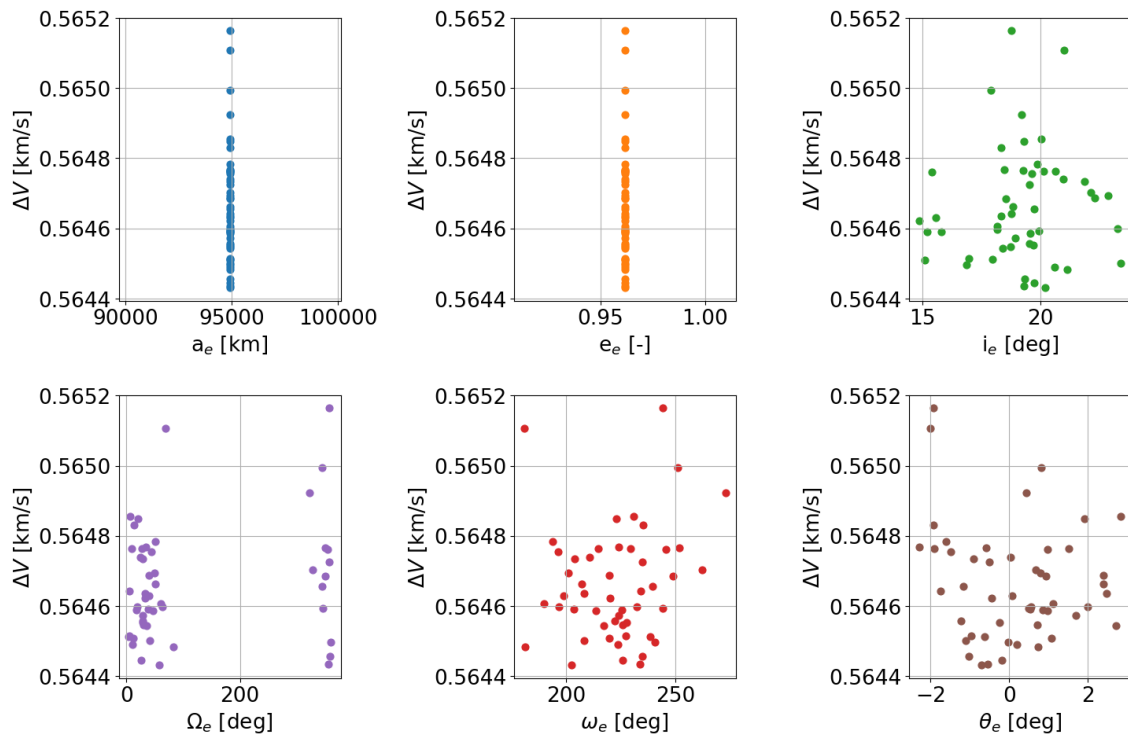
Figure C.17: Results from the final population of elliptical parking orbits, A1-right insertion problem, seed number=3682.
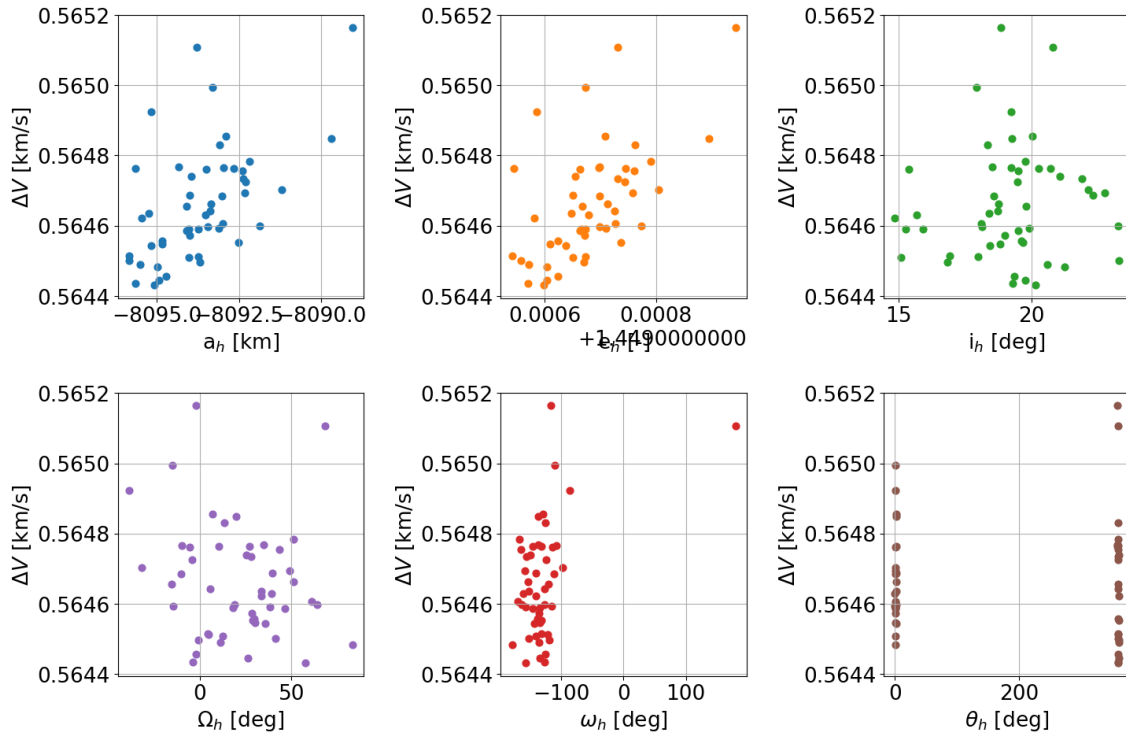
Figure C.18: Results from the final population of hyperbolic orbits, A1-right insertion problem, seed number=3682.

C.3. Case A2-left
Seed 1721
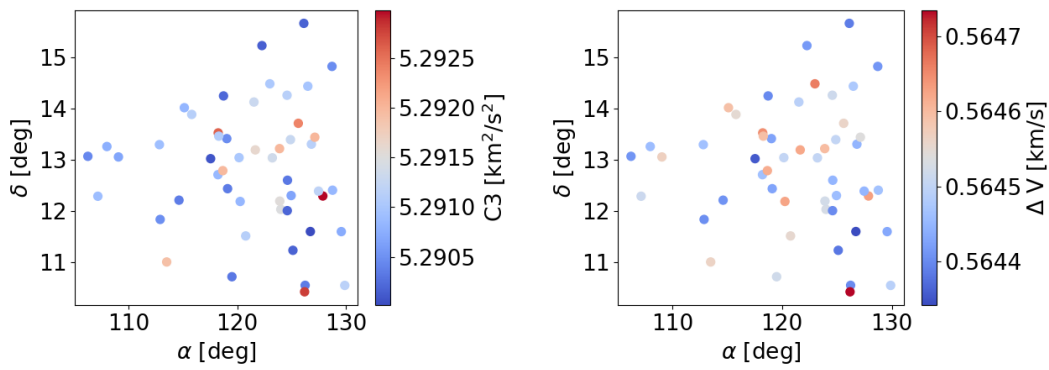
Figure C.19: Results from the final population of hyperbolic orbits, (left) conditions at infinite distance, (right) asymptote angles vs ΔV. A2-left insertion problem, seed number=1721.
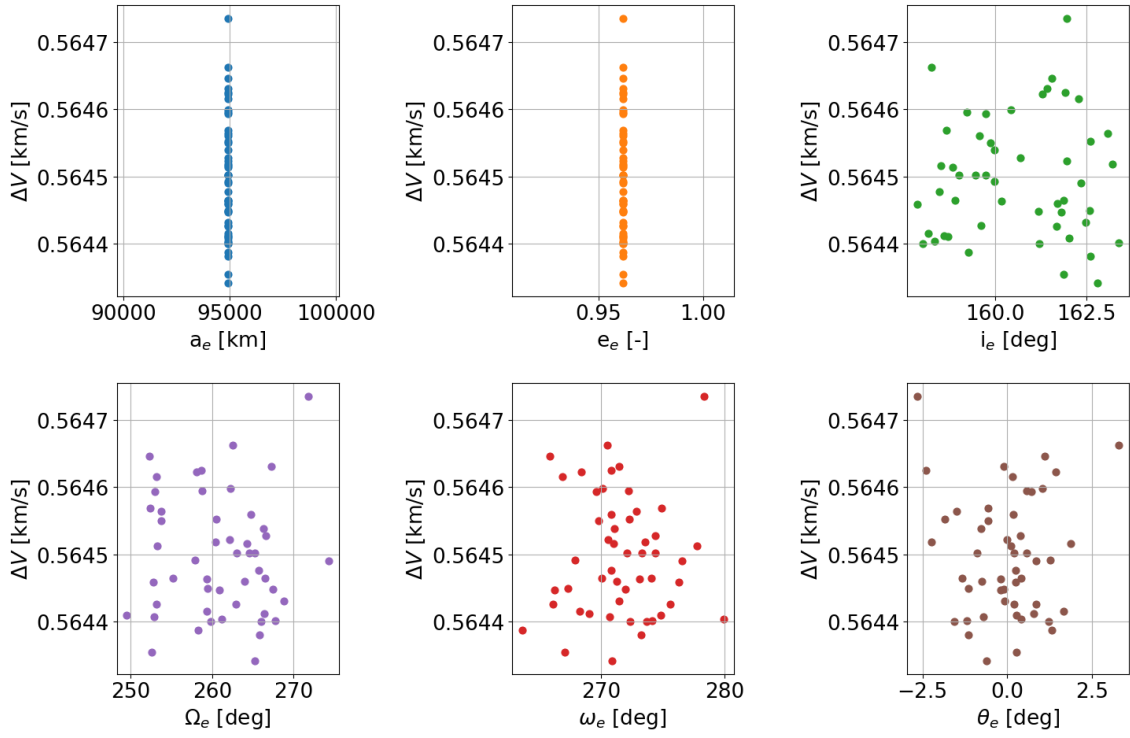
Figure C.20: Results from the final population of elliptical parking orbits, A2-left insertion problem, seed number=1721.
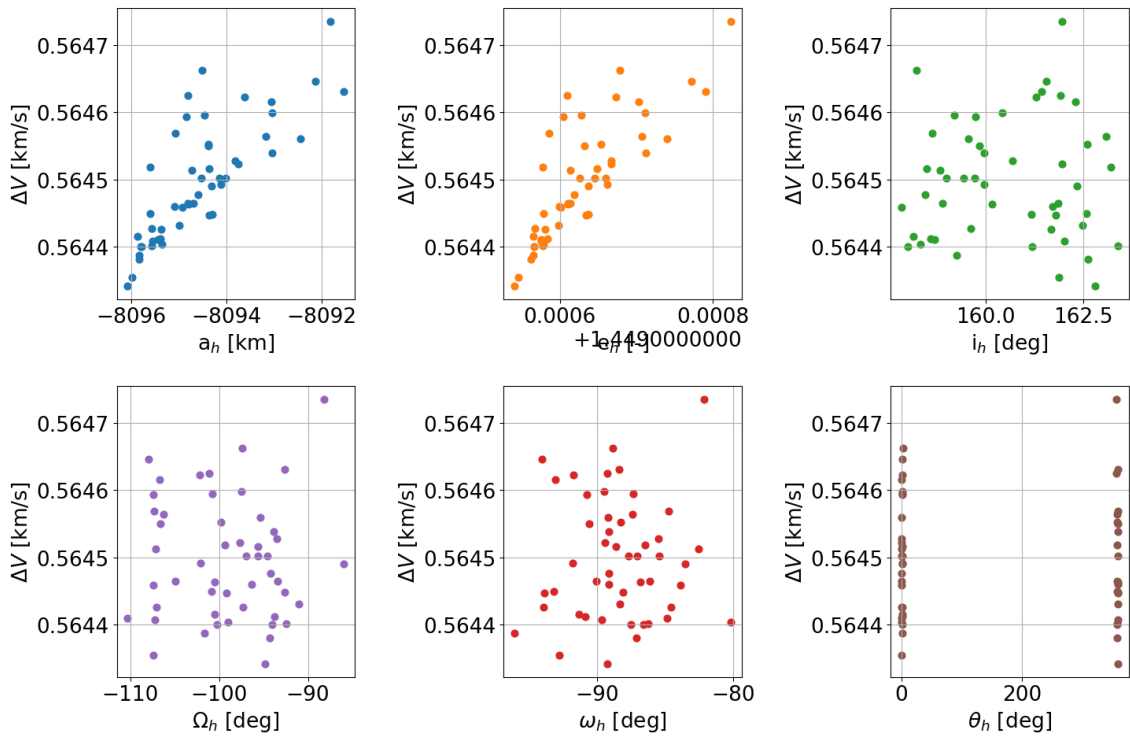
Figure C.21: Results from the final population of hyperbolic orbits, A2-left insertion problem, seed number=1721.

Seed 2358
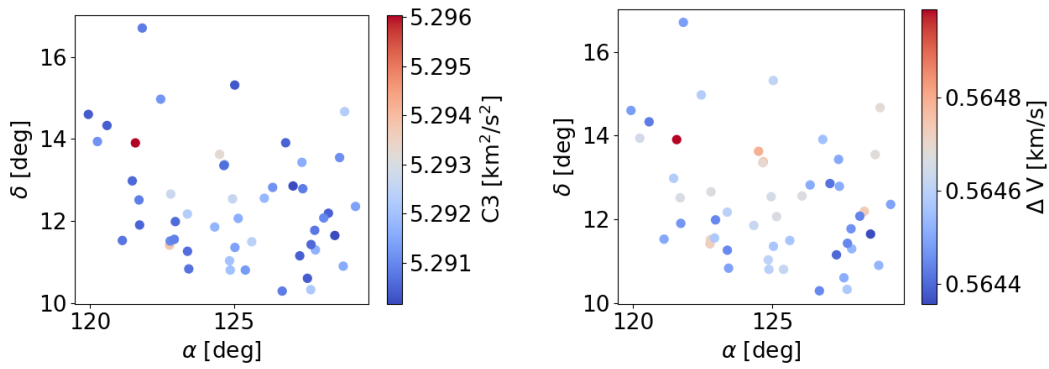
Figure C.22: Results from the final population of hyperbolic orbits, (left) conditions at infinite distance, (right) asymptote angles vs ΔV. A2-left insertion problem, seed number=2358
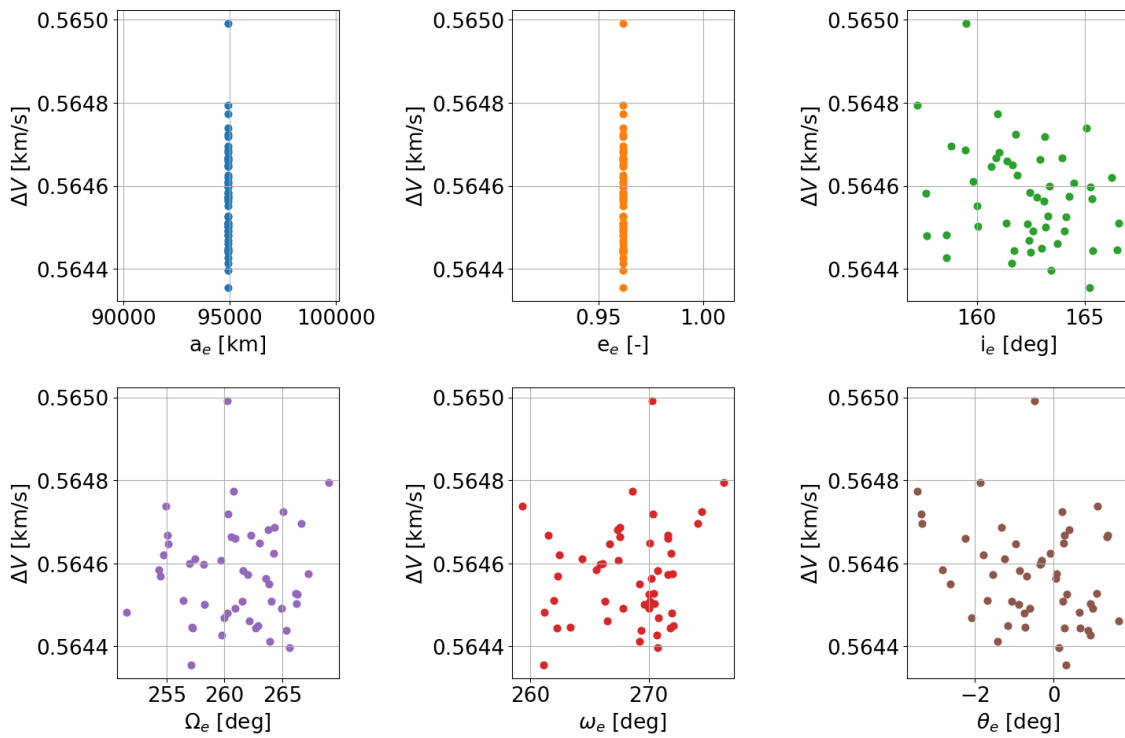
Figure C.23: Results from the final population of elliptical parking orbits, A2-left insertion problem, seed number=2358.
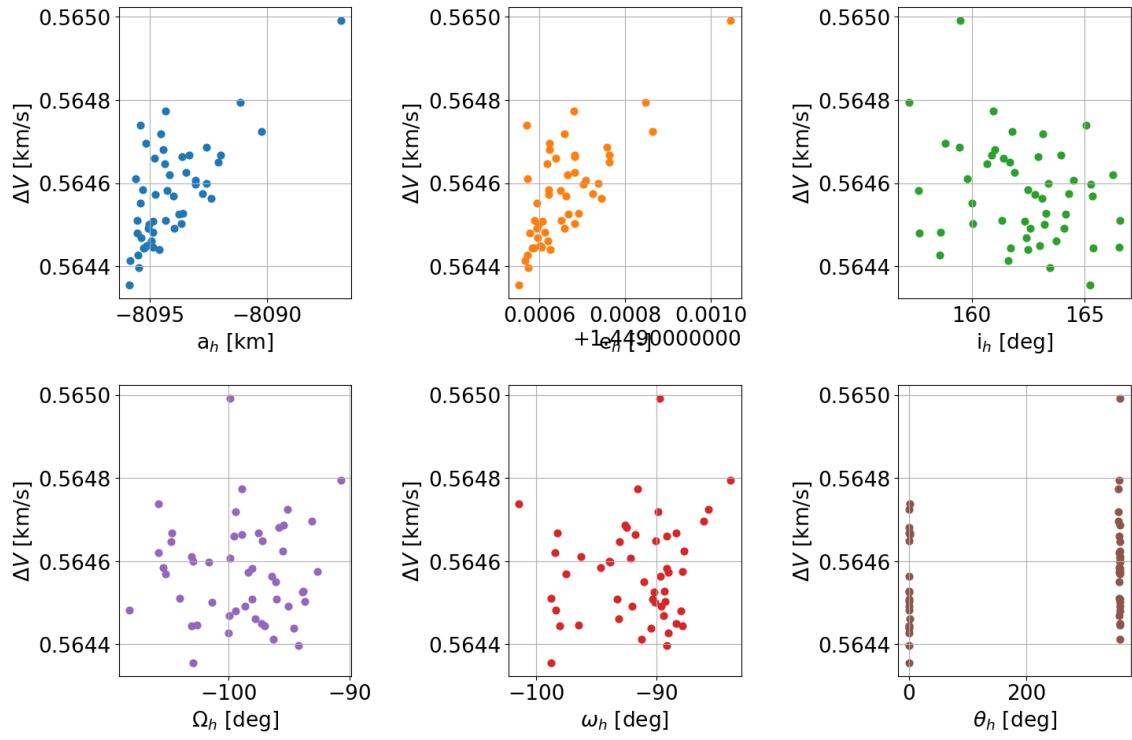
Figure C.24: Results from the final population of hyperbolic orbits, A2-left insertion problem, seed number=2358.

Seed 3682
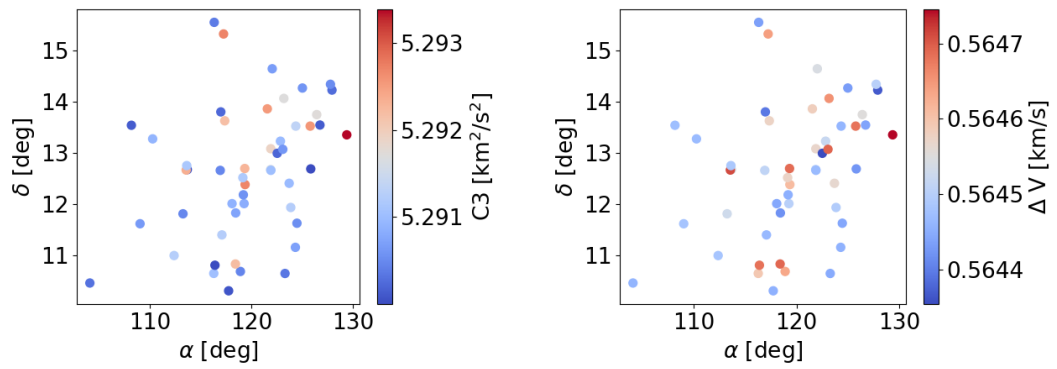
Figure C.25: Results from the final population of hyperbolic orbits, (left) conditions at infinite distance, (right) asymptote angles vs ΔV. A2-left insertion problem, seed number=3682
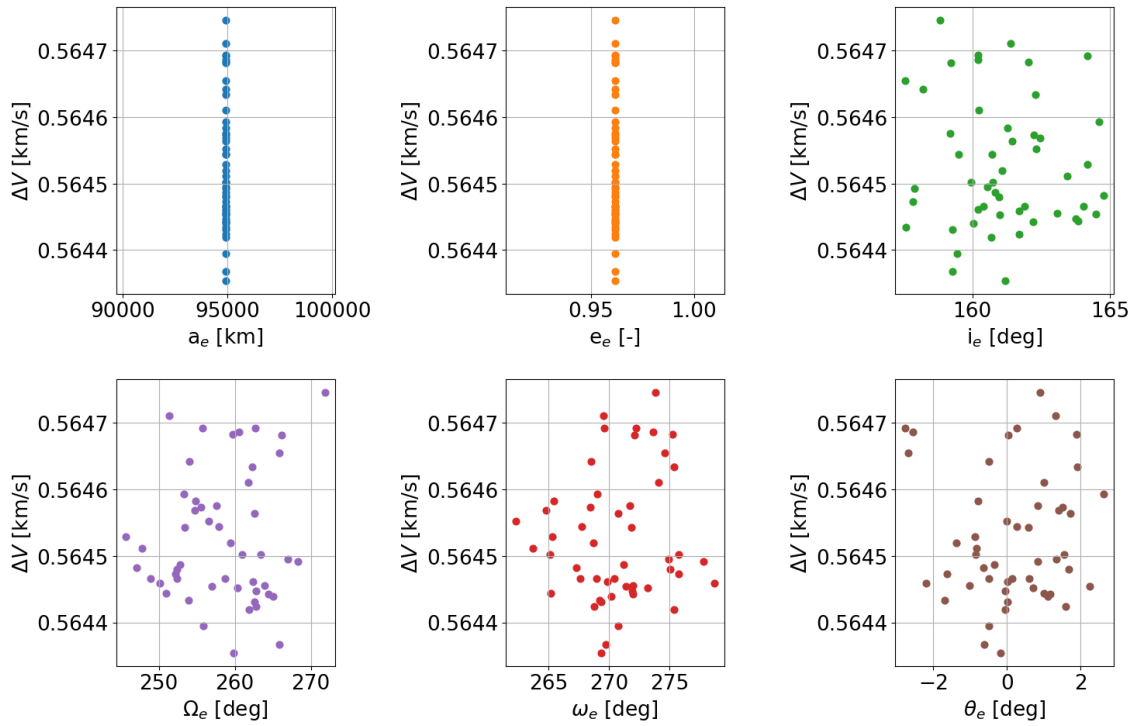
Figure C.26: Results from the final population of elliptical parking orbits, A2-left insertion problem, seed number=3682.
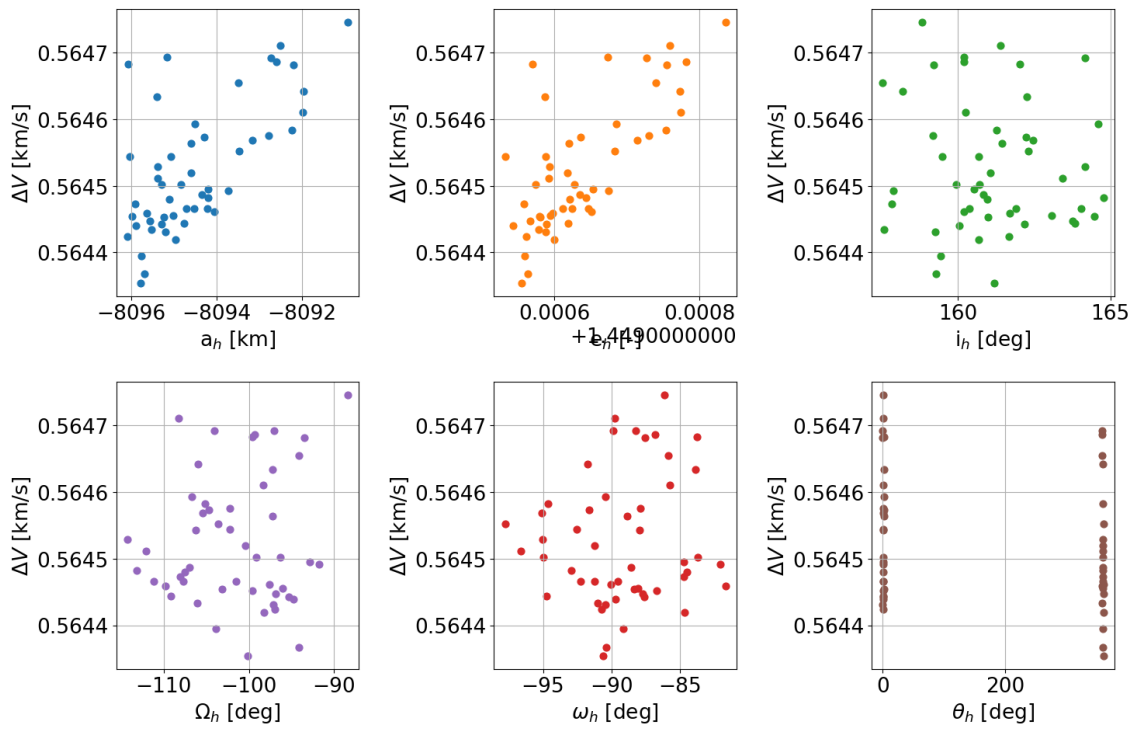
Figure C.27: Results from the final population of hyperbolic orbits, A2-left insertion problem, seed number=3682.

C.4. Case A2-right
Seed 1721
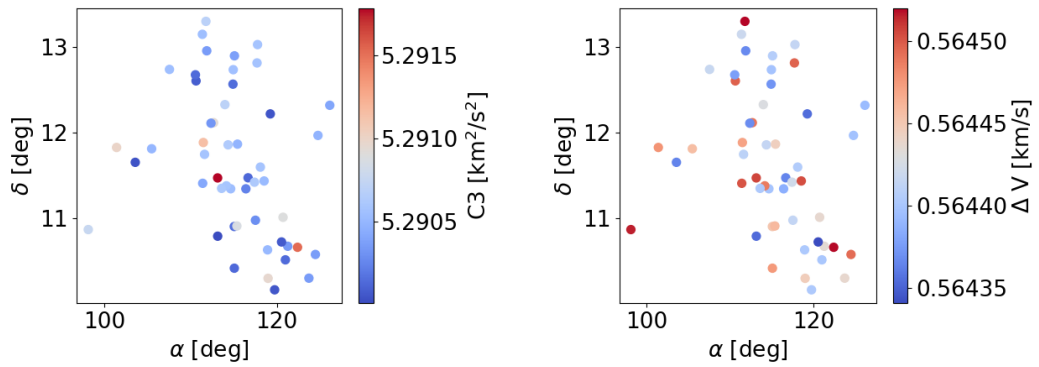
Figure C.28: Results from the final population of hyperbolic orbits, (left) conditions at infinite distance, (right) asymptote angles vs ΔV. A2-right insertion problem, seed number=1721.
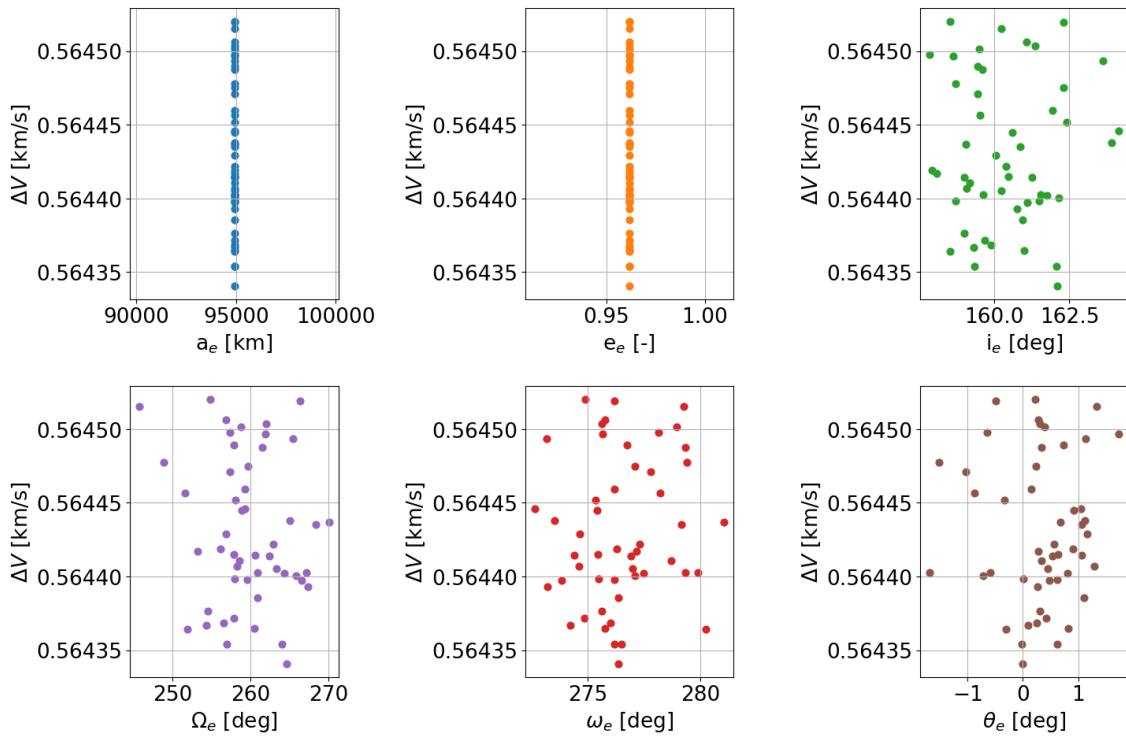
Figure C.29: Results from the final population of elliptical parking orbits, A2-right insertion problem, seed number=1721.
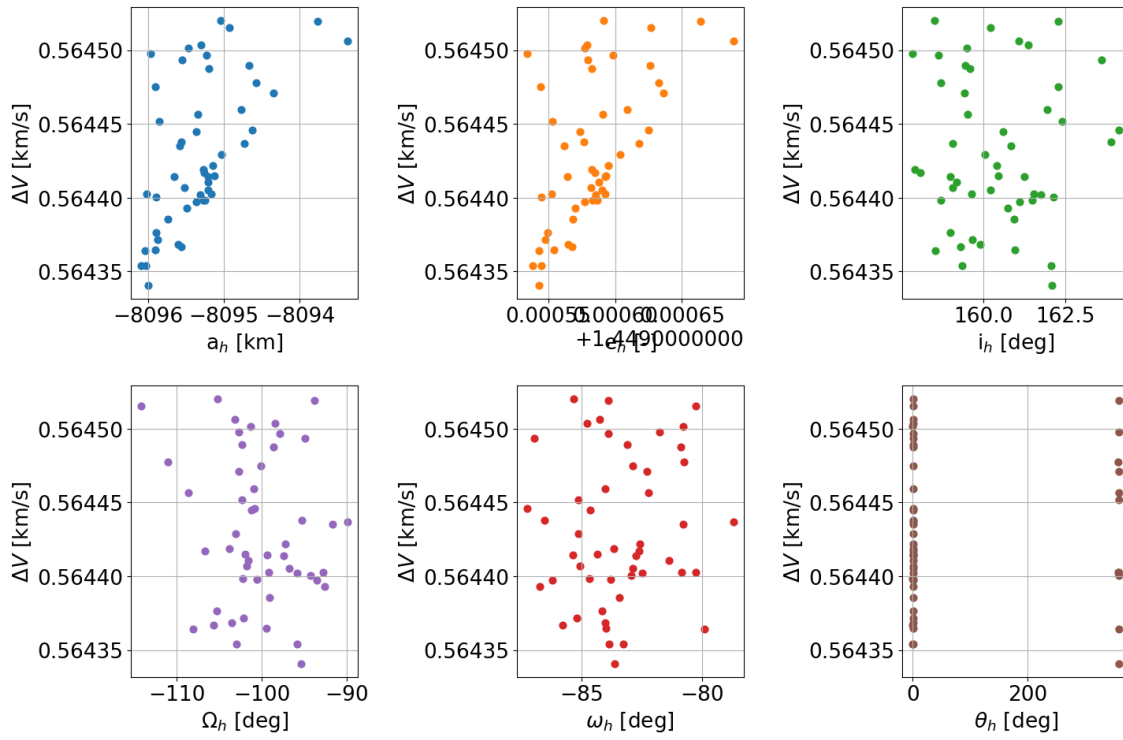
Figure C.30: Results from the final population of hyperbolic orbits, A2-right insertion problem, seed number=1721.

Seed 2358
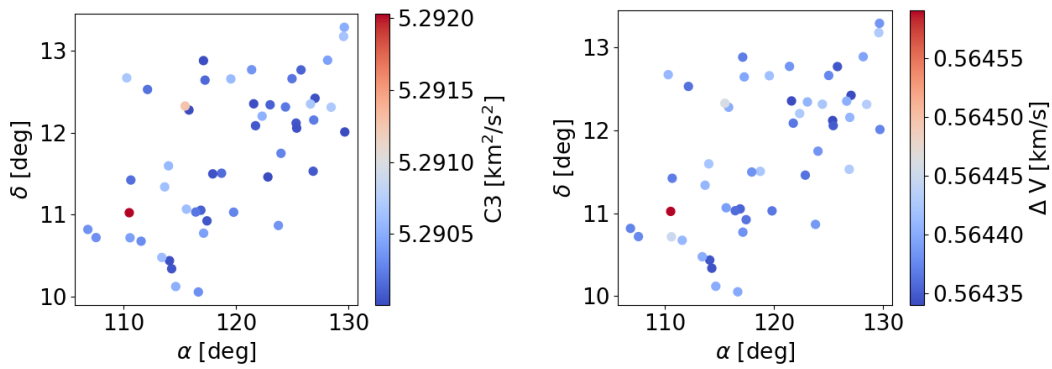
Figure C.31: Results from the final population of hyperbolic orbits, (left) conditions at infinite distance, (right) asymptote angles vs ΔV. A2-right insertion problem, seed number=2358
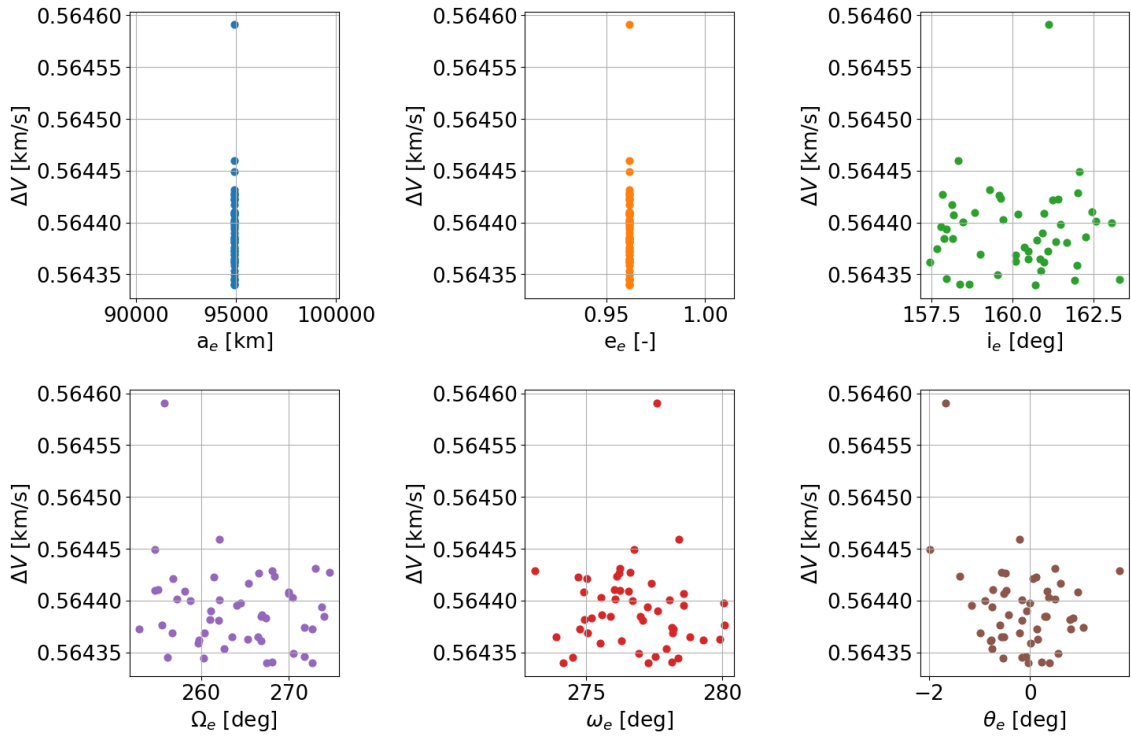
Figure C.32: Results from the final population of elliptical parking orbits, A2-right insertion problem, seed number=2358.
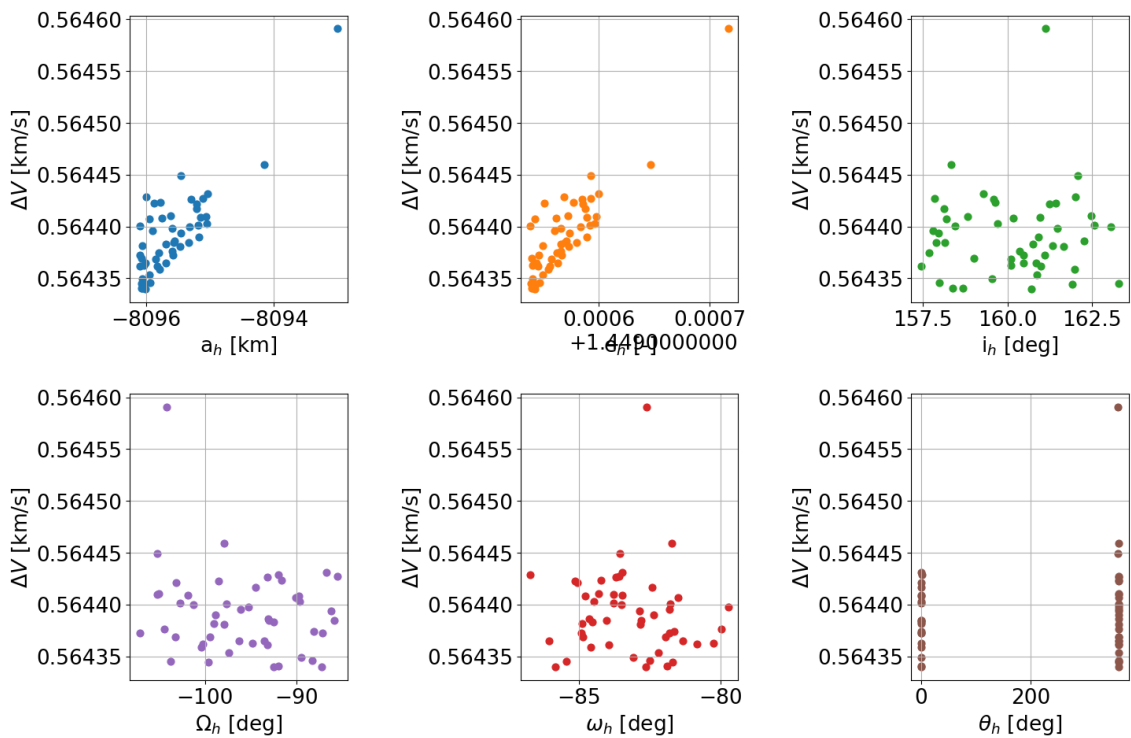
Figure C.33: Results from the final population of hyperbolic orbits, A2-right insertion problem, seed number=2358.

Seed 3682
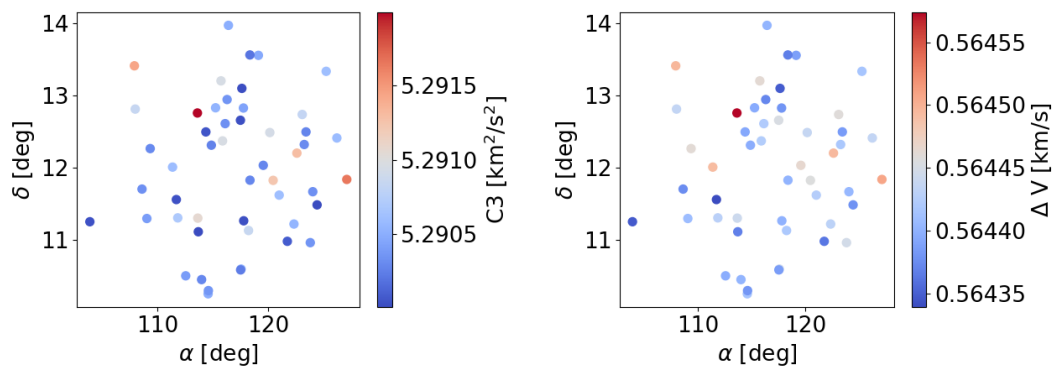
Figure C.34: Results from the final population of hyperbolic orbits, (left) conditions at infinite distance, (right) asymptote angles vs ΔV. A2-right insertion problem, seed number=3682
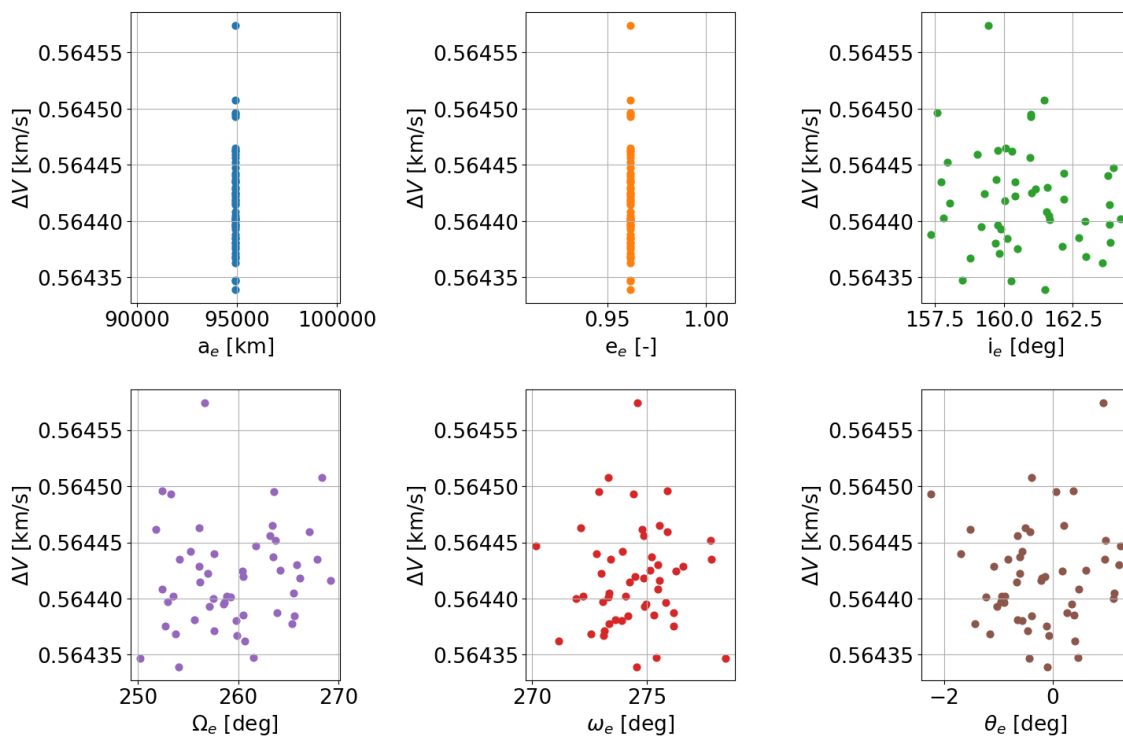
Figure C.35: Results from the final population of elliptical parking orbits, A2-right insertion problem, seed number=3682.
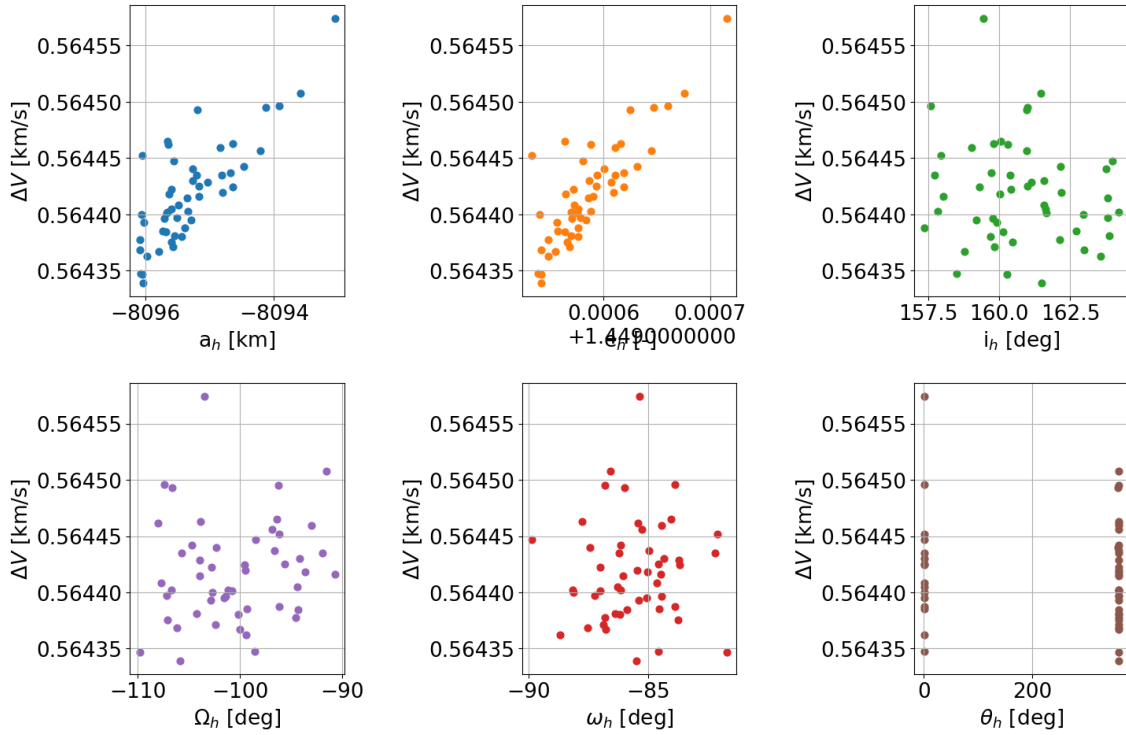
Figure C.36: Results from the final population of hyperbolic orbits, A2-right insertion problem, seed number=3682.

C.5. Case P1-left
Seed 1721
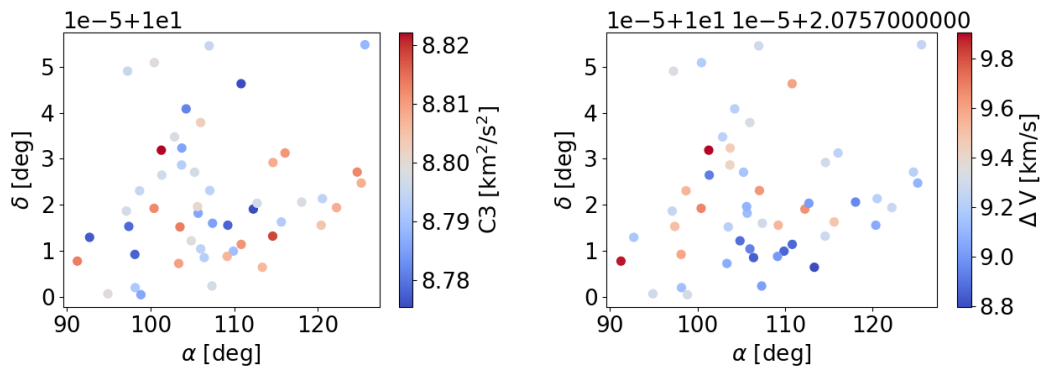
Figure C.37: Results from the final population of hyperbolic orbits, (left) conditions at infinite distance, (right) asymptote angles vs ΔV. P1-left insertion problem, seed number=1721.
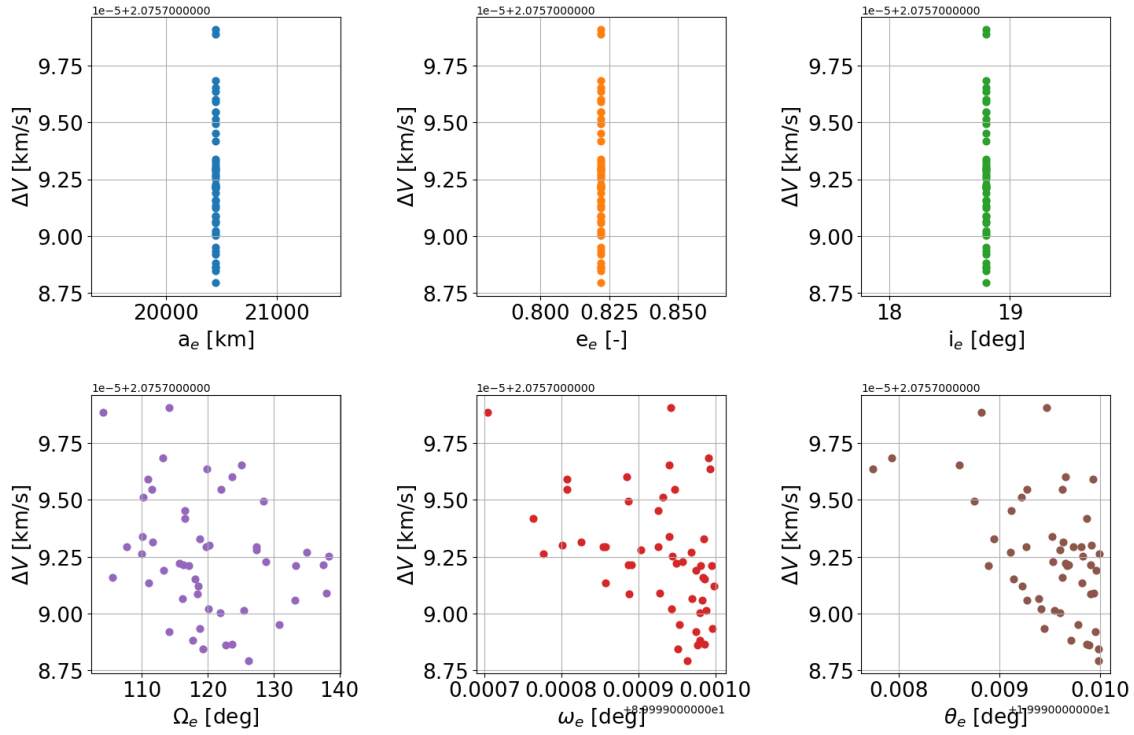
Figure C.38: Results from the final population of elliptical parking orbits, P1-left insertion problem, seed number=1721.
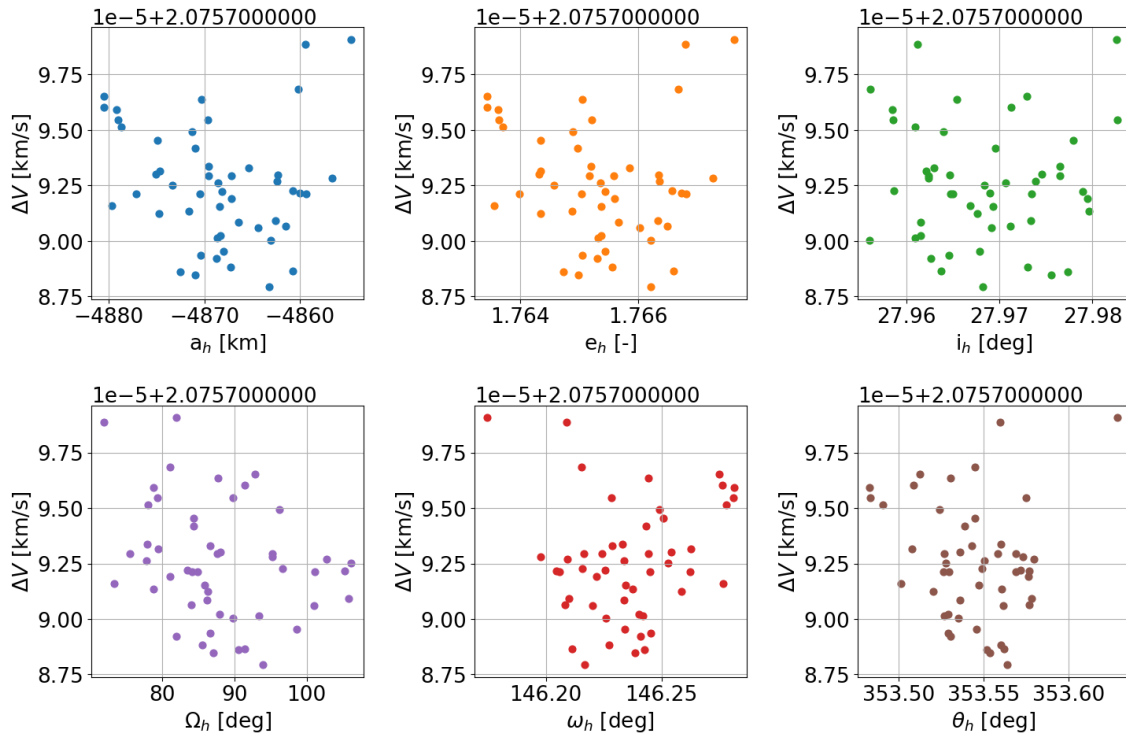
Figure C.39: Results from the final population of hyperbolic orbits, P1-left insertion problem, seed number=1721.

Seed 2358
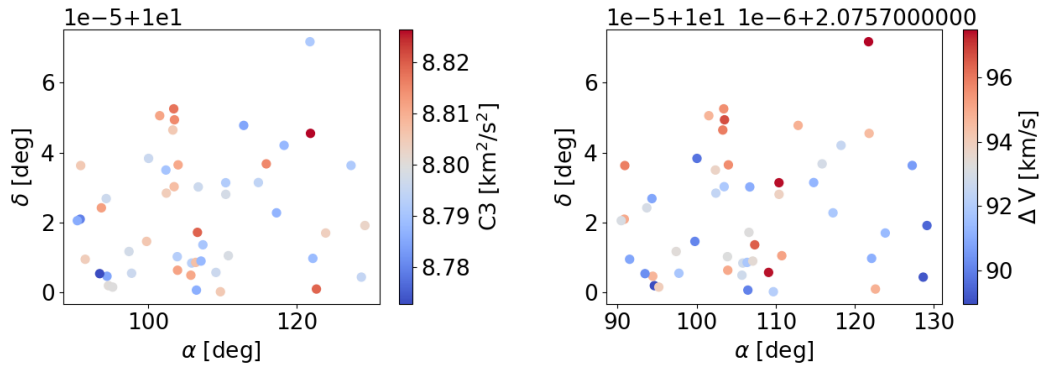
Figure C.40: Results from the final population of hyperbolic orbits, (left) conditions at infinite distance, (right) asymptote angles vs ΔV. P1-left insertion problem, seed number=2358
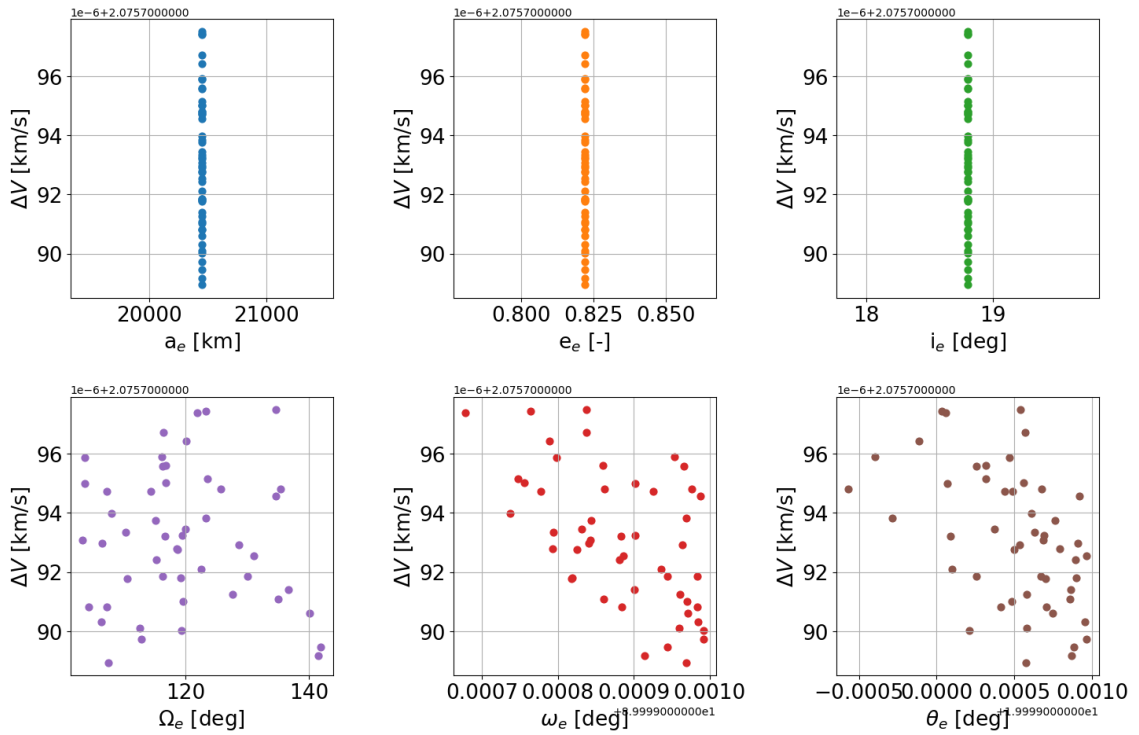
Figure C.41: Results from the final population of elliptical parking orbits, P1-left insertion problem, seed number=2358.
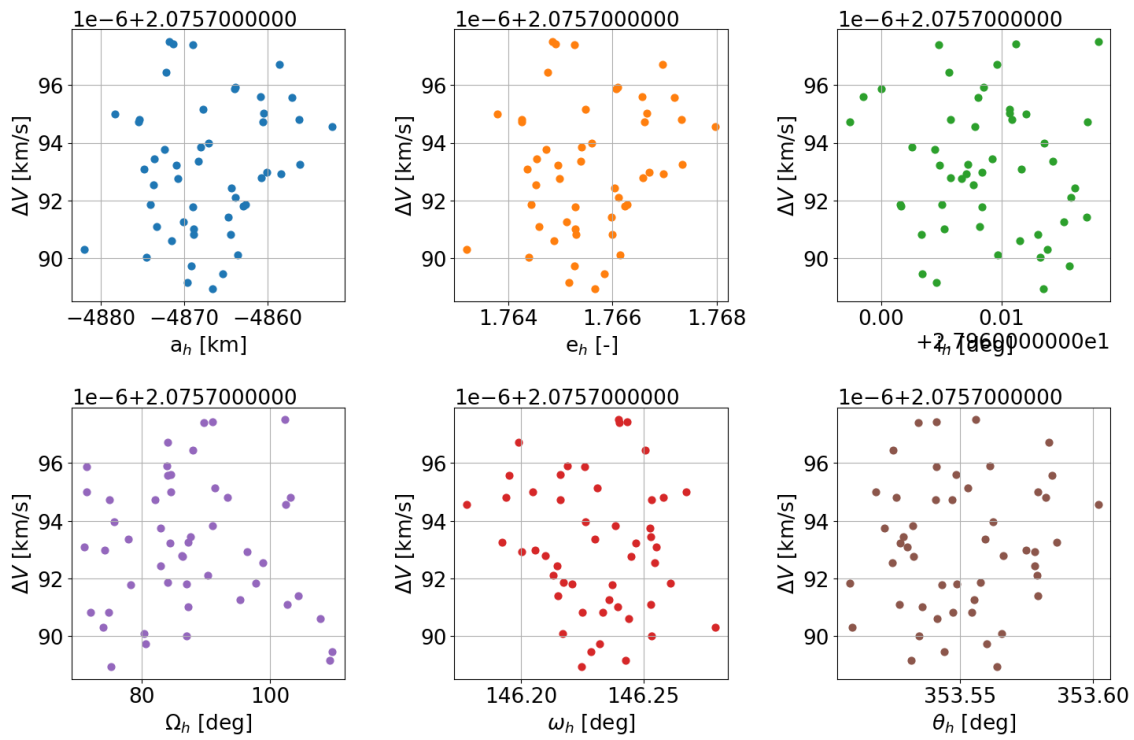
Figure C.42: Results from the final population of hyperbolic orbits, P1-left insertion problem, seed number=2358.

Seed 3682
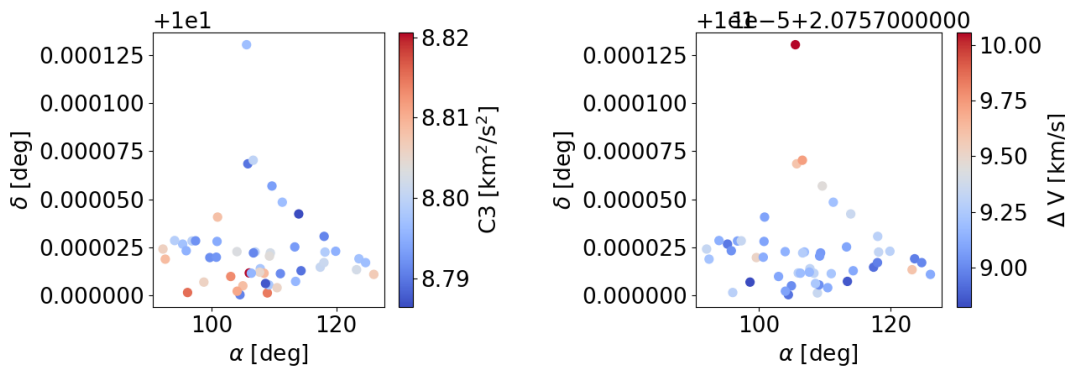
Figure C.43: Results from the final population of hyperbolic orbits, (left) conditions at infinite distance, (right) asymptote angles vs ΔV. P1-left insertion problem, seed number=3682
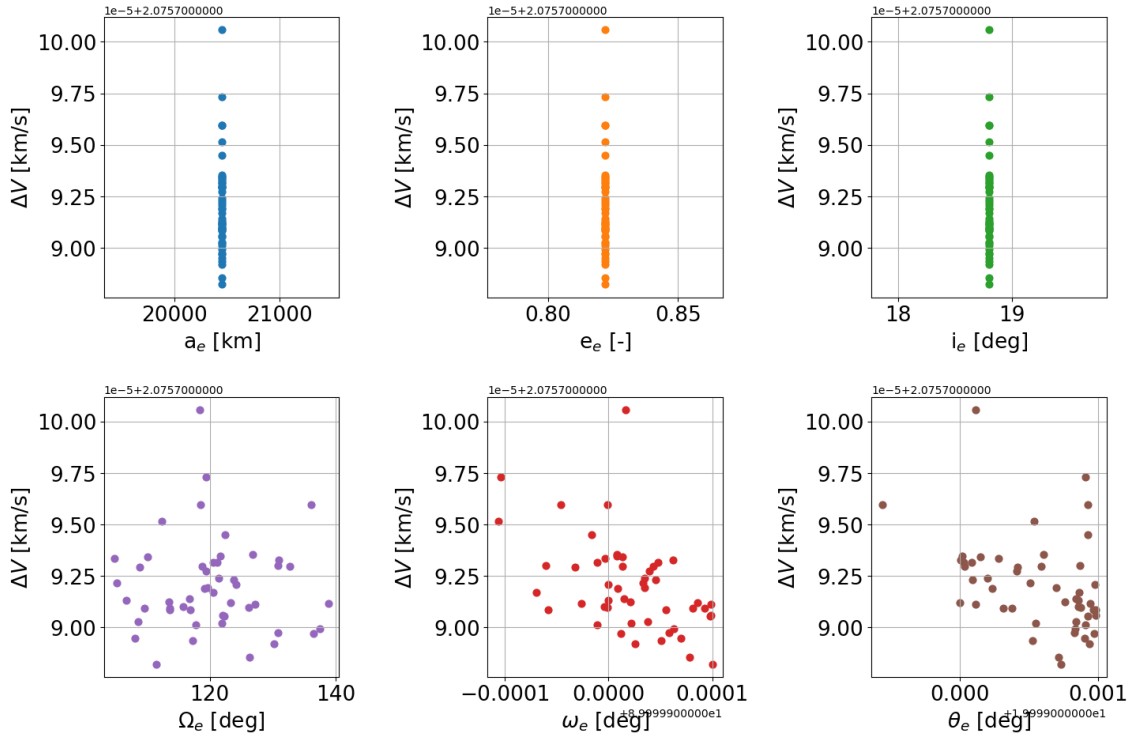
Figure C.44: Results from the final population of elliptical parking orbits, P1-left insertion problem, seed number=3682.
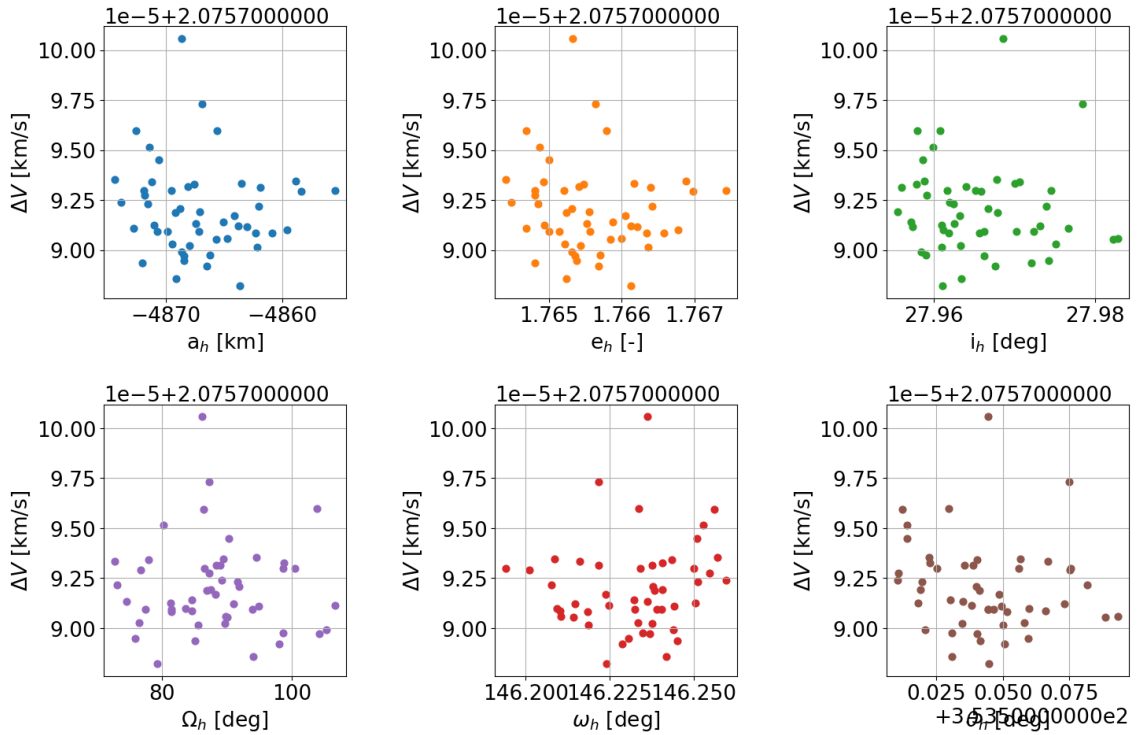
Figure C.45: Results from the final population of hyperbolic orbits, P1-left insertion problem, seed number=3682.

C.6. Case P1-right
Seed 1721
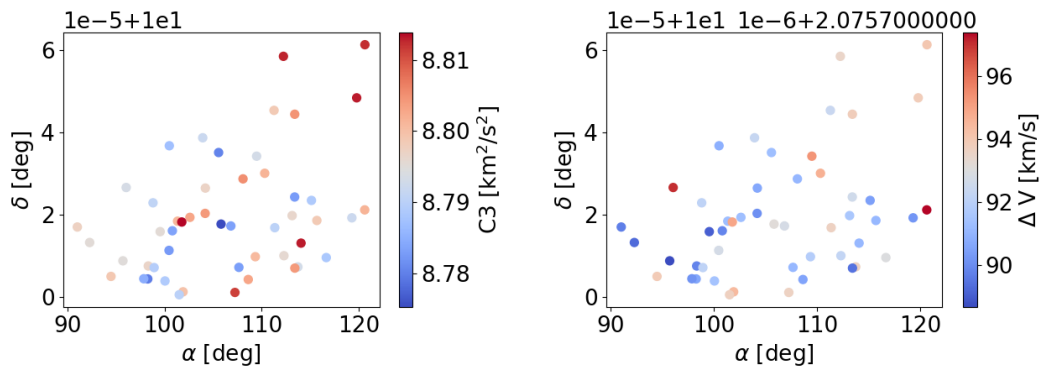
Figure C.46: Results from the final population of hyperbolic orbits, (left) conditions at infinite distance, (right) asymptote angles vs ΔV. P1-right insertion problem, seed number=1721.
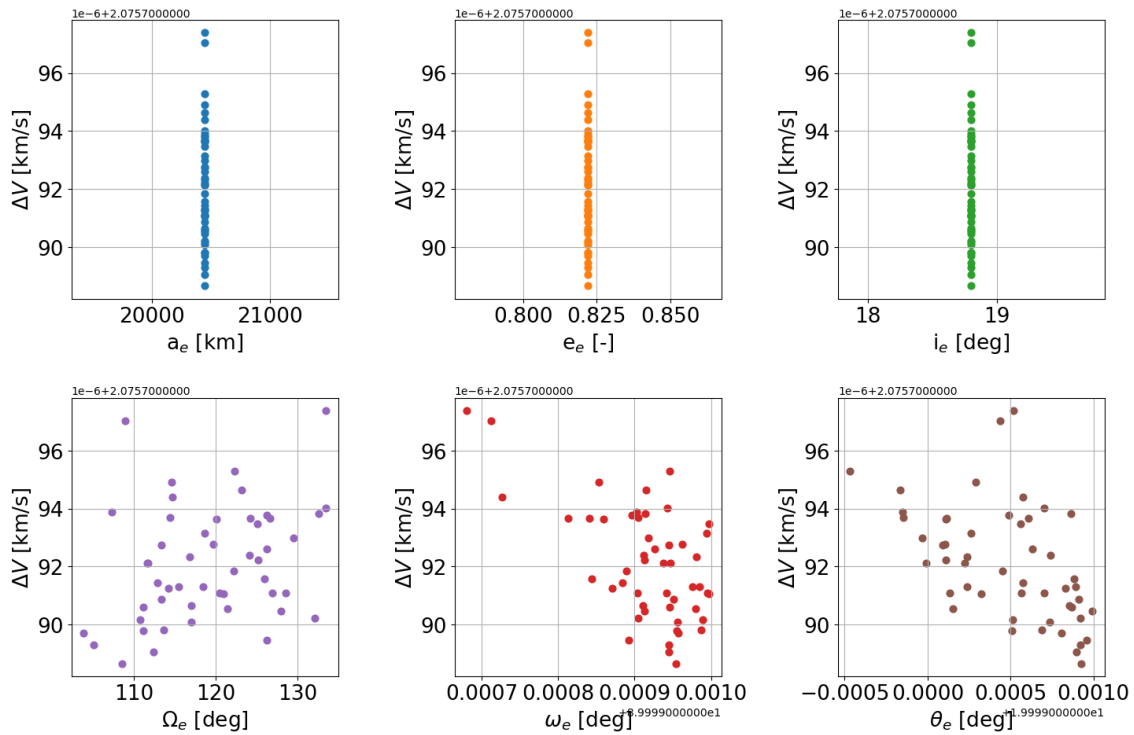
Figure C.47: Results from the final population of elliptical parking orbits, P1-right insertion problem, seed number=1721.
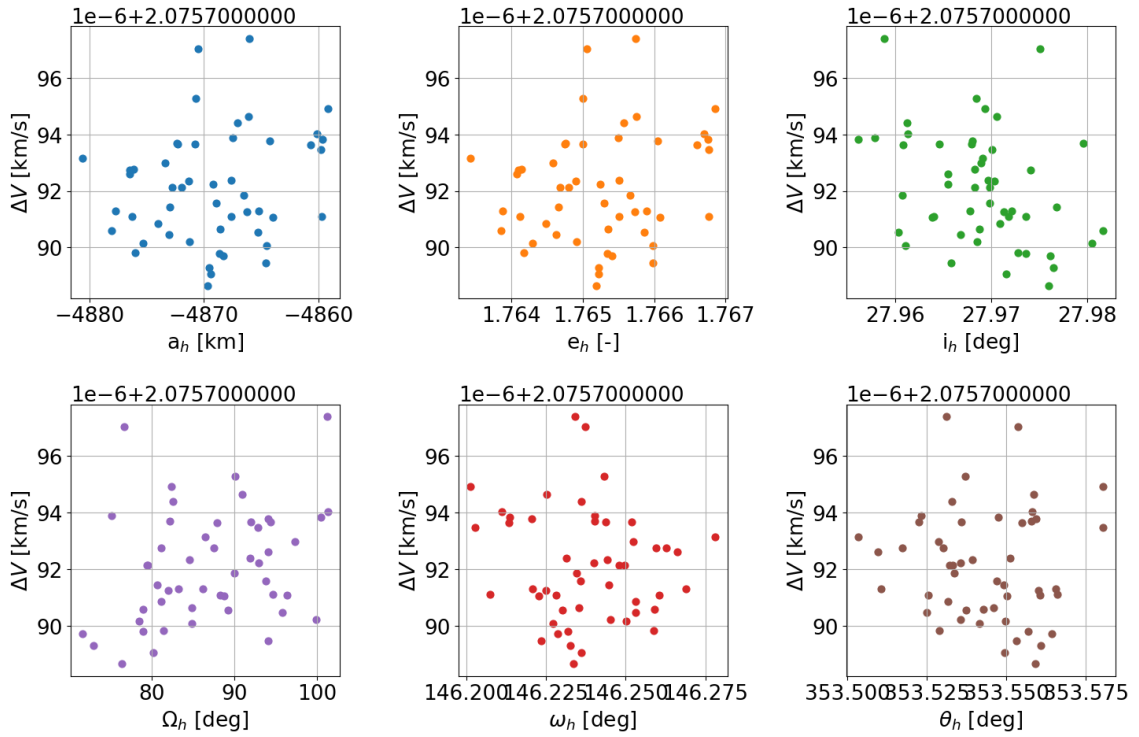
Figure C.48: Results from the final population of hyperbolic orbits, P1-right insertion problem, seed number=1721.

Seed 2358
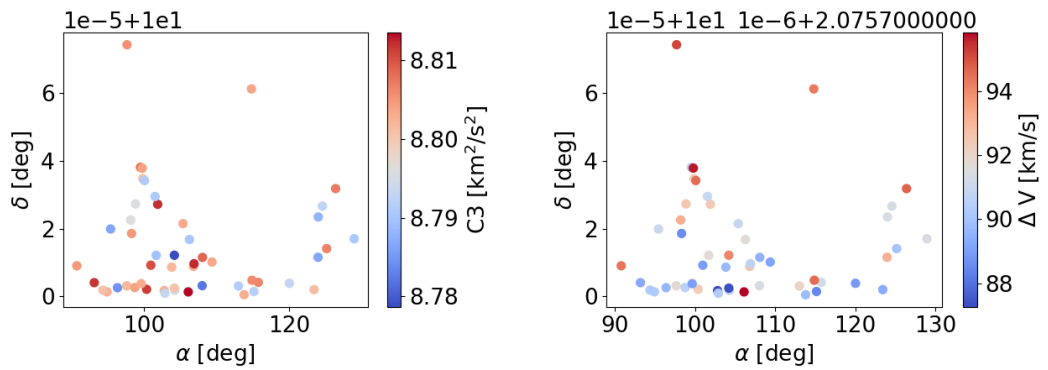
Figure C.49: Results from the final population of hyperbolic orbits, (left) conditions at infinite distance, (right) asymptote angles vs ΔV. P1-right insertion problem, seed number=2358
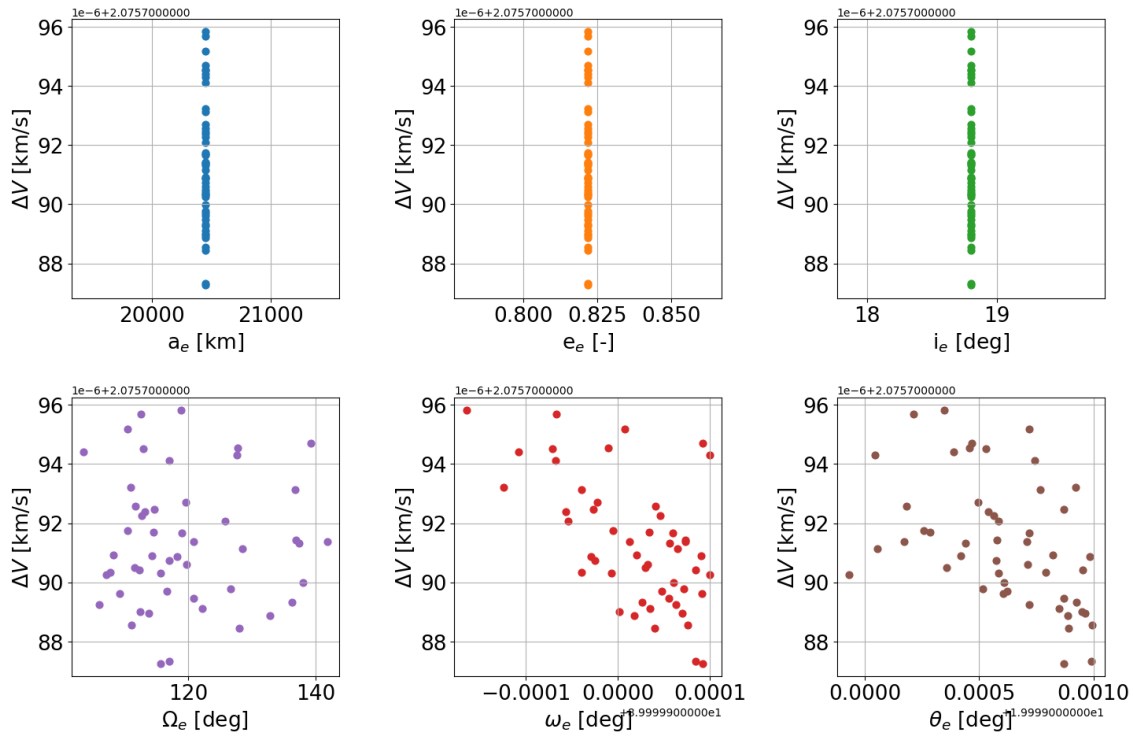
Figure C.50: Results from the final population of elliptical parking orbits, P1-right insertion problem, seed number=2358.
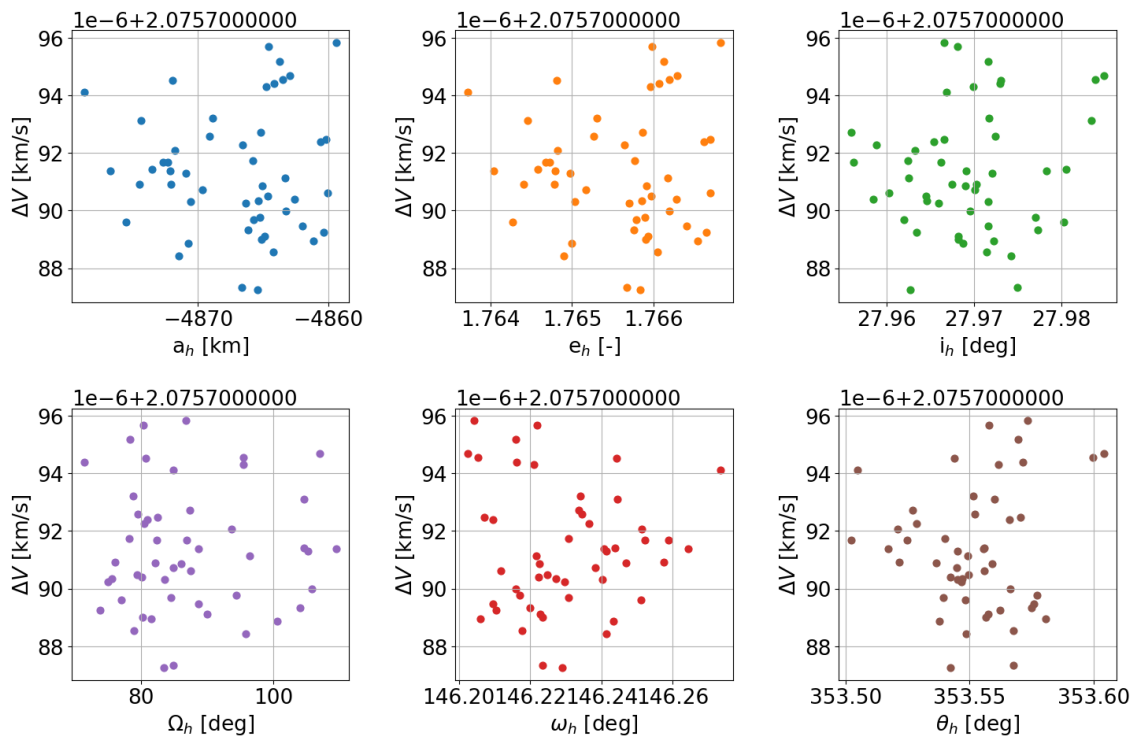
Figure C.51: Results from the final population of hyperbolic orbits, P1-right insertion problem, seed number=2358.

Seed 3682
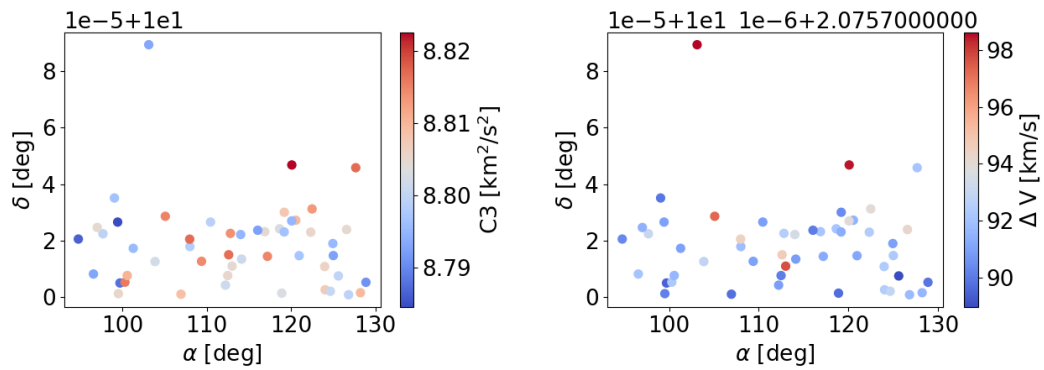
Figure C.52: Results from the final population of hyperbolic orbits, (left) conditions at infinite distance, (right) asymptote angles vs ΔV. P1-right insertion problem, seed number=3682
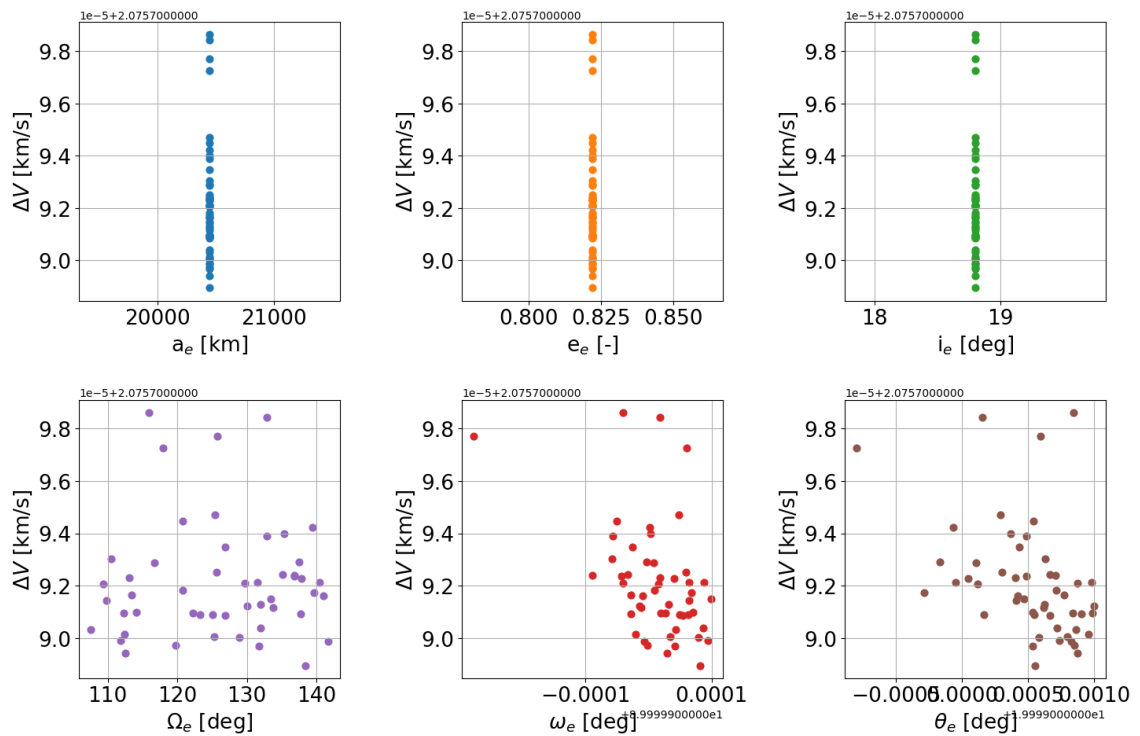
Figure C.53: Results from the final population of elliptical parking orbits, P1-right insertion problem, seed number=3682.
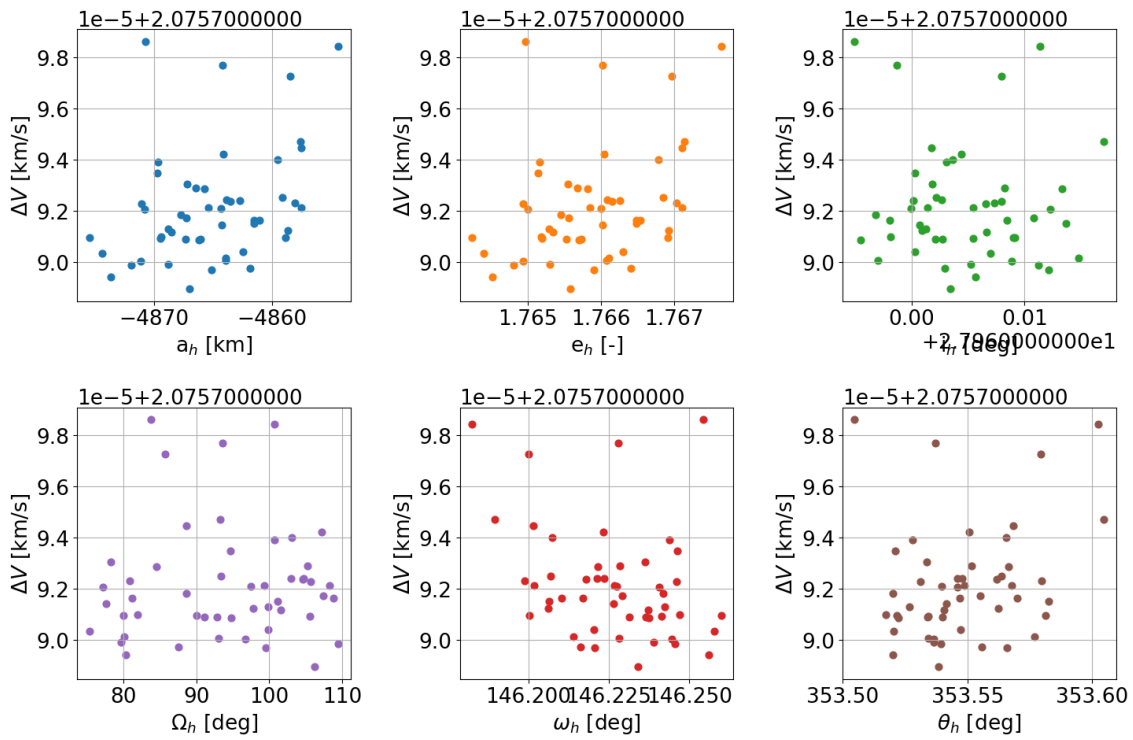
Figure C.54: Results from the final population of hyperbolic orbits, P1-right insertion problem, seed number=3682.

C.7. Case P2
Seed 1721
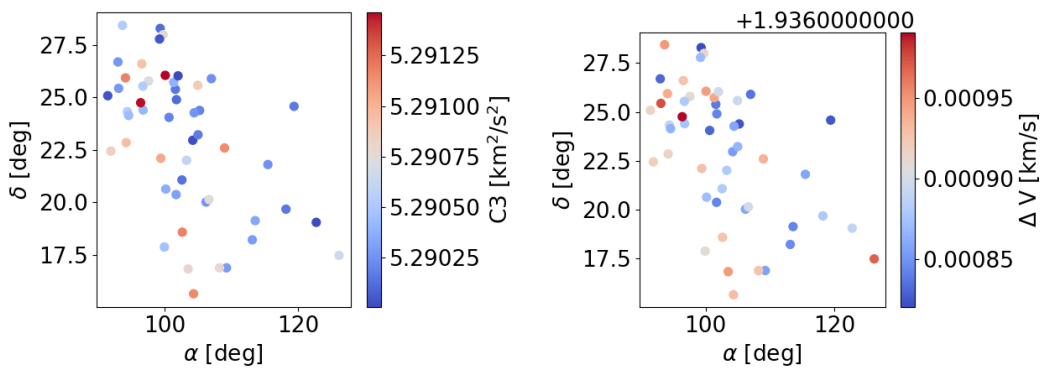
Figure C.55: Results from the final population of hyperbolic orbits, (left) conditions at infinite distance, (right) asymptote angles vs ΔV. P2 insertion problem, seed number=1721.
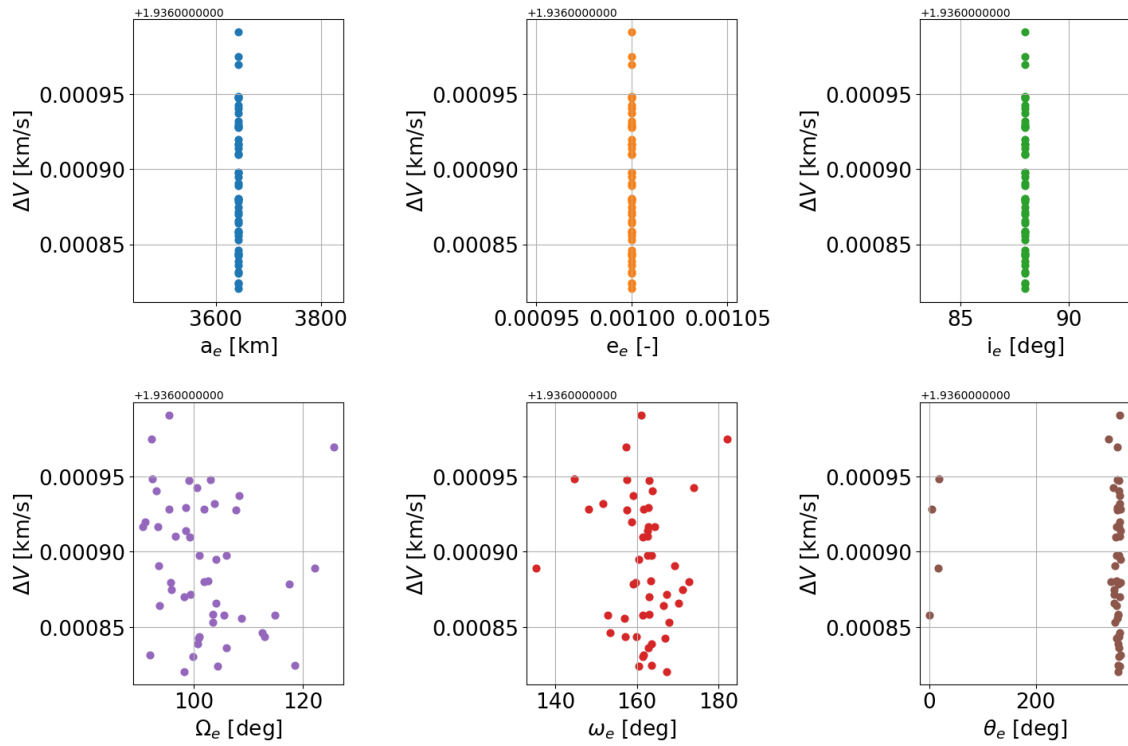
Figure C.56: Results from the final population of elliptical parking orbits, P2 insertion problem, seed number=1721.
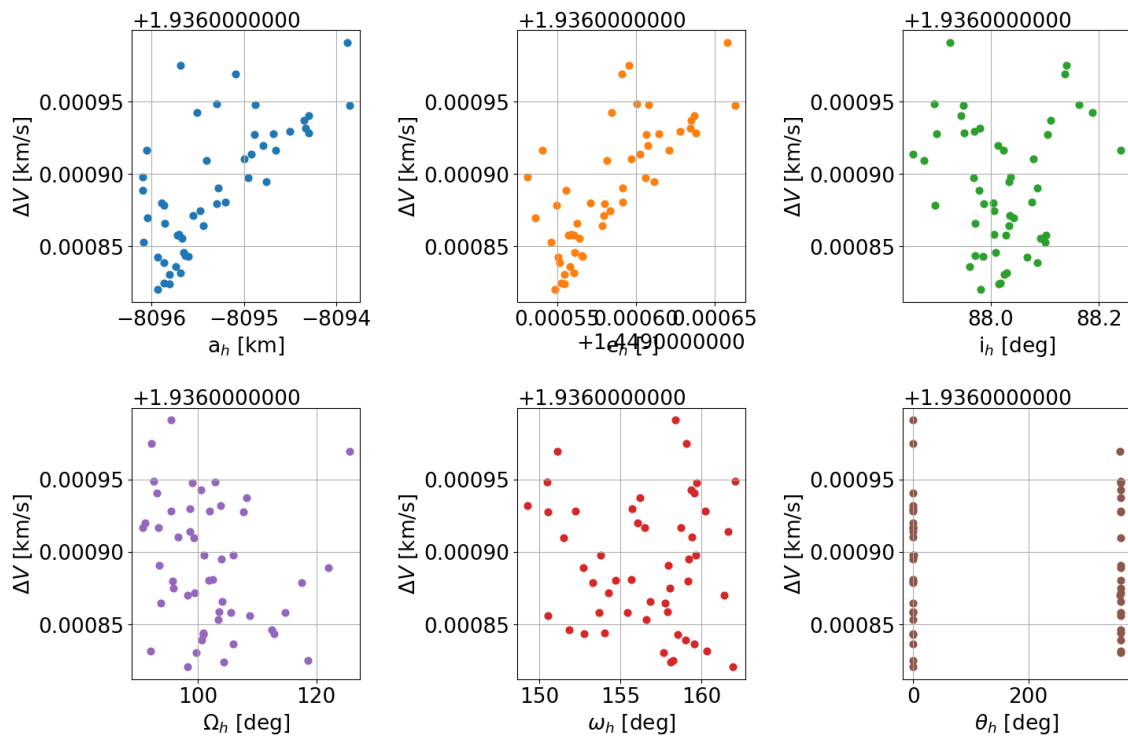
Figure C.57: Results from the final population of hyperbolic orbits, P2 insertion problem, seed number=1721.

Seed 2358
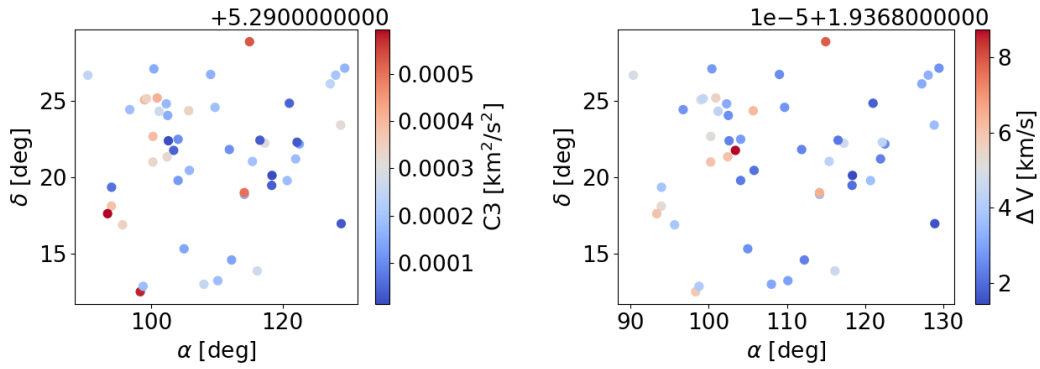
Figure C.58: Results from the final population of hyperbolic orbits, (left) conditions at infinite distance, (right) asymptote angles vs ΔV. P2 insertion problem, seed number=2358
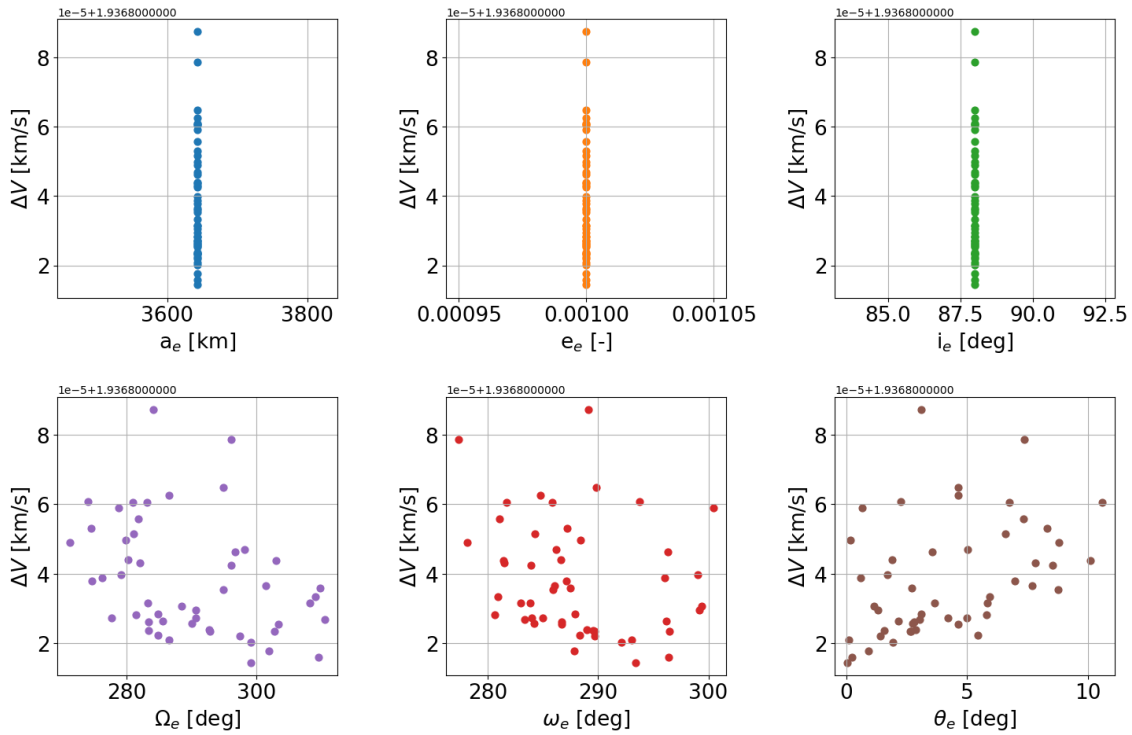
Figure C.59: Results from the final population of elliptical parking orbits, P2 insertion problem, seed number=2358.
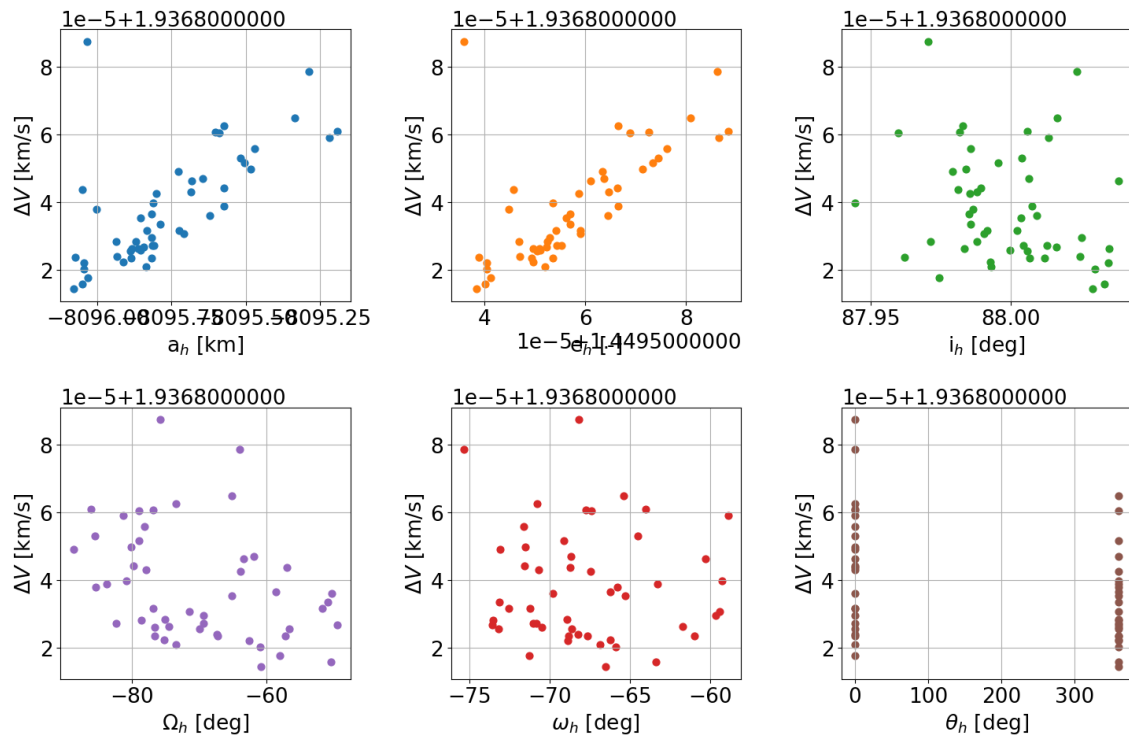
Figure C.60: Results from the final population of hyperbolic orbits, P2 insertion problem, seed number=2358.

Seed 3682
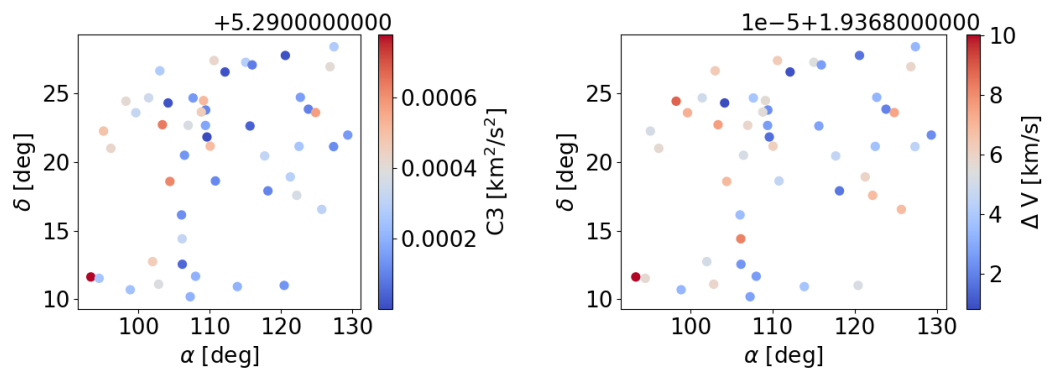
Figure C.61: Results from the final population of hyperbolic orbits, (left) conditions at infinite distance, (right) asymptote angles vs ΔV. P2 insertion problem, seed number=3682
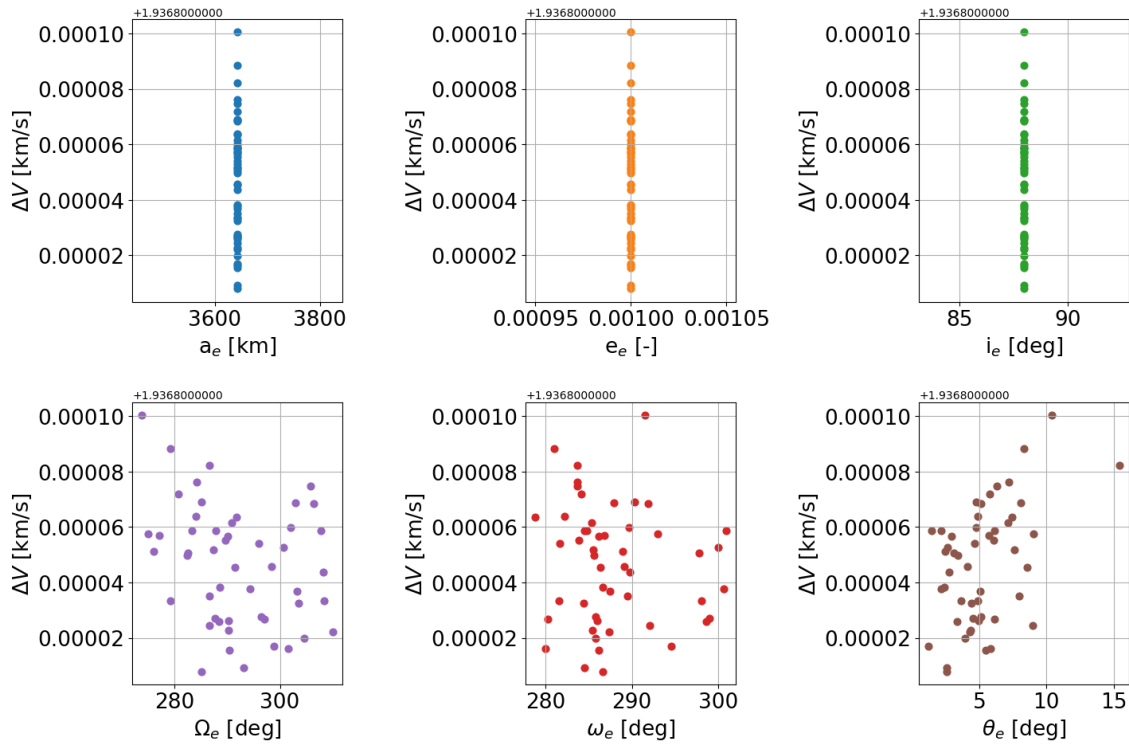
Figure C.62: Results from the final population of elliptical parking orbits, P2 insertion problem, seed number=3682.
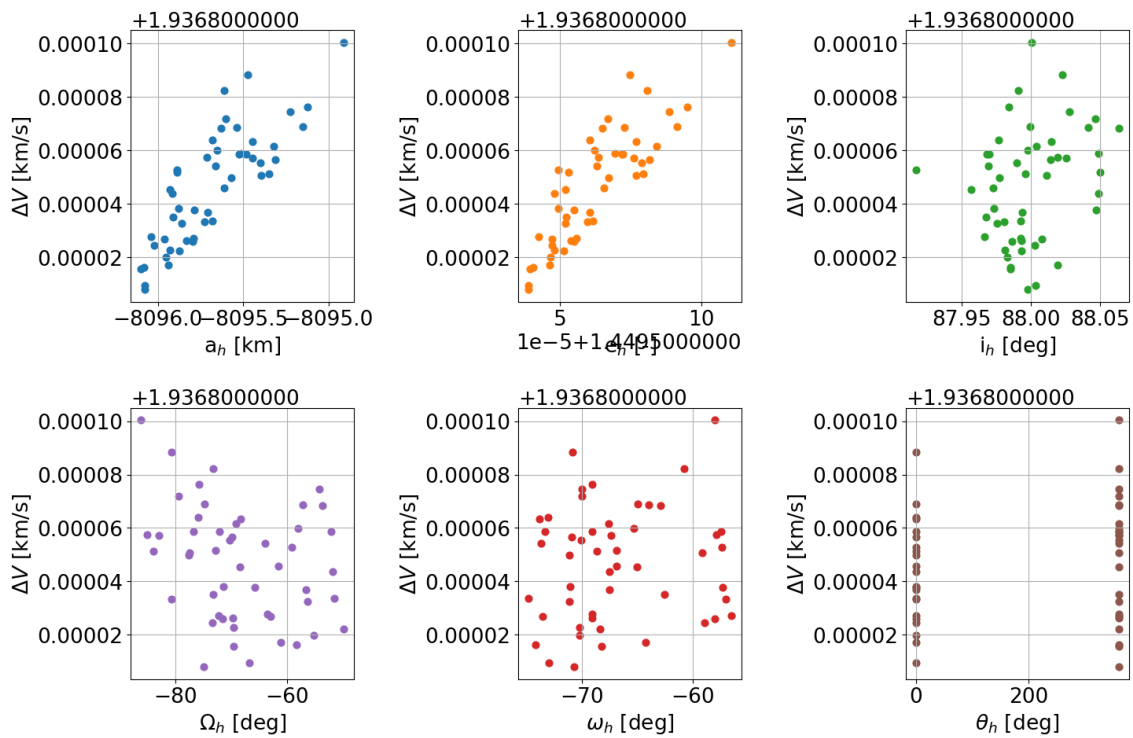
Figure C.63: Results from the final population of hyperbolic orbits, P2 insertion problem, seed number=3682.